
Towards Multi-Agent Reinforcement Learning driven Over-The-Counter Market Simulations

Nelson Vadori J.P. Morgan AI Research	Leo Ardon J.P. Morgan AI Research	Sumitra Ganesh J.P. Morgan AI Research
Thomas Spooner J.P. Morgan AI Research	Selim Amrouni J.P. Morgan AI Research	Jared Vann J.P. Morgan AI Research
Mengda Xu J.P. Morgan AI Research	Zeyu Zheng Computer Science and Engineering University of Michigan	Tucker Balch J.P. Morgan AI Research
	Manuela Veloso J.P. Morgan AI Research	

Abstract

We study a game between liquidity provider and liquidity taker agents interacting in an over-the-counter market, for which the typical example is foreign exchange. We show how a suitable design of parameterized families of reward functions coupled with associated shared policy learning constitutes an efficient solution to this problem. Precisely, we show that our deep-reinforcement-learning-driven agents learn emergent behaviors relative to a wide spectrum of incentives encompassing profit-and-loss, optimal execution and market share, by playing against each other. In particular, we find that liquidity providers naturally learn to balance hedging and skewing as a function of their incentives, where the latter refers to setting their buy and sell prices asymmetrically as a function of their inventory. We further introduce a novel RL-based calibration algorithm which we found performed well at imposing constraints on the game equilibrium, both on toy and real market data.

Contents

1	Introduction	2
2	Supertype-based multi-agent simulation model	6
2.1	Agent types and supertypes	6
2.2	Efficient learning of a spectrum of agent behaviors via reinforcement learning	8
2.2.1	Shared policy conditioned on agent type	8
2.2.2	Reinforcement learning design of OTC agents	9
2.3	ECN model	12
2.3.1	Vanilla model	12
2.3.2	Neural extension of the vanilla model	17

3 Game theoretical analysis and convergence properties	18
3.1 Shared equilibria: convergence of shared-policy learning in the case of stationary LTs	18
3.2 Empirical analysis of game components	23
4 Calibration of agent supertypes to equilibrium targets	25
5 Experiments	28
5.1 Calibration: the case of stationary LTs on toy data	28
5.2 Calibration: the general case on real data	32
5.3 Emergent agent behavior	33
6 Conclusion	40
A Appendix	45

1 Introduction

Market context. We focus on a dealer market, also commonly known as over-the-counter (OTC), where a single security is being traded. Examples of such markets include foreign exchange - the largest financial market in the world - so we can think of the security in question to be eurodollar. Unlike for typical stocks, trading activity between different agents does not occur on a single centralized exchange observable by everyone, rather the market is *decentralized*: an agent willing to trade typically does so via a private connection with another agent, or a liquidity aggregator, a variant thereof which provides the best price from a set of other agents. The nature of these interactions naturally makes the market *partially observable*, since a given agent does not know who other agents are connected to, neither prices which they transact at.

There also exists conventional exchanges (or ECNs, for Electronic Communication Networks), but i) not everyone can access them, typically larger market participants only, ii) trading on such ECNs can contribute to leaking information to other market participants and iii) the smallest price increment in which prices are quoted (tick size) is fixed and potentially higher than what can be obtained via private connections. Although most of the trading occurs via private connections, ECNs are useful in they provide a reference price to market participants, and a platform to trade in case of immediate need (e.g. hedging). For eurodollar, an example of such ECN is Electronic Brokerage Service (EBS), which tick size is 0.5 basis points¹, higher than 0.1 basis points that can be seen in some aggregators.

Market agents. Who are agents trading in such markets? They can mostly be split into two classes: Liquidity Providers (LPs), and Liquidity Takers (LTs)². The former are essentially market makers, whose goal is to provide liquidity to the market by continuously streaming prices to LTs at which they are willing to buy and sell. The latter trade with LPs for various motives, be it for speculative reasons (they have spotted a signal), or because they simply need a specific quantity of the security in question for exogenous purposes.

LPs' problem is to optimally manage the net inventory they are left with after trading with LTs, which is subject to uncertain price fluctuations: this is either done by *skewing*, i.e. optimally adjusting their buy and sell prices asymmetrically so as to reduce their inventory (*internalization*), or by *externalizing* their inventory by trading on the ECN market. While most of the literature - often to preserve analytical tractability - focuses on LPs maximizing risk-penalized profit-and-loss (PnL), in reality LPs also have alternate, important motives in mind, the most significant of which being increasing their market share. The latter is the fraction of total LT flow a specific LP is able to get, and is not trivial to estimate due to the overall partial observability of the OTC market. Interestingly, the market share objective of LPs can be seen as the analogous of the LT's exogenous trading

¹one basis point (bps) equals 10^{-4} .

²an agent can also be a blend of the two, but we do not consider this case in the present paper, however the methods we employ allow for straightforward extension to this case.

target: schematically, one can think of LP and LT agents as aiming to maximize a trade-off between risk-penalized PnL on one side, and a purely quantity related target on the other, reflecting their willingness to trade independently of costs. In the present paper, we want to capture, for each agent class, a spectrum of these incentives reflecting real-life markets. A pictorial view of the market is presented in figure 1.

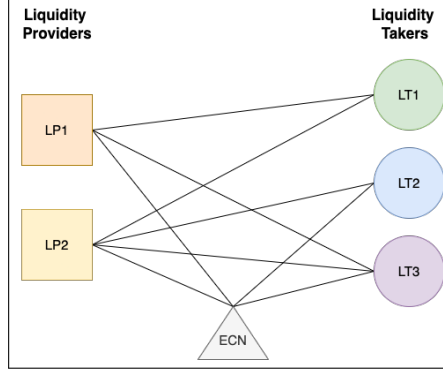


Figure 1: Overview of the simulator. Different colors represent different agent incentives, a mix between risk-penalized PnL, market share and traded quantity targets. Note the partial connectivity structure among agents.

Our goal and desiderata. We aim at designing an OTC market simulation of the above setting - formally *n*-player partially observable general sum Markov game - between LP agents, LT agents, and ECNs, where all agents learn optimal behaviors related to their individual incentives, also called *policies*, by playing against each other. This is now possible using modern AI techniques in multi-agent reinforcement learning (MARL).

Such simulation is powerful in that it allows to study, from an empirical perspective, specific what-if scenarios and equilibrium properties, such as impact on a given LP's market share of increasing risk aversion of specific competitors, or of modifying agent connectivity. This is different from recent, interesting work studying a single LP's optimal pricing and hedging problem from a stochastic optimal control point of view Guéant (2017); Barzykin et al. (2021a,b). There, other agents are modeled as a single "rest of the world" entity, estimated statistically from historical data. By construction, this entity is not "intelligent" and cannot adapt to changes in both the LP's policy, and their own characteristics, such as risk aversion, connectivity and trade-off parameters discussed previously. The reader familiar with finance and stress-tests could make an analogy with historical and monte-carlo value-at-risk.

A central question related to multi-agent simulations is how to instantiate all of these agents' characteristics. This is crucial for practical applications. Typically, one knows some information about the market. For example, we may know the flow response curve of a specific LP as in Guéant (2017), i.e. how much quantity it gets as a function of its pricing. Or we may know the average market share of specific LPs. Our task then becomes to select all simulator hyperparameters, in our case agents' characteristics, so as to match these observations. We will devote a full section on this topic, and introduce a novel RL-driven way to perform such calibration, which we found performed well compared to other approaches on both internal market data, and toy examples. For example, we find interesting that our calibration method allows to find a specific agent population - fully RL-driven - that explains the HSBC EURUSD flow response curve of a specific LP of Barzykin et al. (2021b), cf. figure 8.

The *n*-player game we study is, in spirit, close to that of Bank et al. (2021) who study equilibrium interactions between dealers (LPs), clients (LTs), and open market (ECN), however we deviate from their work via our desiderata below, which will lead us to adopting a deep MARL approach:

- **(Desiderata 1)** Due to the structure of the OTC market, the simulation should account for connectivity between pairs of agents, namely the simulation should take as an input a connectivity graph.

- **(Desiderata 2)** The simulation should allow agents to optimize for a wide spectrum of incentives reflecting real-life dealer markets.
- **(Desiderata 3)** Learning of optimal³ agent actions in (Desiderata 2) should be done from the definition of the game (rules) and by experimenting the game (playing).
- **(Desiderata 4)** The simulation should be flexible and rich enough to reproduce observations that specific agents may have of the market, namely it should allow for calibration to these observations.

(Desiderata 1) is a structural requirement in line with the nature of the market.

For (Desiderata 2), we will focus on the case where LP incentives cover the spectrum from maximizing PnL to market share, and LT incentives cover the spectrum from maximizing PnL to trading for exogenous motives, independent of cost. Both of these are trade-offs between a PnL component and a purely quantity related component, which contributes to compactify our agents' formulation. Note that optimizing for a mix between a trading target and PnL is exactly optimal execution, where the goal is to trade a certain quantity q while minimizing costs. However, as we will see later, our supertype-based design allows for trade-off between an arbitrary set of incentives. In particular, we are not interested in analytical tractability but rather in the ability to learn a wide range of behaviors in line with these incentives.

A reformulation of (Desiderata 3) is that all agents actions should emerge from agents playing the market game while optimizing for a mix of these incentives, as opposed to being handcrafted (exogenous). Note the important point that being optimal isn't necessarily synonym of maximizing wealth, but rather it could be achieving a trading or market share target, in which case optimality is with respect to these criteria. In particular, this opens the door to discovering emergent behaviors from the game itself.

(Desiderata 4) reflects the fact that we want the simulation to capture certain known observations about the market, for example that the market share of a given agent is equal to some level, and the model should be rich and flexible enough to capture these observations. Constraints such as those can be achieved by having agents of different nature, or types, and optimally balancing those types so as to match the desired targets on the emergent behavior of agents. We highlight the fact that this is a highly non trivial requirement: (Desiderata 3) requires learning an equilibrium, hence, together with (Desiderata 4), require learning an equilibrium subject to specific constraints.

Our Contributions. We formalize the game between LPs and LTs based on the concepts of agent type and supertype (section 2.1) and show how to have populations of such agents efficiently learn a family of behaviors corresponding to a spectrum of incentives encompassing profit-and-loss, optimal execution and market share, using RL (section 2.2). The ECN engine that we consider in this paper is "mechanical", in the sense that its limit order book evolves solely as a consequence of agents' orders being sent (market, limit, cancel). To make its evolution realistic in the absence of agents' orders, we equip it with a so-called ECN agent which sends orders to the ECN at every time-step. The construction of this order list is based on a discrete-time Markovian model for the volume at the top levels of the book whose continuous-time limit book volume display a second order polynomial variance structure which generalizes that of Cont and Müller (2021). We show how this model can be extended to the non-Markovian case using neural networks, where the evolution of the order book depends on its history (section 2.3). We study the game theoretic implications of LP agents using a shared policy suitably conditioned on their type and introduce the concept of shared equilibrium, a pure-strategy Nash equilibrium on the extended space of stochastic policies (section 3.1). We show how modern game theoretical tools can help analyze our complex market game (section 3.2), namely differentiable games and their potential-Hamiltonian decomposition of Balduzzi et al. (2019); Candogan et al. (2011). There, we introduce the concepts of Hamiltonian and potential weights of a differentiable game. In particular, we stress the necessity to suitably renormalize the potential component of the game when defining those weights, and show on simple examples how these quantities give interesting insights into our market game. We introduce a novel RL-based calibration algorithm which performs well on both toy and real data (section 4). There, LP and LT players learn to reach an equilibrium jointly with a RL-based calibrator agent aiming at imposing constraints on that equilibrium. In particular, we find interesting that we are able to find a specific agent population - fully RL-driven - that explains the HSBC EURUSD flow response curve of a specific LP of Barzykin

³with respect to some concept of game theoretical equilibrium.

et al. (2021b), cf. figure 8. Finally, we conduct experiments to show i) the efficiency of our novel calibration algorithm, and ii) the emergent behaviors learnt by the LP agents as a function of their incentives (section 5). In particular, we find that LPs naturally learn to balance hedging and skewing, where the latter refers to setting their pricing asymmetrically on the bid and ask sides as a function of their inventory.

Related work. The market making problem has been extensively studied in finance and economics literature, largely as an optimal control problem. Classical models such as Garman (1976), Amihud and Mendelson (1980), Ho and Stoll (1981), and more recently Avellaneda and Stoikov (2008) and Guéant et al. (2013), focus on the role of inventory risk in determining the optimal pricing strategy for a market maker. Other models, such as Glosten and Milgrom (1985), study the role of adverse selection risk arising from informed traders in the market. All these works model a single market maker and make assumptions about the distributions of order arrivals and price to derive analytical solutions for the market maker's pricing policy using stochastic optimal control techniques. Market making has also been studied in the agent-based modeling (ABM) literature (e.g. Darley et al. (2000), Das (2005), Das (2008), Jumadinova and Dasgupta (2010), Wah et al. (2017)), but the agents tend to be simplistic with a view to studying market equilibria and endogenous price formation rather than developing realistic market making strategies. Most previous work focuses on market making in limit order book markets where all agents submit their orders to a central matching facility; there has been relatively little work focused on dealer markets where the agents interact directly with each other. Recently, Guéant (2017), Bank et al. (2021) and Ghoshal and Roberts (2016) have extended the optimal control approach to dealer markets. In Barzykin et al. (2021a,b), liquidity providers' optimal hedging is considered, in addition to the optimal pricing problem. Chan and Shelton (2001), and more recently, Lim and Gorse (2018) and Spooner et al. (2018) have developed RL-based market making approaches for limit order book markets; however, they do not explicitly model the competing market makers or study different competitive scenarios. Cont and Xiong (2022) recently study competition and collusion among a set of market makers, and use reinforcement learning as a mean to solve for the equilibrium of the game. Spooner and Savani (2020) studies a discrete-time zero-sum game between a market maker and adversary and shows that adversarial reinforcement learning can help produce more robust policies. Ganesh et al. (2019); Ardon et al. (2021) are some of the work closest to ours, where competition among a set of market makers and investors is studied by means of reinforcement learning.

There are no MARL algorithms with convergence guarantees to Nash equilibria in general sum Markov games with continuous action and state spaces, as it is the case for our game among LP and LT agents. Our game is further partially observable, which makes matters even worse. Existing algorithms have guarantees in specific settings. For example, fictitious play Brown (1951) (potential games, zero-sum games); double oracle McMahan et al. (2003) (finite action spaces, but in the worst case, all actions of the game need to be enumerated); policy-sparse response oracles (PSRO) Lanctot et al. (2017), which is a modern variant of double oracle, has been proved to be efficient in practice but has no theoretical guarantees: the space of policies is infinite, hence you cannot simply enumerate it as you would do in double oracle. Most of the MARL literature has focused on cooperative games Gupta et al. (2017); Foerster et al. (2016); Rashid et al. (2018); Mahajan et al. (2019). Recently, an extension of normal form potential games to Markov games has been considered under the terminology "Markov potential game" Leonardos et al. (2021). Any Markov game whereby agents take actions and transition from states to states over multiple timesteps can be recast as a one-shot game with utilities $V_i(\pi_i, \pi_{-i})$, where the latter are agents' value functions. The latter game is a one-shot game over a larger pure strategy space, hence it is sometimes called a "meta-game" Lanctot et al. (2017). Markov potential games are related to potential games by the intuitive fact that the meta-game is assumed to be potential. Leonardos et al. (2021) shows that independent RL converges to Nash equilibria in the case of Markov potential games. In our case, we assume extended transitivity, which is weaker than the potential condition. Indeed, it is more similar to generalized ordinal potential games. Further, most MARL algorithms consider n fully heterogeneous agents. In our case, we want to tie these agents together by the concept of type: two agents with similar risk aversion should behave similarly. The latter is not guaranteed using independent RL, in addition of being inefficient. Rather, conditioning the policy on the type represents an efficient alternative. This is the concept of parameter sharing, which has been introduced in Gupta et al. (2017); Foerster et al. (2016), which falls under the popular centralized training with decentralized execution paradigm (CTDE). Gupta et al. (2017) showed that out of the their three proposed approaches, TRPO-based parameter sharing was the best performer (PPO is a more recent variant of TRPO). Although their

work considers a cooperative setting where agents maximize a joint reward, parameter sharing is actually the only method out of their proposed three that doesn't require reward sharing, and we exploit this fact in our work. The approach we employ in this paper (based on a combination of policy sharing and definition of agent types) can be used with any on-policy RL algorithm, such as A2C Mnih et al. (2016), TRPO Schulman et al. (2015), or PPO Schulman et al. (2017). It has been shown that PPO enjoys competitive performance when suitably tuned Yu et al. (2021) and when using sufficient parallelism to generate on-policy experience. For this reason, we use PPO in this paper, with our experiments employing 60 to 90 CPUs in parallel to generate sufficient amount of data for training the shared policy. In contrast, there has been recent academic progress in MARL which has focused on off-policy learning, such as MADDPG Lowe et al. (2017) and value-decomposed Q-learning Sunehag et al. (2018); Rashid et al. (2018).

On the topic of calibration, Zheng et al. (2020) uses a shared policy for worker agents earning individual rewards and paying tax. There, the RL-based tax planner shares some similarities with our RL calibrator, although our calibrator is responsible for optimally picking agent type distribution rather than public information observable by all agents, and updates its policy on a slower timescale so as to allow equilibria to be reached by the shared policy. The idea of using RL to calibrate parameters of a system probably goes back to Eiben et al. (2007), in the context of evolutionary algorithms. As mentioned in Avegliano and Sichman (2019), there is currently no consensus on how to calibrate parameters of agent-based models. Most methods studied so far build a surrogate of the MAS Avegliano and Sichman (2019); Lamperti et al. (2018). The term "surrogate" is very generic, and could be defined as a model that approximates the mapping between the input parameters and some output metric of the MAS. Lamperti et al. (2018) studies classifier surrogates, and in contrast to the latter and other work on calibration, our work is based on a dual-RL approach where our RL calibrator learns jointly with RL agents learning an equilibrium. In our experiments, we compare our approach to a Bayesian optimization baseline that builds such a surrogate. Inverse RL Finn et al. (2016) could be used for calibration, but it aims at recovering unknown rewards from input expert policy: in this work we don't need the latter and assume that rewards are known for each agent type, and that the goal is to find the optimal agent type distribution.

2 Supertype-based multi-agent simulation model

2.1 Agent types and supertypes

Partially Observable Markov Game setting. Throughout, we call *agent class* $\kappa \in \{LP, LT\}$. The game that we consider is a game among n_{LP} LPs and n_{LT} LTs, of finite time horizon T . We write $n_{tot} = n_{LP} + n_{LT}$ the total number of agents, and let n_{ECN} be the number of ECNs. Connectivity among agents, and among agents and ECNs, is given by an input connectivity graph. Two elements of this graph can interact together if and only if they are connected, and are always disconnected if they belong to the same class. Real markets evolve in continuous time, but here, we will consider a discretized version of the game, where time t is integer-valued and each time increment corresponds to a fixed value, for example one second. This will make our framework amenable to RL. We will use the related terminology throughout, where *agents* get *observations*, take *actions* and obtain per-timestep *rewards* as a consequence. We call the simulation of a stochastic game path over $[0, T]$ an *episode*, and the aggregated utility gained by each one of the agents over timesteps its *cumulative reward*.

The schematic and informal game structure is as follows: at each time $t \in [0, T]$, LPs first stream bid and ask prices⁴ at which they are willing to trade with LTs they are connected to, and additionally decide a hedge fraction of their current inventory to trade on the ECN market. Second, LTs decide a trade size (possibly zero) and direction based on the observed prices. When that decision is made, the trade will *always* occur at the best possible price among the LPs and ECN the LT is connected to. In this sense, this is a multi-stage, or stochastic Stackelberg game, since LTs play in response to LPs. The exact definition of players' actions and observations in our OTC context will be given in section 2.2.2, for now we focus on defining the game as a general framework based on the concept of supertype.

⁴these are price curves representing price as a function of quantity traded.

We formalize the game as a n -player partially observable Markov game Hansen et al. (2004). At each time t , each agent observes a fraction of the environment, proceeds to taking an action, and gets a reward which depends in general on all agents' actions and observations. In our Stackelberg context, observations of LTs include connected LPs' actions corresponding to pricing. Within each agent class, all agents share the same action and state spaces \mathcal{A}^κ and \mathcal{S}^κ . We make no specific assumption on the latter spaces unless specifically mentioned, and denote the joint action and state as $\mathbf{a}_t^\kappa := (a_t^{(1,\kappa)}, \dots, a_t^{(n_\kappa,\kappa)})$ and $\mathbf{s}_t^\kappa := (s_t^{(1,\kappa)}, \dots, s_t^{(n_\kappa,\kappa)})$. Partial observability is a consequence of our connectivity graph: an agent observes ECN information only if connected to it. Similarly, a LT observes a LP's pricing only if connected to it. Any agent-specific information such as its inventory or trade history remains private to the agent.

Agent types and supertypes. Before proceeding to the formal definition of agent types and supertypes, we give an informal description to build the reader's intuition, cf. also Vadòri et al. (2020). In addition to the agent class which specifies in particular the structure of observation and action spaces, agents of a given class differ by the utility they are optimizing for, also called *reward* in the context of RL. In our case and as usual in games, agents' rewards depend on players' actions and observations, but also on additional agent-specific parameters capturing their characteristics and incentives, which we call *agent type*. In our market framework, the type of a given agent includes its risk-aversion acting as a regularizer for PnL, its trade-off parameters between PnL, market share and trade quantity targets discussed in section 1, as well as its connectivity structure to other agents. This aspect will be further detailed in section 2.2.2. The point is that agent types correspond to a parametrized family of reward functions capturing a diverse set of incentives. Thinking in terms of agent type within a given agent class will allow us to learn efficiently a spectrum of behaviors using a single neural network suitably conditioned on the type, by exploiting their generalization power. As a simple example, if two agents have risk aversion parameters differing by a small amount ϵ but are identical otherwise, it is not efficient to learn two distinct policies, rather it is better to condition the policy on the risk aversion so as to learn a family of behaviors at once. Note that this generalization trick has also been used in the context of mean-field games Perrin et al. (2022) where they condition policies on the initial agent population so as to learn policies that can generalize well in that variable.

It can be convenient to think of agents in terms of distributions of agents, and not at the individual level. This allows to scale the simulation in a tractable way with fewer parameters, while observing diversity in agents' characteristics. This leads to our concept of *agent supertype*, which are simply parameters driving the distribution of agent type. Types will be sampled from supertypes at the beginning of each episode, and remain constant throughout a given episode. In this sense, supertypes can be seen as behavioral templates according to which agents can be cloned probabilistically. Note that introducing noise via the randomization of types can help convergence to equilibria, as noted in Hambly et al. (2021) in a linear-quadratic framework. Typically, we create groups of agents who share the same supertype, so that the number of distinct supertypes is typically much less than the number of agents. In our setting, agent supertypes will include in particular probabilities of being connected to other agents, so that actual connectivities between agents of different supertypes can be sampled as Bernoulli random variables.

Formally, we assign to each agent i a supertype $\Lambda_i^\kappa \in \mathcal{S}^{\Lambda_i^\kappa}$, with $\Lambda^\kappa := (\Lambda_i^\kappa)_{i \in [1, n_\kappa]}$. At the beginning of each episode, agent i is assigned a type $\lambda_i^\kappa \in \mathcal{S}^{\lambda^\kappa}$ sampled probabilistically as a function of its supertype, namely $\lambda_i^\kappa \sim p_{\Lambda_i^\kappa}$ for some probability density function $p_{\Lambda_i^\kappa}$, and initial states $s_0^{(i,\kappa)}$ are sampled independently according to the initial distribution $\mu_{\lambda_i^\kappa}^0$. This is formally equivalent to extending agents' state space to $\mathcal{S}^\kappa \times \mathcal{S}^{\lambda^\kappa}$, with a transition kernel that keeps λ_i^κ constant throughout an episode and equal to its randomly sampled value at $t = 0$. Note that typically, $\mathcal{S}^{\Lambda_i^\kappa}$ and $\mathcal{S}^{\lambda^\kappa}$ are subsets of \mathbb{R}^d .

Rewards, state transition kernel and type-symmetry assumption. In the following we make symmetry assumptions whose only purpose is to guarantee that an agent's expected reward only depends on its supertype, given that all agents' policies are fixed. Let $z_t^{(i,\kappa)} := (s_t^{(i,\kappa)}, a_t^{(i,\kappa)}, \lambda_i^\kappa)$. At each time t , LP agent i receives an individual reward $\mathcal{R}^{LP}(z_t^{(i,LP)}, z_t^{(-i,LP)}, z_t^{(LT)})$, where the vector $z_t^{(-i,\kappa)} := (z_t^{(j,\kappa)})_{j \neq i}$. Similarly, LT agent i receives an individual reward $\mathcal{R}^{LT}(z_t^{(i,LT)}, z_t^{(-i,LT)}, z_t^{(LP)})$. Denote $\mathcal{Y}^\kappa := \mathcal{S}^\kappa \times \mathcal{A}^\kappa \times \mathcal{S}^{\lambda^\kappa}$. The state transition kernel $\mathcal{T} : (\mathcal{Y}^{LP})^{n_{LP}} \times (\mathcal{Y}^{LT})^{n_{LT}} \times (\mathcal{S}^{LP})^{n_{LP}} \times (\mathcal{S}^{LT})^{n_{LT}} \rightarrow [0, 1]$ is denoted $\mathcal{T}(z_t^{(LP)}, z_t^{(LT)}, s_t^{LP}, s_t^{LT})$,

and represents the probability of reaching the joint state (s_t^{LP}, s_t^{LT}) conditionally on agents having the joint state-action-type structure $(z_t^{(LP)}, z_t^{(LT)})$.

We now proceed to making assumptions on the rewards and state transition kernel that we call *type-symmetry*, since they are similar to the anonymity/role-symmetry assumption in Li and Wellman (2020), which only purpose is to guarantee that the expected reward of an agent in (2) only depends on its supertype Λ_i^κ . In plain words, the latter guarantees that from the point of view of a given agent, all other agents are interchangeable, and that two agents with equal supertypes and policies have the same expected cumulative reward.

Assumption 2.1. (Type symmetry) For $\kappa \in \{LP, LT\}$, \mathcal{R}^κ is invariant w.r.t. permutations of both its second and third arguments, namely for any permutations ρ, μ we have $\mathcal{R}^\kappa(\cdot, z_1^\rho, z_2^\mu) = \mathcal{R}^\kappa(\cdot, z_1, z_2)$ for any z_1, z_2 , and $\mathcal{T}(z_1^\rho, z_2^\mu, s_1^\rho, s_2^\mu) = \mathcal{T}(z_1, z_2, s_1, s_2)$ for any z_1, z_2, s_1, s_2 , where superscripts denote the permuted vectors.

2.2 Efficient learning of a spectrum of agent behaviors via reinforcement learning

2.2.1 Shared policy conditioned on agent type

Multi-agent learning in partially observable settings is a challenging task. When all agents have the same action and observation spaces, the work of Foerster et al. (2016); Gupta et al. (2017) has shown that using a single shared policy π across all agents represents an efficient training mechanism. This falls in the centralized training with decentralized execution paradigm (CTDE). In that case, π is a neural network that takes as input the individual agent observations $s_t^{(i)}$ and outputs (a probability over) individual agent actions $a_t^{(i)}$, hence the terminology *decentralized execution*. The network is trained by collecting all agent experiences simultaneously and treating them as distinct sequences of local observations, actions and rewards experienced by the shared policy, hence the terminology *centralized training*. Due to the finite time-horizon of our setting, we assume that agents observations include time, which allows to consider time-independent policy on an extended space⁵. In our case, we have two classes of homogenous agents, LPs and LTs, so we will use one shared policy per class.

We innovate by including the agent type λ_i^κ in the local states and hence define the shared policy over the extended agent state space $\mathcal{S}^\kappa \times \mathcal{S}^{\lambda^\kappa}$. Denoting \mathcal{X}^κ the space of functions $\mathcal{S}^\kappa \times \mathcal{S}^{\lambda^\kappa} \rightarrow \Delta(\mathcal{A}^\kappa)$, where $\Delta(\mathcal{A}^\kappa)$ is the space of probability distributions over actions, we then define:

$$\mathcal{X}^\kappa := \left[\mathcal{S}^\kappa \times \mathcal{S}^{\lambda^\kappa} \rightarrow \Delta(\mathcal{A}^\kappa) \right], \quad \pi^\kappa(da|s, \lambda) := \mathbb{P} \left[a_t^{(i, \kappa)} \in da | s_t^{(i, \kappa)} = s, \lambda_i^\kappa = \lambda \right], \quad \pi^\kappa \in \mathcal{X}^\kappa. \quad (1)$$

Note that as often done so in imperfect information games, we can add the hidden variable of a LSTM h in $\pi(\cdot | s_t^{(i, \kappa)}, h_{t-1}^{(i, \kappa)}, \lambda_i^\kappa)$ to encode the agent history of observations Gupta et al. (2017): to ease notational burden we do not include it in the following, but this is without loss of generality since h can always be encapsulated in the state $s_t^{(i, \kappa)}$.

Due to our type-symmetry assumption 2.1, we see that the expected reward $V_{\Lambda_i^\kappa}$ of each agent i only depends on its supertype Λ_i^κ and the shared policies π^{LP}, π^{LT} ⁶.

$$V_{\Lambda_i^\kappa}(\pi^{LP}, \pi^{LT}) := \mathbb{E}_{\substack{\lambda_i^\kappa \sim p_{\Lambda_i^\kappa} \\ a_t^{(i, \kappa)} \sim \pi^\kappa(\cdot | \cdot, \lambda_i^\kappa)}} \left[\sum_{t=0}^T \mathcal{R}^\kappa(z_t^{(i, \kappa)}, z_t^{(-i, \kappa)}, z_t^{(-\kappa)}) \right], \quad \pi^\kappa \in \mathcal{X}^\kappa. \quad (2)$$

where the superscript $(-\kappa)$ denotes the agent class - LP or LT - which is not κ .

Considering the expected agent rewards in (2), we will aim to find Nash equilibria of the game. Our game is not analytically tractable, so we will focus on reaching empirical convergence of agents rewards, using RL. This is done in sections 3.2, 5.2 and 5.3. In the case where LT's do not learn, i.e.

⁵in the contexts of Markov semigroups, a time-dependent semigroup on a given space can be recast as a time-homogenous semigroup in the space-time domain.

⁶it also depends on other agents' supertypes Λ_{-i}^κ independent of their ordering, but since we work with a fixed supertype profile Λ^κ for now, Λ_{-i}^κ is fixed when Λ_i^κ is.

their policy π^{LT} is fixed⁷, we investigate in section 3.1 the nature of equilibria that can be reached by the LPs using a shared policy.

Since agents may have different observations at a given point in time, sharing a network still allows different actions across agents. Our *rationality assumption* underlying parameter sharing is the following: if two agents have equal types and equal sequences of historical observations at a given point in time, then they should behave the same way, i.e. the distributions of their actions should be equal. Agents do not directly observe types nor supertypes of other agents, rather they observe these quantities indirectly via the outcome of their own actions $a_t^{(i,\kappa)}$, which is encoded in their observations $s_t^{(i,\kappa)}$, including historical information h as previously discussed. For example, a LP agent quoting a given price will not receive the same trading activity from LTs depending on the risk aversion of other LPs. Although our focal LP cannot observe the risk aversion of his competitors, he observes the resulting trading activity and can tailor his behavior to the latter.

2.2.2 Reinforcement learning design of OTC agents

In the remainder of the paper, we assume for simplicity that there is one ECN, $n_{ECN} = 1$, and we denote P_t its mid price at the beginning of timestep t . Our framework supports $n_{ECN} > 1$, in which case a reference price P_t would typically be computed as a liquidity-weighted average mid-price over the n_{ECN} mid-prices. The ECN, and in particular the construction of P_t , is discussed in section 2.3.

Following our discussion in section 1, we represent the utilities of both LP and LT agents as a trade-off between a risk-penalized PnL term, and a purely quantity-related, PnL-independent term. In the case of the LP agent, the latter is market share. In the case of the LT agent, it is a pair of trade objectives on the bid and ask sides. This makes our agent formulation compact and unified as a hybrid wealth-volume objective. We summarize the RL formulation of our LP and LT agents in table 1 and proceed to the description of the details in the remainder of the section.

Agent risk-penalized PnL. Let PnL_{t+1} be the cumulative PnL of a given agent at the end of time t (i.e. beginning of time $t+1$), and $\Delta PnL_{t+1} := PnL_{t+1} - PnL_t$ the incremental PnL. We then have the usual decomposition of PnL into inventory and spread terms, which follows by simple "accounting":

$$\begin{aligned} PnL_t &= PnL_{\text{inv},t} + PnL_{\text{spread},t} + \ell(q_t), \quad PnL_{\text{inv},t} := \sum_{i=1}^t q_i (P_i - P_{i-1}) \\ PnL_{\text{spread},t} &:= \sum_{i=1}^t \sum_{b \in \mathcal{B}_i} q_i^b (P_{i-1} - P_{i-1}^b) + \sum_{a \in \mathcal{A}_i} q_i^a (P_{i-1}^a - P_{i-1}) \end{aligned} \quad (3)$$

We denote $\ell(q_t)$ the usual terminal inventory penalty capturing the fact that liquidating q_t cannot usually be done exactly at price P_t Guéant (2017), where q_t is the agent's net inventory at the beginning of time step t . In this work we take $\ell \equiv 0$ since we are not specifically interested in studying the impact of this penalty, but our framework allows for arbitrary ℓ .

$PnL_{\text{inv},t}$ is the inventory PnL and captures the fluctuations of the reference mid-price P_t over time.

$PnL_{\text{spread},t+1}$ is the cumulative spread PnL obtained at the end of time step t as a consequence of the trades performed during time step t and before. It captures the local profit of individual trades relative to the mid-price P_t . Let \mathcal{A}_{t+1} be the set of trades performed by the agent on its ask side during time step t at prices $\{P_t^a\}_{a \in \mathcal{A}_{t+1}}$ and absolute quantities $\{q_{t+1}^a\}_{a \in \mathcal{A}_{t+1}}$ (i.e. sold by the agent). Similarly, for trades on the agent's bid side, we use the notations \mathcal{B}_t , q_t^b , P_t^b . Note that with these notations, $\Delta q_t = \sum_{b \in \mathcal{B}_t} q_t^b - \sum_{a \in \mathcal{A}_t} q_t^a$.

Trades occurring on the OTC market between LPs and LTs can be assimilated to market orders. Indeed, LPs stream prices at which they are willing to trade with LTs, which in turn decide if and how much they want to trade. In particular, LTs cannot send limit orders to LPs. Precisely, these prices take the form of a pair of price curves, bid and ask, representing price as a function of quantity traded. Equivalently, one can see this pair of curves as an order book. As specified below and to keep consistency with the LP-LT interaction, we consider that the orders performed by LP and LT

⁷for example, they buy or sell with equal probability.

agents at the ECN are market orders, but we discuss how to extend their action spaces to include the possibility of limit orders.

Liquidity Provider Agent. Let m_{t+1} be the LP's market share during time step t , namely the fraction of the total quantity traded by all LTs that the LP was able to attract (buy and sell included), and $\hat{m}_{t+1} = \frac{1}{t+1} \sum_{k=1}^{t+1} m_k$ its running average. Note that a given LP competes with all other LPs but also with ECNs. For example, if all LPs decide to stream noncompetitive prices to LTs, and that each LT is connected to at least one ECN, then the market share of each LP will be zero, and the sum of all ECNs market share will be one. We define the term \mathcal{M}_{t+1} as the distance to a target m_{target} :

$$\mathcal{M}_{t+1}(m_{\text{target}}) := |\hat{m}_{t+1} - m_{\text{target}}|$$

In this work we take $m_{\text{target}} = 1$, so that \mathcal{M}_{t+1} will simply relate to maximizing market share (since it cannot be more than one). The parameters η, ω are trade-off parameters between PnL and market share: the former is a normalizer to make both quantities comparable, while the latter is a weight that gives more or less importance to the PnL.

In real markets, LPs aim at maximizing both PnL and market share, as opposed to PnL only. We reflect this in our reward formulation \mathcal{R}_{t+1}^{LP} , which is the reward obtained by the LP agent at the end of time t , due to actions performed during time t :

$$\begin{aligned} \mathcal{R}_{t+1}^{LP} &:= \omega \cdot \eta \cdot \Delta PnL_{t+1}^{\gamma} - (1 - \omega) \cdot \Delta \mathcal{M}_{t+1}(m_{\text{target}}), \quad \eta > 0, \quad \omega \in [0, 1] \\ PnL_t^{\gamma} &:= PnL_t - \gamma \sum_{k=1}^t |\Delta PnL_{\text{inv},k}| \end{aligned} \tag{4}$$

The parameter γ is the risk aversion which typically relates to a quadratic penalty on inventory Guéant (2017), so as to preserve analytical tractability, which we are not concerned with due to our RL approach. We chose a L_1 penalty on the inventory PnL variation since it makes the penalty homogeneous to PnL, and we chose to penalize inventory PnL rather than inventory since morally, the penalty should be zero when the volatility of P_t is zero. If P_t were a Brownian motion with volatility σ , the expected value of our inventory PnL penalty would be $\mathbb{E} |\Delta PnL_{\text{inv},t}| = \sqrt{\frac{2}{\pi}} \sigma q_t$. Our penalty formulation allows to adapt to changes in the volatility rather than assuming it is constant.

Let $x_t^b(q), x_t^a(q)$ be the quantity-normalized ECN spreads of trading q on the bid and ask, corresponding to prices $P_t - x_t^b(q)$ and $P_t + x_t^a(q)$. Let $x_t(q) := \frac{1}{2}(x_t^a(q) + x_t^b(q))$ be the symmetrized spread, and $x_t := 2 \lim_{q \rightarrow 0} x_t(q)$ the market spread, i.e. difference between best ask and best bid. The LP constructs its prices on both sides by tweaking the ECN reference price:

$$\begin{aligned} P_t^a(q, \epsilon_{t,\text{spread}}, \epsilon_{t,\text{skew}}) &= P_t + x_t(q) + \frac{1}{2} \epsilon_{t,\text{spread}} x_t + \epsilon_{t,\text{skew}} x_t \\ P_t^b(q, \epsilon_{t,\text{spread}}, \epsilon_{t,\text{skew}}) &= P_t - x_t(q) - \frac{1}{2} \epsilon_{t,\text{spread}} x_t + \epsilon_{t,\text{skew}} x_t \end{aligned} \tag{5}$$

The term $x_t(q)$ is the reference ECN price of trading q . The spread tweak $\epsilon_{t,\text{spread}} \geq -1$ controls the price difference $P_t^a - P_t^b$ and impacts both sides symmetrically. The skew tweak $\epsilon_{t,\text{skew}} \in \mathbb{R}$ shifts prices asymmetrically towards one side or another. Typically, the LP chooses the latter so as to attract flow to reduce its inventory: this is referred to as *skewing* or *internalization*, and we will see in section 5.3 that our agents are able to learn such behavior in an emergent manner. Note that the lower bound for $\epsilon_{t,\text{spread}}$ comes from the condition $\lim_{q \rightarrow 0} P_t^a(q, \epsilon_{t,\text{spread}}, \epsilon_{t,\text{skew}}) - P_t^b(q, \epsilon_{t,\text{spread}}, \epsilon_{t,\text{skew}}) \geq 0$. We could also equivalently have defined, in the spirit of Barzykin et al. (2021a), $\epsilon_{t,\text{ask}} := \frac{1}{2} \epsilon_{t,\text{spread}} + \epsilon_{t,\text{skew}}$, $\epsilon_{t,\text{bid}} := \frac{1}{2} \epsilon_{t,\text{spread}} - \epsilon_{t,\text{skew}}$. It is a simple bijection between the two formulations, but the spread-skew formulation is more intuitive since it allows to decouple the willingness of the LP to stream competitive prices (spread) to his asymmetric treatment of the two sides (skew). We allow the LP to quote prices at a granularity equal to $\xi_{LP} = 0.1$ bp, which is the typical granularity that we can observe in FX liquidity aggregators. Concretely, P_t^a and P_t^b are projected on such grid.

In the RL terminology, LP's actions at time t are the pricing parameters $\epsilon_{t,\text{spread}} \geq -1, \epsilon_{t,\text{skew}} \in \mathbb{R}$ and a hedge fraction $\epsilon_{t,\text{hedge}} \in [0, 1]$, which results in a market order $\epsilon_{t,\text{hedge}} q_t$ at the ECN.

Due to the partial observability of the game, optimal agents' action should depend on the whole history of the per-timestep observations Lockhart et al. (2019). The LP's observations $s_t^{(i,LP)}$ contain

the reference mid-price P_t , its own net inventory q_t , the fraction of time elapsed $\frac{t}{T}$, its market share m_t , liquidity available on the top m levels of the ECN order book, and the cost of hedging a fraction $\epsilon_{t,\text{hedge}} q_t$ of the current inventory, for a vector of values of $\epsilon_{t,\text{hedge}} \in [0, 1]$. Note that time is included in the observations since we are working on a finite time-horizon, hence optimal actions should be time-dependent.

The parameters characterizing the agent type are: $\eta, \omega, \gamma, m_{\text{target}}$ in (4), as well as the empirical fraction of LTs of each supertype that the agent is connected to. The latter is a vector of size the number of LT supertypes, containing, for each episode, the empirical fraction of LT agents that are connected to the LP.

In this work, we assume that orders $\epsilon_{t,\text{hedge}} q_t$ sent by the LP to the ECN are market orders. It is possible to extend this framework to include the possibility of limit orders, by extending the action space \mathcal{A}^{LP} to include the distance (in ticks) from the top of book to place the order at. The same observation holds for LTs.

Liquidity Taker Agent. At each time t , the LT agent decides a trade size and direction based on the observed prices. When that decision is made, the trade will always occur, independently of the LT's policy, at the best possible price among connected LPs and ECN. In this work, we consider a simplification where each LT trades a unit quantity q_{LT} (possibly different across LT agents) and only decides to buy or sell q_{LT} , or not to trade. In this sense its action space can be assimilated to $\{1, -1, 0\}$. Note that in order to have a population of LTs trading different sizes, we can define different supertypes with specific distributions for q_{LT} . We define \mathcal{R}_{t+1}^{LT} the reward obtained by the LT agent at the end of time t , due to actions performed during time t :

$$\begin{aligned} \mathcal{R}_{t+1}^{LT} &:= \omega \cdot \eta \cdot \Delta PnL_{t+1}^{\gamma} - (1 - \omega) \cdot \Delta \mathcal{Q}_{t+1}(q^a, q^b), \quad \eta > 0, \quad \omega \in [0, 1] \\ \mathcal{Q}_{t+1}(q^a, q^b) &:= \frac{1}{2} \sum_{j \in \{a, b\}} \left| \hat{q}_t^j - q^j \right|, \quad q^a, q^b \in [0, 1], \quad q^a + q^b \leq 1 \\ \hat{q}_t^j &:= \frac{1}{t+1} \sum_{k=0}^t 1_{\{a_k=j\}} \end{aligned} \tag{6}$$

Similar to the LP, \mathcal{R}_{t+1}^{LT} is a trade-off between PnL and a quantity-related term. Similar to the running average of the market share \hat{m}_t , \hat{q}_t^b and \hat{q}_t^a represent the fraction of time the LT has bought and sold, which targets are q^a, q^b . The LT can decide not to trade, so we have $\hat{q}_t^b + \hat{q}_t^a \leq 1$. Since when the LT trades, it trades the fixed quantity q_{LT} , the total quantities traded on both sides over an episode of length T are $\hat{q}_T^a q_{LT} T, \hat{q}_T^b q_{LT} T$, hence \hat{q}_t^b, \hat{q}_t^a can alternatively be seen as trade objectives. When the weight ω is strictly between zero and one, we can interpret the utility (6) as a form of optimal execution, since we wish to reach trade objectives q^a, q^b while minimizing cost, i.e. maximizing PnL.

We illustrate this reward formulation in figure 2. We fix the shape of the ECN mid-price curve P_t in blue, train a single shared policy network π^{LT} by randomizing the PnL weight ω at the beginning of the episode, conditioning $\pi^{LT} \equiv \pi^{LT}(\cdot | \cdot, \omega)$ on ω , and look at how the LT's trading behavior varies as a function of ω . We see that as ω increases, the agent switches from achieving its $q^b = 75\%$, $q^a = 25\%$ bid-ask targets to maximizing PnL (buy low, sell high). When $\omega = 0$, the agent exactly achieves its targets but does not necessarily trade at the most cost-efficient points in time. As ω increases, the agent tries to match its targets while trading in the best regions from a PnL point of view. As ω approaches one, the targets will stop playing any role in the agent's behavior.

In order to further show the relevance of our LT formulation, we show in figure 3 the impact on the LP's flow response curve $\epsilon \rightarrow \mathcal{F}(\epsilon)$ of increasing the number of PnL driven LTs characterized by $\omega = 1$, cf. definition in section 5.3. We see that such LTs introduce convexity in this curve, due to their eagerness to trade when the prices offered by the LP become particularly attractive. Such convexity is observed in HSBC EURUSD data in figure 8, which shows the ability of our LT formulation to generate interesting features of the market.

The LT's observations $s_t^{(i, LT)}$ contain the reference mid-price P_t , the LP's net inventory q_t , the fraction of time elapsed $\frac{t}{T}$, its running trade fractions \hat{q}_t^a, \hat{q}_t^b , and the cost of buying and selling q_{LT} from the set of LPs and ECNs it is connected to.

The parameters characterizing the agent type are: $\eta, \omega, \gamma, q^a, q^b, q_{LT}$ in (6) and the fraction of LPs of each supertype that the agent is connected to.

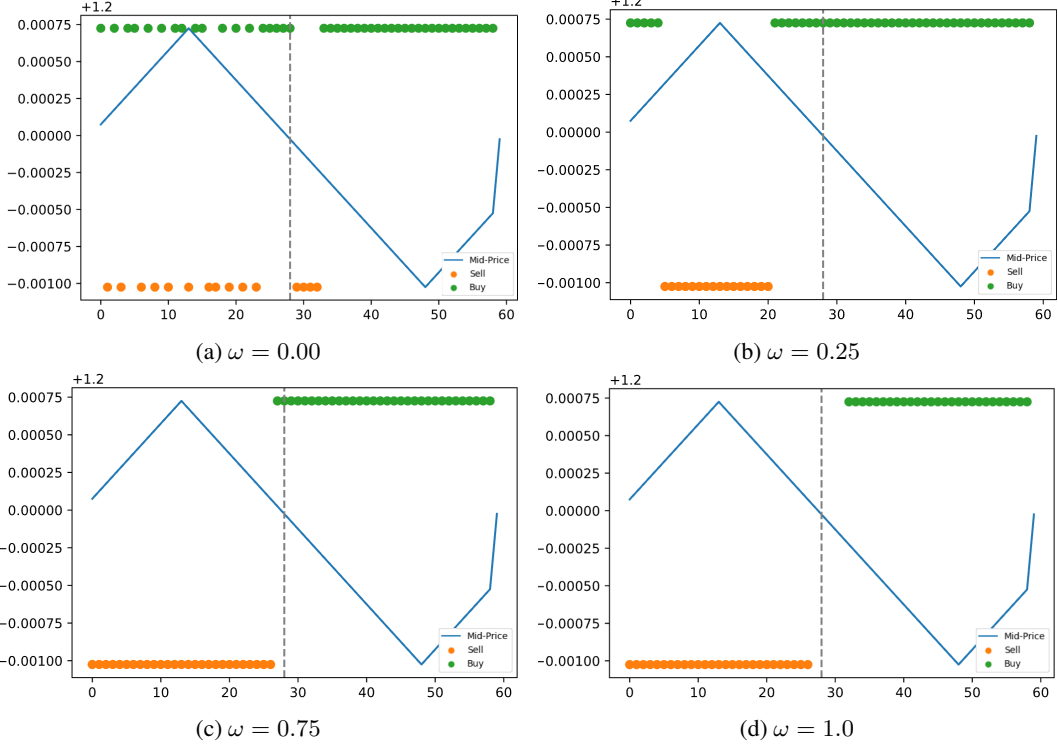


Figure 2: Spectrum of learnt optimal actions by the shared LT agent policy π^{LT} , as a function of PnL weight ω . Mid-price as a function of time (blue), LT buy actions (green), sell actions (orange). Quantity targets $q^a = 25\%$, $q^b = 75\%$. The agent gradually shifts from exactly achieving its quantity targets to maximizing PnL (buy low, sell high).

Table 1: Summary of the RL formulation of market agents.

Agent class	Liquidity Provider	Liquidity Taker
Observations s_t	reference price \bar{P}_t , net inventory q_t time $\frac{t}{T}$, market share m_t ECN liquidity for top m levels, cost of hedging ϵ_{qt} for various ϵ .	reference price P_t , net inventory q_t time $\frac{t}{T}$, running quantity traded \hat{q}_t^a, \hat{q}_t^b cost of trading q_{LT} from the best LP or ECN.
Type λ	$\gamma, \eta, \omega, m_{\text{target}}$, fraction of LTs of each supertype it is connected to	$\gamma, \eta, \omega, q^a, q^b, q_{LT}$, fraction of LPs of each supertype it is connected to
Actions a_t	Pricing parameters $\epsilon_{\text{spread}} \geq -1$, $\epsilon_{\text{skew}} \in \mathbb{R}$, and hedge fraction $\epsilon_{\text{hedge}} \in [0, 1]$	$\{1, -1, 0\}$: buy or sell a unit quantity q_{LT} , or remain inactive.
Rewards \mathcal{R}_{t+1}	$\omega \cdot \eta \cdot \Delta PnL_{t+1} \gamma_{t+1} - (1 - \omega) \cdot \Delta M_{t+1}(m_{\text{target}})$	$\omega \cdot \eta \cdot \Delta PnL_{t+1} \gamma_{t+1} - (1 - \omega) \cdot \Delta Q_{t+1}(q^a, q^b)$

2.3 ECN model

2.3.1 Vanilla model

The ECN is not the main focus of our study, rather it is the OTC interactions between LPs and LTs. We however need an ECN engine so as to provide a reference price to market participants, and allow LPs to hedge a fraction of their inventory or LTs to trade if need be. This ECN plays the same role as the open market of Bank et al. (2021), or the inter-dealer segment of Barzykin et al. (2021b). We code an ECN engine that supports market, limit and cancel orders on the bid and ask sides, in particular it keeps track of individual orders and their originators, with a classical first-in-first-out mechanism.

Our two desiderata for the ECN is that i) LP and LT agents can impact the ECN limit order book when sending orders to it, and ii) in the absence of LP and LT agents orders, the ECN evolves realistically over the input RL simulation timestep dt , in particular its volume remains stable over time and does

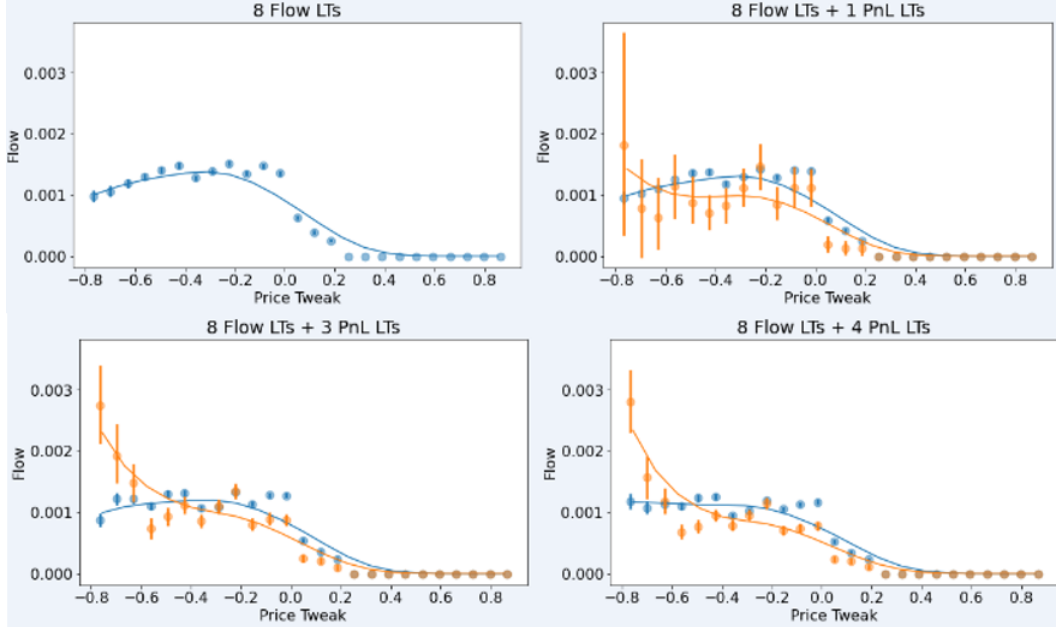


Figure 3: Flow response curve $\epsilon \rightarrow \mathcal{F}(\epsilon)$. Impact on LP's flow of increasing the number of LTs with PnL weight $\omega = 1$. Flow coming from flow LT's $\omega = 0$ (blue) and PnL LT's $\omega = 1$ (orange). The flow for each agent class is normalized by the number of agents in that class, so that all curves are comparable and can be interpreted as the average flow received from a typical agent of that class.

not explode nor vanish. The former is a structural requirement that follows from the ability of agents to send orders as explained in section 2.2.2. We solve the latter by equipping the ECN with a so-called ECN agent in charge of sending orders to it at every timestep. In this section we proceed to specifying the nature of this ECN agent, i.e. how it constructs a list of orders at each timestep of the simulation. We emphasize that although the ECN agent will use the model in (7)-(8) to build a list of orders, the ECN dynamics are not given by these equations, rather the limit order book evolves solely as a consequence of orders sent by LPs, LTs, and the ECN agent. This can be seen as a hybrid impact model between RL-agents and the "rest of the world", where the LT trade sizes q_{LT} drive the extent to which RL-based agents impact the ECN.

We equip the ECN with a fixed price grid with a fixed granularity ξ , also called tick size. In the case of eurodollar on EBS, $\xi = 0.5$ bp. This price grid is upper and lower bounded by P_{max} , P_{min} and we let $K_{max} := \lfloor \xi^{-1}(P_{max} - P_{min}) \rfloor$ be the total number of ticks. We call *limit order book snapshot* the associated pair of vectors of size K_{max} representing the volumes available for each price, on each side. We denote P_t , P_t^a , P_t^b the ECN mid-price, best ask and best bid prices, i.e. $2P_t = P_t^a + P_t^b$.

The training data \mathcal{D} that we use to calibrate the ECN agent is level two limit order book data, namely a dataset containing the limit order book snapshot at different times. Such data doesn't contain volumes for all prices from P_{min} to P_{max} , typically it contains volume and price data for the top m non-empty levels on each side, typically $m = 5$. Our ECN agent model will therefore consider the associated volumes $(V_{i,t})_{i \in [1,2m]}$. In order to always have a snapshot for prices from P_{min} to P_{max} , we extrapolate volumes for levels k further than m with exponential decay $e^{-\alpha k}$, where $\alpha > 0$ is fitted to the top m levels using our dataset \mathcal{D} . To further reduce the dimensionality of the model, we assume that the price difference between two consecutive non-empty levels is always one tick, except for the difference between the best ask and best bid - also called market spread - which can be greater, typically 1 to 3 ticks. This is typical of liquid markets. With these assumptions, in order to construct the order book at time $t + 1$ from the order book at time t , it is enough to know the mid price change $\xi^{-1}(P_{t+1} - P_t)$, the new market spread $\xi^{-1}(P_{t+1}^a - P_{t+1}^b)$, and the change in volume $(V_{i,t+1} - V_{i,t})_{i \in [1,2m]}$ for the top m levels on both sides. The vanilla version of the model that we consider in this section will, in short, assume that the vectors of these $2m + 2$ quantities at two distinct times are independent and identically distributed, although we account for correlation among the $2m + 2$ random variables at a fixed time. We revisit this independence assumption in the

neural extension of the vanilla model in section 2.3.2, where we will allow the order book variation to depend on its history.

The mechanism of the ECN agent can be broken down into the following steps. First, at the beginning of the simulation, it creates an initial limit order book snapshot. Then, at each timestep, i) it generates a limit order book snapshot variation, precisely two vectors of size K_{max} , one for each side, containing volume variations associated to the price grid; ii) it creates a sequence of orders associated to the latter snapshot variation, in the sense that sending those orders to the ECN would reproduce exactly that variation, in the absence of other orders.

Initial limit order book snapshot. We fix the initial mid-price P_0 and model the initial limit order book snapshot as a vector \mathcal{S}_0 of size $2m + 1$ consisting of log-quantities $(\ln V_{i,0})_{i \in [1,2m]}$ plus the market spread, in ticks:

$$\mathcal{S}_0 := ((\ln V_{i,0})_{i \in [1,2m]}, \xi^{-1}(P_0^a - P_0^b))$$

From our training dataset \mathcal{D} , we construct samples of \mathcal{S}_0 that we fit to a multivariate Gaussian mixture distribution with typically 5 components, so as to capture higher moments and cross-moments between log-volumes and market spread. We then sample from this fitted distribution to generate the initial snapshot.

Breaking down the limit order book snapshot variation into smaller orders of typical size. For now, assume that we have a way to draw samples of order book snapshot variation over a timestep. Remember that such variation consist of precisely two vectors of size K_{max} , one for each side, containing volume variations associated to the price grid. Given such variation, we constitute a list of market, limit, cancel orders such that sending those orders to the ECN reproduces exactly that variation, in the absence of other orders. In this sense it is a purely mechanical process. We describe below such transformation for the ask side (the bid side being similar).

We first build a list of meta-orders which we then break up into smaller pieces of typical size. Let $(\Delta V_i)_{i=1..K_{max}}$ be the vector of signed volume variation on the ask size, where entries of the latter vector correspond to increasing prices. If the first non-zero entry of ΔV is negative, we create a meta market order, and continue incrementing the size of the order until we reach a nonnegative variation. The subsequent meta orders will be set as limit or cancellation depending if the variation is positive or negative. Otherwise, if the first non-zero entry is positive, we simply skip the market order step. Precisely, let $i_0 := \inf\{i : \Delta V_i \neq 0\}$. If $\Delta V_{i_0} > 0$, then we create a list of size $K_{max} - i_0$ where the k^{th} element is a meta limit or cancellation order of size $|\Delta V_k|$, depending on the sign of ΔV_k . On the other hand if $\Delta V_{i_0} < 0$, let $i_1 := \inf\{i > i_0 : \Delta V_i \geq 0\}$, then we create a meta market order of size $\sum_{k=i_0}^{i_1-1} |\Delta V_k|$, and create meta limit and cancellation orders using $(\Delta V_k)_{i \geq i_1}$ as specified previously. Then, from our training data \mathcal{D} , we compute the order book volume differences for the smallest time interval available, which gives us an empirical distribution of typical individual orders, and then break down each large meta order into a sequence of small orders of random size sampled from this empirical distribution.

Limit order book snapshot variation. We now proceed to specifying our model for generating order book snapshot variation over a timestep from time n to time $n + 1$, from which the ECN agent constructs its orders. Similarly to the initial snapshot, we consider the vector \mathcal{S}_{n+1} of dimension $2m + 2$, where the last 2 entries are the market spread at time $n + 1$ (in ticks) and the mid price change (in ticks) between times n and $n + 1$. The first $2m$ entries consist of relative volume variations $\delta_{i,n}$ at book level i related to the dynamics (8). The knowledge of \mathcal{S}_{n+1} is enough to construct the limit order book at time $n + 1$ from the order book at time n .

$$\mathcal{S}_{n+1} := ((\delta_{i,n})_{i \in [1,2m]}, \xi^{-1}(P_{n+1}^a - P_{n+1}^b), \xi^{-1}(P_{n+1} - P_n)), \quad n \geq 0. \quad (7)$$

From our training dataset \mathcal{D} , we construct samples of \mathcal{S}_{n+1} that we fit to a multivariate Gaussian mixture distribution with typically 5 components, so as to capture the correlation structure and higher order moments/cross-moments between volume variations, market spread and mid price change. We then sample from this fitted distribution independently at each timestep to generate the snapshot variation.

We consider the following discrete-time dynamics for the volume $V_{i,n}$ at time n and level i :

$$\begin{aligned} \Delta V_{i,n} &:= V_{i,n+1} - V_{i,n} = -\delta_{i,n}^- V_{i,n} + \delta_{i,n}^+ \\ \delta_{i,n}^+ &:= \max(\delta_{i,n}, 0) \geq 0, \quad \delta_{i,n}^- := \max(-\delta_{i,n}, 0) \in [0, 1] \end{aligned} \quad (8)$$

We treat positive and negative volume variations differently since when a volume variation is negative, it cannot be more than the current volume at that level, so it is coherent to express the variation as a multiple of the latter quantity. On the other hand, when it is positive, it is better to express it in absolute terms. If it were expressed multiplicatively, a close to empty book would remain empty, and a book with more liquidity would increase its liquidity exponentially: this hybrid formulation allows us to obtain a provably stable ECN evolution over arbitrary time horizons, i.e. $\lim_{n \rightarrow \infty} \mathbb{E}[V_{i,n}] < +\infty$, as will be seen in theorem 2.2 and proposition 2.3. This would not be true without this hybrid "multiplicative-absolute" $\delta^+ - \delta^-$ formulation, for example in the purely multiplicative or absolute cases $\Delta V = (\delta^+ - \delta^-)V$, $\Delta V = \delta^+ - \delta^-$ (unless in the very specific case $\mathbb{E}[\delta_{i,n}^+] = \mathbb{E}[\delta_{i,n}^-]$, which is usually not true when calibrating to empirical data). We illustrate these dynamics in figure 4.

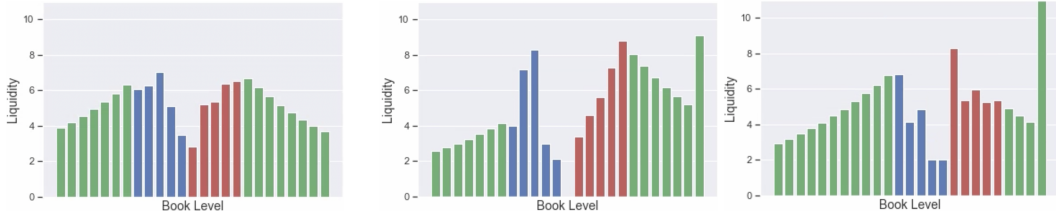


Figure 4: Example of ECN order book evolution associated to the dynamics (7)-(8) over time an episode, in the absence of LP and LT orders (from left to right). Top 5 levels on the ask (red), bid (blue), levels in green are extrapolated. The middle plot displays a market spread of 2 ticks, contrary to 1 tick in the other cases. In accordance to the theory, running these dynamics over arbitrary time horizons keeps the order book stable, in the sense that volumes do not vanish nor explode.

Our hybrid formulation is similar in spirit to that of Cont and Müller (2021), which models the order book volume by means of a SDE. Their drift contains a term $-\alpha_x V_{x,t} + \beta_x$ with $\alpha, \beta \geq 0$ deterministic and x the (continuous) book level. Their dynamics assume multiplicative volatility for the volume $\sigma^- V_{x,t}$, which they justify by "*the multiplicative nature of the noise accounts for the high-frequency cancellations associated with HFT orders*". Interestingly, we will see that the continuous-time diffusion approximation limit of our discrete-time dynamics (8) generalizes their work in that when the volatility σ^+ of positive volume variations δ^+ is zero, we recover multiplicative book volume volatility $\sigma^- V_{i,t}$ generated by negative volume variations (remark 2.5). When σ^+ is not zero, the book volume variance will be shown to be a quadratic polynomial in $V_{i,t} - \mu_i^\infty$, where $\mu_i^\infty := \lim_{t \rightarrow \infty} \mathbb{E}[V_{i,t}]$ is the long-range mean. The deviation of the book volume from its long-range mean can be seen as a proxy for market activity, hence we can define regions for the book volume where its variance is higher or lower than the (constant) long-range variance. This self-exciting behavior is studied in proposition 2.6. Cont and Müller (2021) further considers convection and diffusion terms in their SDE drift, which relate to correlation across their infinite set of book levels. In our case we instead model a finite number of book levels i which are correlated through the joint distributions of $(\delta_i^+, \delta_i^-)_{i \in [1, 2m]}$. This can be seen as a "practical equivalent" of the convection and diffusion terms.

In theorem 2.2 and corollary 2.4, we look at the continuous-time limit of our discrete-time dynamics (8). As mentioned previously, the covariance structure Q generalizes that of Cont and Müller (2021), which corresponds to the specific case $\sigma^+ = 0$. In the general case, we see that Q is modulated by the position of the volume $V_{i,t}$ relative to its long-range mean μ_i^∞ . This aspect is further analyzed in proposition 2.6. Interestingly, looking at the continuous-time limit allows us to quantify the impact of the model parameters $\sigma_\pm, \mu_\pm, \rho$ on the nature of the fluctuations of the order book volume, which is compactly captured by the polynomial Q .

Theorem 2.2. *Let $((\delta_{i,n}^+, \delta_{i,n}^-)_{i \in [1, 2m]})_{n \geq 0}$ be a sequence of independent and identically distributed vectors of random variables taking value in $(\mathbb{R} \times [0, 1])^{2m}$ where $\delta_{i,n}^\pm$ has mean μ_i^\pm , standard deviation σ_i^\pm , and such that $\mu_i^- > 0$. Let $\text{corr}(\delta_{i,n}^-, \delta_{j,n}^+) =: \rho_{ij}$, $\text{corr}(\delta_{i,n}^+, \delta_{j,n}^+) =: \rho_{ij}^+$, $\text{corr}(\delta_{i,n}^-, \delta_{j,n}^-) =: \rho_{ij}^-$. Assume that V_i satisfies the discrete-time recursion:*

$$V_{i,n+1} = (1 - \delta_{i,n}^-)V_{i,n} + \delta_{i,n}^+ \quad a.s., \quad V_{i,0} \in \mathbb{R}_+, \quad n \geq 0.$$

Denote $V_{i,n+1}^\epsilon$ the process associated to the scaling $\delta_{i,n,\epsilon}^\pm := \epsilon \mu_i^\pm + \sqrt{\epsilon}(\delta_{i,n}^\pm - \mu_i^\pm)$, and $V_{i,t}^\epsilon := V_{i,\lfloor \epsilon^{-1}t \rfloor}^\epsilon$. Under the assumption that $\delta_{i,n}^+$ are bounded in $L^{2+\eta}$ for some $\eta > 0$, V^ϵ converges

weakly in the Skorokhod topology to a multivariate Ornstein–Uhlenbeck process V^* with quadratic covariance structure:

$$dV_{i,t}^* = \mu_i^- (\mu_i^\infty - V_{i,t}^*) dt + [q(V_t^* - \mu^\infty) dB_t]_i$$

where B is a standard vector Brownian motion and q is a square-root of the matrix Q , $q(V_t^* - \mu^\infty)q(V_t^* - \mu^\infty)^T = Q(V_t^* - \mu^\infty)$, with $[Q(V_t^* - \mu^\infty)]_{ij} =: \tilde{Q}_{ij}(V_{i,t}^* - \mu_i^\infty, V_{j,t}^* - \mu_j^\infty)$, and \tilde{Q}_{ij} the quadratic polynomial:

$$\tilde{Q}_{ij}(x, y) := \sigma_{ij}^\infty + \rho_{ij}^- \sigma_i^- \sigma_j^- xy + \sigma_i^- (\mu_j^\infty \rho_{ij}^- \sigma_j^- - \rho_{ij} \sigma_j^+) x + \sigma_j^- (\mu_i^\infty \rho_{ij}^- \sigma_i^- - \rho_{ji} \sigma_i^+) y$$

where:

$$\sigma_{ij}^\infty := \rho_{ij}^+ \sigma_i^+ \sigma_j^+ + \mu_i^\infty \mu_j^\infty \rho_{ij}^- \sigma_i^- \sigma_j^- - \mu_i^\infty \rho_{ij} \sigma_j^+ \sigma_i^- - \mu_j^\infty \rho_{ji} \sigma_i^+ \sigma_j^-, \quad \mu_i^\infty := \frac{\mu_i^+}{\mu_i^-}$$

The long-range moments in proposition 2.3 follow easily by direct computation⁸.

Proposition 2.3. *We have for every $i, j \in [1, 2m]$:*

$$\begin{aligned} \lim_{n \rightarrow \infty} \mathbb{E}[V_{i,n}] &= \lim_{t \rightarrow \infty} \mathbb{E}[V_{i,t}^*] = \mu_i^\infty \\ \lim_{n \rightarrow \infty} \text{cov}[V_{i,n}, V_{j,n}] &= \frac{\sigma_{ij}^\infty}{\mu_i^- + \mu_j^- - \mu_i^- \mu_j^- - \rho_{ij}^- \sigma_i^- \sigma_j^-} \\ \lim_{t \rightarrow \infty} \text{cov}[V_{i,t}^* V_{j,t}^*] &= \frac{\sigma_{ij}^\infty}{\mu_i^- + \mu_j^- - \rho_{ij}^- \sigma_i^- \sigma_j^-} \end{aligned}$$

In particular when looking at a single level i in theorem 2.2, we get immediately the corresponding univariate version presented in corollary 2.4.

Corollary 2.4. *Under the same notations as theorem 2.2, the rescaled volume V^ϵ at a single book level converges weakly in the Skorokhod topology to a Ornstein–Uhlenbeck process V^* with quadratic variance:*

$$dV_t^* = \mu^- (\mu^\infty - V_t^*) dt + \sqrt{Q(V_t^* - \mu^\infty)} dB_t$$

where B is a standard Brownian motion and Q the quadratic polynomial:

$$Q(x) := \sigma^{\infty 2} + \sigma^-^2 x^2 + 2\sigma^- (\mu^\infty \sigma^- - \rho \sigma^+) x$$

where:

$$\sigma^{\infty 2} := \sigma^{+2} + \mu^\infty \sigma^- (\mu^\infty \sigma^- - 2\rho \sigma^+), \quad \mu^\infty := \frac{\mu^+}{\mu^-}$$

Remark 2.5. *If $\sigma^+ = 0$ in corollary 2.4, $\sqrt{Q(V_t^* - \mu^\infty)} = \sigma^- V_t^*$ as in Cont and Müller (2021) (section 1, equation 1.2).*

The equivalent vanilla Ornstein–Uhlenbeck process would have constant volatility σ^∞ . In our case, the quadratic variation Q is a second order polynomial in $V_t^* - \mu^\infty$. The latter quantity can be seen as a proxy for market activity, since when the market is calm, the volume is close to its long-range mean, whereas when it is volatile, it is perturbed away from it. Depending on the parameters $\sigma_\pm, \mu_\pm, \rho$ of corollary 2.4, we can define in proposition 2.6 regimes where the variance is higher, or lower than the equivalent "flat" Ornstein–Uhlenbeck variance $\sigma^{\infty 2}$, which is also the long-range variance of V^* by proposition 2.3.

Proposition 2.6. *Under the notations of corollary 2.4, let $\mathcal{V}(x) := Q(x) - Q(0)$ be the variance impact due to the polynomial nature of Q . We define the self-exciting and self-inhibiting regimes of V^* as the regions $\mathcal{V} > 0, \mathcal{V} < 0$. If $\sigma^- = 0$, V^* is not self-exciting nor self-inhibiting since $\mathcal{V} \equiv 0$.*

⁸Note that the term $\mu_i^- \mu_j^-$ disappears from the covariance denominator when passing to the continuous-time limit, since n is of order ϵ^{-1} , μ_i^\pm or order ϵ and σ_i^\pm of order $\sqrt{\epsilon}$, hence $\sigma_i^- \sigma_j^-, \mu_i^-, \mu_j^-$ are all of order ϵ , but $\mu_i^- \mu_j^-$ is of order ϵ^2 and hence vanishes.

If $\sigma^- > 0$, the self-exciting regimes of V^* are $(-\infty, \gamma_*), (\gamma^*, +\infty)$, and its self-inhibiting regime is (γ_*, γ^*) , with:

$$\gamma^* = \max \left[\mu^\infty, 2 \frac{\sigma^+}{\sigma^-} \rho - \mu^\infty \right], \quad \gamma_* = \min \left[\mu^\infty, 2 \frac{\sigma_+}{\sigma_-} \rho - \mu^\infty \right]$$

In particular, V^* is never self-inhibiting if and only if $\sigma^+ \mu^- \rho = \sigma^- \mu^+$. The parameters μ^\pm, σ^\pm and ρ impact the regime change only through the ratios $\frac{\sigma^+}{\sigma^-} \rho$ and $\frac{\mu^+}{\mu^-}$. Further, we have $\partial_\rho V(x) > 0$ if and only if $x < 0$.

2.3.2 Neural extension of the vanilla model

In this section we show how the vanilla model in section 2.3.1 can be extended easily. The main drawback of this model is that the $p = 2m + 2 = 12$ dimensional snapshot variation vectors \mathcal{S}_t in (7) for different times t are assumed to be independent, identically distributed, sampled from a multivariate Gaussian mixture with constant, non history-dependent parameters. These parameters consist of, for each component of the mixture, a nonnegative weight, as well as the mean (vector of size p), variance (vector of size p) and $p \times p$ correlation matrix of a multivariate normal distribution, associated to the vector of random variables \mathcal{S}_t in (7).

More realistically, we would like the parameters of this Gaussian mixture to depend on the book history, namely on the history of previous \mathcal{S} 's.

We achieve this using the architecture in figure 5 similar to Ha and Schmidhuber (2018), built with a long short-term memory network (LSTM) and a mixture density network (MDN). A LSTM layer first transforms a batch $(\mathcal{S}_j)_{j \in [t-k+1, t]} \in \mathbb{R}^{k \cdot p}$ of historical window size $k = 20$ into a latent space of dimension $\mathcal{L} = 32$. This encoding is obtained by taking the hidden state of the LSTM. Using the hidden state as a projection method for the history of a vector-valued stochastic process is a well-known method and is typically used in modern game theory to represent the history of actions and observations experienced by an agent in imperfect-information games Gupta et al. (2017). Then, the hidden state is concatenated with the most recent book snapshot variation \mathcal{S}_t and fed into a fully connected neural network with one input layer (width 32), 2 hidden layers (width 64) and multiple output layers, one per parameter type of the Gaussian mixture with n components, cf. figure 5. This consists of, for each component, its weight $\pi \in \mathbb{R}_+$, mean $\mu \in \mathbb{R}^p$, variance $\sigma^2 \in \mathbb{R}_+^p$ and $p \times p$ correlation matrix ρ , a total of $n \left(1 + 2p + \frac{p(p-1)}{2} \right)$ parameters. This is because the correlation matrix is symmetric and contains ones on the diagonal. Note that we use suitable output activation functions (exponential, tanh, softmax) to ensure that variances are non-negative, correlations are in $[-1, 1]$ and mixture weights are nonnegative and sum to one. The network is trained to maximize the log-likelihood between the training data and that of the Gaussian mixture distribution.

In our case, $p = 12$, so the total number of Gaussian mixture parameters to learn is dominated by the number of correlation parameters $\mathcal{O}(np^2)$. In order to reduce the number of parameters to learn, we consider two cases. For the first case, *fixed correlation*, a correlation matrix between the p random variables \mathcal{S}_t is precomputed from our training data and used by each mixture component. Consequently, our network solely outputs component weights, means, variances, a total of $n \cdot (1 + 2p)$ parameters. The training loss is evaluated using the precomputed correlation matrix. For the second case, *shared correlation*, the network learns one correlation matrix that is shared across all mixture components, i.e. each component uses the same learnt correlation matrix. Note that *shared correlation* includes *fixed correlation* as a particular case, however distinguishing these two cases is useful to quantify the benefit of learning the correlations vs. computing it in a classical, statistical way using the training data.

We train the network using an Adam optimizer with learning rate 10^{-3} up to epoch 110, then 10^{-4} , and a minibatch size of 100. We initialize the network weights using the Xavier initialization, also known as Glorot initialization, associated to the uniform distribution. We use the same training, validation and test data when assessing performance of the vanilla model and of its neural extension. The vanilla model fit is performed using the standard expectation-maximization (EM) algorithm, using *sklearn*. We do not use dropout, but use early stopping as a way to prevent overfitting. That is, we stop training when the validation loss starts increasing. In total we trained on approximately 20,000 epochs.

We present in table 2 the scores (log-likelihood) of all three models. We see that the neural architecture outperforms significantly the vanilla model, and that learning correlations improves performance.

Our internal FX data is confidential, so to conduct the experiment in table 2, we used Lobster⁹ INTC data from Jan 28th 2015. We considered the last two hours before close as it is highly liquid, the timestep value $dt = 1s$, and split the data into training, validation and test sets of sizes 70%, 15%, 15%. The data that we feed as input to our network is standardized, namely we subtract the mean and divide by the standard deviation.

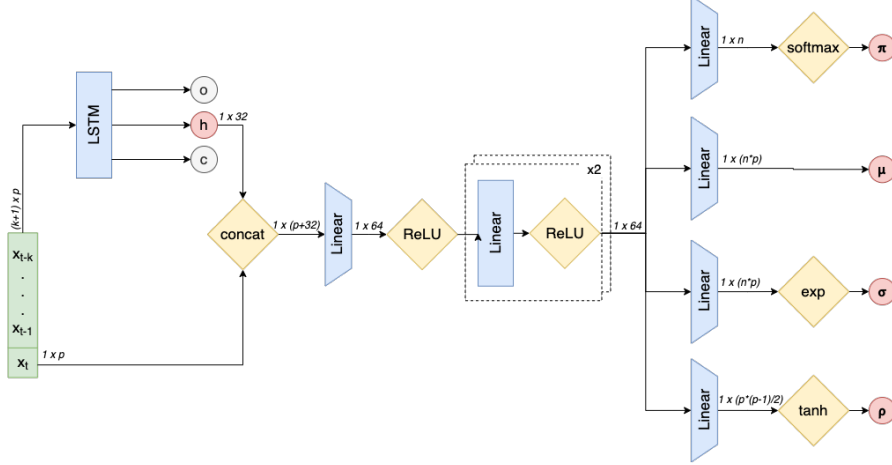


Figure 5: Architecture of the Neural ECN model. We output parameters of a multivariate Gaussian mixture distribution (component weights, means, variances and correlations) with n components fitted to the $p = 2m + 2 = 12$ dimensional vector \mathcal{S}_t in (7). An order book history $h_t := (\mathcal{S}_j)_{j \in [t-k+1, t]}$ of size $k = 20$ is fed as input to the network and first encoded into a latent space of size 32. We concatenate the latter with the most recent book information \mathcal{S}_t , and feed it to a fully connected neural network with 2 hidden layers of width 64.

Table 2: Summary of ECN model scores (log-likelihood). Gaussian mixture with 5 components.

Model	Train Score	Validation Score	Test Score
Vanilla	8.89	6.23	8.94
Neural w/ fixed correlation	18.32	15.79	15.64
Neural w/ shared correlation	23.40	21.90	21.63

3 Game theoretical analysis and convergence properties

3.1 Shared equilibria: convergence of shared-policy learning in the case of stationary LTs

In this section, we focus on LPs. That is, we assume that LTs do not learn, i.e. π^{LT} is a fixed distribution and can therefore be considered as part of the environment, i.e. transition dynamics \mathcal{T} . Our goal is to understand what are the game theoretic implications of LP agents of different types using a shared policy.

Intuitively, assume 2 players are asked to submit algorithms to play chess that will compete against each other. Starting with the white or dark pawns presents some similarities as it is chess in both cases, but also fundamental differences, hence the algorithms need to be good in all cases, whatever the type (white or dark) assigned by the random coin toss at the start of the game. The 2 players are playing a higher-level game on the space of algorithms that requires the submitted algorithms to be good in all situations. This also means we will consider games where there are "good" strategies, formalized by the concept of extended transitivity in assumption 3.3, needed in theorem 3.6.

⁹www.lobsterdata.com

We will actually need the following definition, which is slightly more general than (2) in that it allows LP agents $j \neq i$ to use a different policy $\pi_2 \in \mathcal{X}^{LP}$, where $i \neq j$, $\pi_1, \pi_2 \in \mathcal{X}^{LP}$:

$$\tilde{V}_{\Lambda_i^{LP}}(\pi_1, \pi_2) := \mathbb{E}_{\lambda_i^{LP} \sim p_{\Lambda_i^{LP}}, a_t^{(i,LP)} \sim \pi_1(\cdot | \cdot, \lambda_i^{LP})} \left[\sum_{t=0}^T \mathcal{R}^{LP}(z_t^{(i,LP)}, z_t^{(-i,LP)}, z_t^{(LT)}) \right] \quad (9)$$

$$\lambda_j^{LP} \sim p_{\Lambda_j^{LP}}, a_t^{(j,LP)} \sim \pi_2(\cdot | \cdot, \lambda_j^{LP})$$

$\tilde{V}_{\Lambda_i^{LP}}(\pi_1, \pi_2)$ is to be interpreted as the expected reward of a LP agent of supertype Λ_i^{LP} using π_1 , while all other LP agents are using π_2 . $\tilde{V}_{\Lambda_i^{LP}}$ also depends on π^{LT} , but since we assume it to be fixed in this section, we do not write the dependence explicitly. This method of having an agent use π_1 and all others use π_2 is mentioned in Hefti (2017) under the name "symmetric opponents form approach" (SOFA) in the context of symmetric games. Our game as we formulated it so far is not symmetric since different supertypes get different rewards, however we will see below that we will introduce a symmetrization of the game via the function \hat{V} .

Shared policy gradient and the higher-level game \hat{V} . In the parameter sharing framework, $\pi \equiv \pi_\theta$ is a neural network with weights θ , and the gradient $\nabla_{\theta, B}^{shared}$ according to which the shared policy π_θ is updated (where B is the number of episodes sampled) is computed by collecting all agent experiences simultaneously and treating them as distinct sequences of local states, actions and rewards experienced by the shared policy Gupta et al. (2017), yielding the following expression under vanilla policy gradient, similar to the single-agent case:

$$\nabla_{\theta, B}^{shared} = \frac{1}{n_{LP}} \sum_{i=1}^{n_{LP}} g_i^B \quad (10)$$

$$g_i^B := \frac{1}{B} \sum_{b=1}^B \sum_{t=0}^T \nabla_\theta \ln \pi_\theta \left(a_{t,b}^{(i,LP)} | s_{t,b}^{(i,LP)}, \lambda_{i,b}^{LP} \right) \sum_{t'=t}^T \mathcal{R}^{LP}(z_{t',b}^{(i,LP)}, z_{t',b}^{(-i,LP)}, z_{t',b}^{(LT)})$$

Note that one may use an advantage critic in equation (10) in place of the sampled rewards \mathcal{R}^{LP} , but this is related to sample efficiency and doesn't change the methods and observations developed subsequently. By the strong law of large numbers, taking $B = +\infty$ in (10) simply amounts to replacing the average by an expectation as in (9) with $\pi_1 = \pi_2 = \pi_\theta$. Proposition 3.1 is a key observation of this paper and sheds light upon the mechanism underlying parameter sharing in (10): in order to update the shared policy, we **a**) set all agents to use the same policy π_θ and **b**) pick one agent at random and take a step towards improving its individual reward while keeping other agents on π_θ : by (11), this yields an unbiased estimate of the gradient $\nabla_{\theta, \infty}^{shared}$. Sampling many agents at random $\alpha \sim U[1, n_{LP}]$ in order to compute the expectation in (11) will yield a less noisy gradient estimate but will not change its bias. In (11), \hat{V} is to be interpreted as the utility received by a randomly chosen agent behaving according to π_1 while all other agents behave according to π_2 .

Proposition 3.1. *For a function $f(\theta_1, \theta_2)$, let $\nabla_{\theta_1} f(\theta_1, \theta_2)$ be the gradient with respect to the first argument, evaluated at (θ_1, θ_2) . We then have:*

$$\nabla_{\theta, \infty}^{shared} = \nabla_{\theta_1} \hat{V}(\pi_\theta, \pi_\theta), \quad \hat{V}(\pi_1, \pi_2) := \mathbb{E}_{\alpha \sim U[1, n_{LP}]} \left[\tilde{V}_{\Lambda_\alpha^{LP}}(\pi_1, \pi_2) \right], \quad \pi_1, \pi_2 \in \mathcal{X}^{LP} \quad (11)$$

where $\mathbb{E}_{\alpha \sim U[1, n_{LP}]}$ indicates that the expectation is taken over α random integer in $[1, n_{LP}]$.

Proof. It is known (although in a slightly different form in Lockhart et al. (2019) or Srinivasan et al. (2018) appendix D) that the term g_i^∞ in (10) is nothing else than $\nabla_{\theta_1} \tilde{V}_{\Lambda_i^{LP}}(\pi_\theta, \pi_\theta)$, that is the sensitivity of the expected reward of an agent of supertype Λ_i^{LP} to changing its policy while all other agents are kept on π_θ , cf. (9). The latter can be seen as an extension of the likelihood ratio method to imperfect information games, and allows us to write concisely, using (10):

$$\nabla_{\theta, \infty}^{shared} = \frac{1}{n_{LP}} \sum_{i=1}^{n_{LP}} \nabla_{\theta_1} \tilde{V}_{\Lambda_i^{LP}}(\pi_\theta, \pi_\theta)$$

$$= \nabla_{\theta_1} \frac{1}{n_{LP}} \sum_{i=1}^{n_{LP}} \tilde{V}_{\Lambda_i^{LP}}(\pi_\theta, \pi_\theta) = \nabla_{\theta_1} \mathbb{E}_{\alpha \sim U[1, n_{LP}]} \left[\tilde{V}_{\Lambda_\alpha^{LP}}(\pi_\theta, \pi_\theta) \right]$$

□

Shared Equilibria. We remind Duersch et al. (2012) that a 2-player game is said to be symmetric if the utility received by a player only depends on its own strategy and on its opponent's strategy, but not on the player's identity, and that a pure strategy¹⁰ Nash equilibrium (π_1^*, π_2^*) is said to be symmetric if $\pi_1^* = \pi_2^*$. For such games, due to symmetry, we call $\text{payoff}(\pi_1, \pi_2)$ the utility received by a player playing π_1 while the other player plays π_2 .

Equation (11) suggests that the shared policy is a Nash equilibrium of the 2-player symmetric game with payoff \hat{V} , where by our definition of the term "payoff", the first player receives $\hat{V}(\pi_1, \pi_2)$ while the other receives $\hat{V}(\pi_2, \pi_1)$. This is because $\nabla_{\theta_1} \hat{V}(\pi_\theta, \pi_\theta)$ in (11) corresponds to trying to improve the utility of the first player while keeping the second player fixed, starting from the symmetric point (π_θ, π_θ) . If no such improvement is possible, we are facing by definition a symmetric Nash equilibrium, since due to symmetry of the game, no improvement is possible either for the second player starting from the same point (π_θ, π_θ) . The game with payoff \hat{V} can be seen as an abstract game (since the 2 players are not part of the n_{LP} agents) where each element of the strategy set (that is, every pure strategy) is a policy $\pi \in \mathcal{X}^{LP}$ defined in (1). This type of game has been introduced in Balduzzi et al. (2019) as a *Functional Form Game* (FFG), since pure strategies of these games are stochastic policies themselves (but of the lower-level game among the n_{LP} agents). This motivates the following definition.

Definition 3.2. (Shared Equilibrium) A shared (resp. ϵ -shared) equilibrium π^* associated to the supertype profile $\Lambda := (\Lambda^{LP}, \Lambda^{LT})$ is defined as a pure strategy symmetric Nash (resp. ϵ -Nash) equilibrium (π^*, π^*) of the 2-player symmetric game with pure strategy set \mathcal{X}^{LP} and payoff \hat{V} in (11).

Note that the previously described mechanism **a)-b)** occurring in parameter sharing is exactly what is defined as **self-play** in Balduzzi et al. (2019) (algorithm 2), but for the game of definition 3.2 with payoff \hat{V} . That is, we repeat the following steps for iterations k (i) set all agents on π_{θ_k} (ii) pick one agent at random and improve its reward according to the gradient update (11), thus finding a new policy $\pi_{\theta_{k+1}}$.

Consider for a moment only the case where types are defined to be agents' indexes: $\Lambda_i := \lambda_i := i$: this is a particular case of our formalism. Define the "underlying game" among n_{LP} LP agents to be the game where each agent i chooses a (stochastic) policy π_i from states to actions, and receives a utility equal to its value function $V_i(\pi_i, \pi_{-i})$, defined as the expected value of its cumulative reward (cf. (2)). This definition is classical, cf. Leonardos et al. (2021) for the study of Markov Potential games, and amounts to recasting a Markov game whereby agents take actions and transition from states to states over multiple timesteps as a one-shot game with utilities V_i on a larger (pure) strategy space, namely the space of stochastic policies. This trick was also used in PSRO Lanctot et al. (2017), where they call the larger one-shot game a "meta-game". When types and supertypes are both equal to agents' indexes, heterogeneity of agents is entirely subsumed in the "type" variable and Nash equilibria of the underlying game among the n_{LP} agents exactly coincide with shared equilibria. Indeed, assume that $(\pi_i^*)_{i \in [1, n_{LP}]}$ is any Nash equilibria of the underlying game, i.e. $V_i(\pi_i, \pi_{-i}^*) \leq V_i(\pi_i^*, \pi_{-i}^*) \forall i, \forall \pi_i$. We can simply define $\pi^*(\cdot | \cdot, i) := \pi_i^*$ to get a shared equilibrium, where π^* is the shared policy being used by all agents (but seen through a different prism $\pi^*(\cdot | \cdot, i)$ for each agent i). Indeed, by definition of the Nash, no agent can deviate in a profitable way. In particular, no randomly selected agent can deviate in a profitable way, hence by definition of the game \hat{V} , π^* is a shared equilibrium. Conversely, every shared equilibrium is a Nash of the underlying game.

Why is the abstract game \hat{V} useful? The abstract game characterizes the learning mechanism according to which an equilibrium is reached, rather than the equilibrium itself. Such an abstract game is used as a mean to find equilibria of the underlying game among the n_{LP} agents. In our case, the learning mechanism is that at each step, a randomly selected agent tries to find a profitable deviation. This is by definition of \hat{V} . Such sequences of improvements by individual players are known as "improvement paths" since the seminal work on potential games Monderer and Shapley (1996). One of our contributions is to give a rigorous, game-theoretical explanation to the policy sharing algorithms that have been used in the literature Gupta et al. (2017). Policy sharing has been used in practice via (variants of) equation (10), but without theoretical grounding. Therefore, nothing

¹⁰"pure strategy" in the terminology of game theory, as opposed to "mixed strategy".

is known about its convergence properties, nor what it means for agents to be using a shared policy. We show that policy sharing precisely corresponds to the learning mechanism described above, where a randomly chosen player tries to deviate profitably at each step. Importantly, such characterization allows to relate policy sharing to potential games, giving us insights on conditions required for the learning mechanism to converge, namely our "extended transitivity" assumption 3.3.

We now discuss the case where Λ_i and λ_i are general quantities rather than the agents' indexes i . In this case, the reasoning is the same except that shared equilibria will now coincide with symmetric Bayesian Nash equilibria of the underlying game, instead of Nash equilibria. One-shot Bayesian games are a natural generalization of normal form games in which at every instance of the game, each player is given a type λ_i randomly sampled from an exogenous distribution of types, which we call supertype. We refer to Li and Wellman (2021) for the definition of Bayesian games and Bayesian Nash equilibria. An agent policy in a Bayesian game is a mapping from types to state-action policies of the original game, $\pi \equiv \lambda \rightarrow \pi(\cdot | \cdot, \lambda)$, i.e. agents need to specify their behavior for every type they can possibly be given. Therefore, Bayesian Nash equilibria are Nash equilibria on a larger pure strategy space where policies have been augmented with the agent type. In our case, all agents use the same shared policy π , but seen through a different prism $\pi(\cdot | s_t^{(i, \kappa)}, \lambda_i)$ for each agent i . This means that the Bayesian Nash equilibria we are looking for are symmetric. As mentioned in section 2.2.1, since agents may have different observations $s_t^{(i, \kappa)}$ at a given point in time, policy sharing still allows different actions across agents. Our *rationality assumption* underlying parameter sharing is the following: if two agents have equal types and equal sequences of historical observations at a given point in time, then they should behave the same way.

Although shared equilibria coincide with symmetric Bayesian Nash equilibria of the underlying game among n_{LP} LP agents, we have chosen to use the new terminology "shared equilibria" to highlight the new interpretation of parameter sharing in terms of the abstract game \hat{V} , which relates to the learning mechanism that agents will employ to reach equilibria. This learning mechanism, from a practical point of view, further allows us to use all agents' experiences to interpolate policies $\pi(\cdot | \cdot, \lambda)$ in the type variable λ , using the generalization power of neural nets. For example, if in a specific instance of the game, the sampled risk aversions γ for 2 LP agents are 0.5 and 1, the related experience will be used at the next stage of the game for an agent which risk aversion is 0.6.

The natural question is now *under which conditions do Shared equilibria exist, and can the self-play mechanism in (11) lead to such equilibria?* We know Balduzzi et al. (2019) that self-play is related to transitivity in games, so to answer this question, we introduce a new concept of transitivity that we call *extended transitivity* as it constitutes a generalization to 2-player symmetric general sum games of the concept of transitivity for the zero-sum case in Balduzzi et al. (2019). There, such a transitive game has payoff $u(x, y) := t(x) - t(y)$. One can observe that this game satisfies extended transitivity in assumption 3.3 with $\delta_\epsilon := \epsilon$ and $T(x) := t(x)$. Note also that their monotonic games for which $u(x, y) := \sigma(t(x) - t(y))$ (where σ is increasing) satisfy extended transitivity as well with $\delta_\epsilon := \sigma^{(-1)}(\epsilon + \sigma(0))$ and $T(x) := t(x)$.

Assumption 3.3. (extended transitivity) A 2-player symmetric game with pure strategy set S and payoff u is said to be extended transitive if there exists a bounded function T such that:

$$\forall \epsilon > 0, \exists \delta_\epsilon > 0 : \forall x, y \in S : \text{if } u(y, x) - u(x, x) > \epsilon, \text{ then } T(y) - T(x) > \delta_\epsilon.$$

The intuition behind assumption 3.3 is that T can be seen as the game "skill" that is being learnt whenever a player finds a profitable deviation from playing against itself. It will be required in theorem 3.6 to prove the existence of shared equilibria, which is the main result of this section. Actually, it will be proved that such equilibria are reached by following self-play previously discussed, thus showing that policy updates based on (11) with per-update improvements of at least ϵ achieve ϵ -shared equilibria within a finite number of steps. In order to do so, we need definition 3.4 of a *self-play sequence*, which is nothing else than a rigorous reformulation of the mechanism occurring in self-play Balduzzi et al. (2019) (algo 2). For ϵ -shared equilibria, assumption 3.3 is sufficient, but for shared equilibria, we need the continuity result in lemma 3.5.

Definition 3.4. A (f, ϵ) -self-play sequence $(x_n, y_n)_{0 \leq n \leq 2N}$ of size $0 \leq 2N \leq +\infty$ generated by $(z_n)_{n \geq 0}$ is a sequence such that for every n , $x_{2n} = y_{2n} = z_n$, $(x_{2n+1}, y_{2n+1}) = (z_{n+1}, z_n)$ and $f(x_{2n+1}, y_{2n+1}) > f(x_{2n}, y_{2n}) + \epsilon$.

Lemma 3.5. Assume that the rewards \mathcal{R}^{LP} are bounded, and that \mathcal{S}^{LP} , \mathcal{A}^{LP} and $\mathcal{S}^{\lambda^{LP}}$ are finite. Then $V_{\Lambda_i^{LP}}$ is continuous on $\mathcal{X}^{LP} \times \mathcal{X}^{LP}$ for all i , where \mathcal{X}^{LP} is equipped with the total variation metric.

Theorem 3.6. Let Λ^{LP} be a supertype profile. Assume that the symmetric 2-player game with pure strategy set \mathcal{X}^{LP} and payoff \widehat{V} is extended transitive. Then, there exists an ϵ -shared equilibrium for every $\epsilon > 0$, which further can be reached within a finite number of steps following a (\widehat{V}, ϵ) -self-play sequence. Further, if \mathcal{S}^{LP} , \mathcal{A}^{LP} and $\mathcal{S}^{\lambda^{LP}}$ are finite and the rewards \mathcal{R}^{LP} are bounded, then there exists a shared equilibrium. In particular, if $(\pi_{\theta_n})_{n \geq 0}$ is a sequence of policies obtained following the gradient update (11) with $\widehat{V}(\pi_{\theta_{n+1}}, \pi_{\theta_n}) > \widehat{V}(\pi_{\theta_n}, \pi_{\theta_n}) + \epsilon$, then $(\pi_{\theta_n})_{n \geq 0}$ generates a finite (\widehat{V}, ϵ) -self-play sequence and its endpoint $(\pi_\epsilon, \pi_\epsilon)$ is an ϵ -shared equilibrium.

In theorem 3.6, we assume that at each step, a randomly selected player is able to get an ϵ -improvement from current policy π_{θ_n} to a new policy $\pi_{\theta_{n+1}}$, if other players stay fixed to π_{θ_n} . This ϵ -improvement can be obtained in different ways depending on the context, in our case it is via a step of RL policy gradient update. In the game theory literature, this is a classical assumption known under the name " ϵ -best response oracle", and is assumed in many works. This represents the ability of agents to find locally profitable deviations. For example, one of the most recently cited multi-agent algorithm, policy-sparse response oracles (PSRO), is studied under this oracle assumption Lanctot et al. (2017); Balduzzi et al. (2019). The Double Oracle algorithm McMahan et al. (2003) also assumes the existence of oracles for individual players. Fictitious play, in the same way, assumes that players have an oracle that allows them to best respond to the time-averaged opponent policies.

We should comment on the relationship between our extended transitivity and potential games Monderer and Shapley (1996). Extended transitivity may seem a bit abstract, but it is well-rooted in the game theory literature. In simple terms, it corresponds to games of skill where there are some universally good strategies Czarnecki et al. (2020). For example in chess or tennis, some players are universally "good". This is because there is a skill underlying the game that players need to master. Mathematically, that skill is the function T in our extended transitivity assumption. This is in contrast to cyclic games like rock-paper-scissors where there is no dominating strategy. Precisely, our extended transitivity is very closely related to *generalized ordinal potential games* in the seminal work of Monderer and Shapley (1996). A 2 player symmetric game u as in assumption 3.3 is said to be generalized ordinal potential with potential function \mathcal{P} if Monderer and Shapley (1996):

$$(\text{GOP}) \quad \forall x, y, z \in S : \text{ if } u(y, z) - u(x, z) > 0, \text{ then } \mathcal{P}(y, z) - \mathcal{P}(x, z) > 0.$$

The first comment is that our $\epsilon - \delta_\epsilon$ requirement is a "uniform" version of the > 0 requirement in (GOP), like continuity vs. uniform continuity. We need it for technical reasons in Lemma A.1 in appendix. In the discussion below, we omit this technical aspect and consider the two to be the same. The second comment is that extended transitivity only assumes deviations from symmetric points (x, x) , contrary to all points (x, z) in (GOP). There are two ways to connect extended transitivity and (GOP). The first way is to assume that $\mathcal{P}(y, z) - \mathcal{P}(x, z)$ in (GOP) does not depend on z , which occurs for example if \mathcal{P} is a separable function, i.e. $\mathcal{P}(x, y) = p_1(x) + p_2(y)$. Then (GOP) implies extended transitivity by taking $z = x$. The second way is to assume that:

$$(\text{A1}) \quad \forall x, y \in S : \text{ if } u(y, x) - u(x, x) > 0, \text{ then } u(y, y) - u(x, y) > 0.$$

(A1) is a very intuitive assumption. If $u(y, x) - u(x, x) > 0$, it means that the strategy y is "good" when the other player plays x . If y is good in some universal way, then it is also good when the other player plays y , i.e. $u(y, y) - u(x, y) > 0$. If \mathcal{P} is a symmetric function¹¹, we have that (GOP) together with (A1) imply extended transitivity with $T(x) := \mathcal{P}(x, x)$. Indeed, assume that $u(y, x) - u(x, x) > 0$. Then by (GOP), $\mathcal{P}(y, x) - \mathcal{P}(x, x) > 0$. By (A1), $u(y, y) - u(x, y) > 0$, which by (GOP) yields $\mathcal{P}(y, y) - \mathcal{P}(x, y) > 0$. This implies, using the symmetry of \mathcal{P} , that $T(y) - T(x) = \mathcal{P}(y, y) - \mathcal{P}(x, x) = \mathcal{P}(y, y) - \mathcal{P}(x, y) + \mathcal{P}(y, x) - \mathcal{P}(x, x) > 0$, which proves extended transitivity. However, for extended transitivity to be true, we only need the weaker $\mathcal{P}(y, y) > \mathcal{P}(x, x)$.

It is possible to check empirically that extended transitivity holds for the game \widehat{V} : for this, we need to check that our learning mechanism based on a random player finding a profitable deviation at each

¹¹If the 2 player symmetric game u is exact potential - which is stronger than (GOP) - then it is well-known that \mathcal{P} is symmetric, namely $\mathcal{P}(x, y) = \mathcal{P}(y, x)$.

training iteration makes the cumulative reward of the shared policy approximately monotonically increasing during training. If extended transitivity were false, we would observe a cyclic behavior of the shared policy reward, as as in the case of rock-paper-scissors for example. We observe that LPs' shared policy reward indeed has the correct behavior in figures 7 and 19.

3.2 Empirical analysis of game components

In this section we show how modern game theoretical tools, and precisely differentiable games and their potential-Hamiltonian decomposition introduced in Letcher et al. (2019), can help us analyze the nature of our financial game between LPs and LTs. Our contribution is definition 3.9, where we introduce weights that quantify to which extent the game is potential or Hamiltonian. We notice that it is important, in order to analyze the interactions between market players, to remove the players' self-interactions from the potential term of the game Jacobian when comparing it to its Hamiltonian counterpart, so as to obtain a fair comparison between the two game components that only involves interactions across players $i \neq j$.

A differentiable game is a game where players' pure strategies are vectors of real numbers. For example, these vectors can be weights of a neural network, and hence games where each player controls its own neural network are examples of differentiable games. In this section, we write $\theta_i \in \mathbb{R}^d$ the weights of player i , and π_{θ_i} its neural net-driven policy. Letcher et al. (2019) introduce two quantities of interest. One is the game gradient \mathcal{G} quantifying the sensitivity of each player's expected utility V_i w.r.t. its own strategy θ_i :

$$\mathcal{G}(\theta) := (\nabla_{\theta_i} V_i)_{i \in [1, n]} \quad (12)$$

The second is the game Jacobian defined as the gradient of \mathcal{G} , namely the square (block) matrix $\mathcal{J}(\theta)$ ¹² of size $\sum_{i=1}^n |\theta_i|$ such that its block (i, j) is the matrix:

$$[\mathcal{J}(\theta)]_{ij} := \nabla_{\theta_j} \mathcal{G}_i = \nabla_{\theta_i, \theta_j}^2 V_i \quad (13)$$

What distinguishes a game from classical function optimization is that in general, there exists no function which admits \mathcal{G} as its gradient, unless the game is potential. In the seminal paper on potential games Monderer and Shapley (1996), these games are defined as games where the change in the utility of a player i due to a change in its own strategy is equal to that of some function called the potential. It is proved that if utilities V_i are smooth and $\theta_i \in \mathbb{R}$, a game is potential if and only if:

$$\frac{\partial^2 V_i}{\partial \theta_i \partial \theta_j}(\theta) = \frac{\partial^2 V_j}{\partial \theta_i \partial \theta_j}(\theta) \quad \forall i, j \quad (14)$$

Potential games constitute a very important class of games, and in short, correspond to games where there is an underlying "skill" that players can learn (the potential). Note that a game can be potential and zero-sum, for example the 2 player game where utilities of players playing respectively x and y are $f(x) - f(y)$ and $f(y) - f(x)$ for some function f . In that case, the potential function is f , which both players are trying to maximize, and hence f can be thought of as the game skill that both players are trying to master.

In the case $d = 1$ and with the definition of \mathcal{J} in (13), an equivalent formulation of (14) is that \mathcal{J} is a symmetric matrix. An extension to the case $\theta_i \in \mathbb{R}^d$ with $d > 1$ was considered in Letcher et al. (2019): defining \mathcal{J} as in (13), we get that the game is potential if and only if \mathcal{J} is symmetric. Since any matrix M can be decomposed uniquely into symmetric and antisymmetric parts, $M = \mathcal{S}_* + \mathcal{A}_*$ with $\mathcal{S}_* = \frac{1}{2}(M + M^T)$, $\mathcal{A}_* = \frac{1}{2}(M - M^T)$, we can do so for \mathcal{J} , which yields the decomposition of any differentiable game into potential and Hamiltonian components. Hamiltonian games are in spirit, the same as harmonic games in Candogan et al. (2011). The game is potential if and only if $\mathcal{A}_* = 0$, and is Hamiltonian if and only if $\mathcal{S}_* = 0$. This is discussed in Letcher et al. (2019).

Definition 3.7. Letcher et al. (2019) Let $\mathcal{J} := \mathcal{S}_* + \mathcal{A}_*$ the unique decomposition of \mathcal{J} into symmetric and antisymmetric matrices. The game is Hamiltonian if $\mathcal{S}_* = 0$, and potential if $\mathcal{A}_* = 0$.

Definition 3.8. Let $\mathcal{J} := \mathcal{D} + \mathcal{S} + \mathcal{A}$ the unique decomposition of \mathcal{J} into a diagonal matrix, a symmetric matrix with zero diagonal, and an antisymmetric matrix. We say that the game is weak Hamiltonian if $\mathcal{S} = 0$.

¹²we denote $\mathcal{J}(\theta)$ by \mathcal{J} when there is no ambiguity.

By our previous discussion and definition 3.8, we have $\mathcal{S}_* = \mathcal{S} + \mathcal{D}$ and $\mathcal{A}_* = \mathcal{A}$. Therefore, the game is potential if and only if $\mathcal{A}_* = 0$, if and only if $\mathcal{A} = 0$. Hamiltonian and weak Hamiltonian games differ in that the former require both \mathcal{D} and \mathcal{S} to be zero, whereas the latter only require \mathcal{S} to be zero. Since we are interested in quantifying interactions among players, we exclude its diagonal \mathcal{D} from the symmetric component of the game Jacobian, which quantifies the self-interaction of a player with itself $\nabla_{\theta_i}^2 V_i$. Doing so yields that both matrices \mathcal{S} and \mathcal{A} in definition 3.8 only include interactions across players $i \neq j$ as both have zero diagonal elements. This makes the comparison between the potential and weak Hamiltonian components fair. Not removing the players' self-interactions from our weights in definition 3.9 would make the symmetric component dominate artificially its antisymmetric counterpart, which is also what we see in practice.

In our case, θ_i are the weights of a neural network, and therefore it is impossible to store these matrices since they are too large. Instead, we can compute the "Jacobian-gradient-product" $\mathcal{J}^T \mathcal{G}$, simply obtained by taking the gradient of $\frac{1}{2} \|\mathcal{G}\|^2$ in modern Automatic Adjoint Differentiation (AAD) frameworks such as tensorflow. From there, we can compute its symmetric and antisymmetric parts $\mathcal{S}\mathcal{G}$ and $\mathcal{A}^T\mathcal{G}$ (cf. Letcher et al. (2019), appendix A). The latter constitute the interaction of the matrices \mathcal{A} and \mathcal{S} with the gradient \mathcal{G} , and allow us to approximate their norms by the norms of $\mathcal{A}^T\mathcal{G}$ and $\mathcal{S}\mathcal{G}$, which we will use as a practical replacement for the norms of \mathcal{A} and \mathcal{S} . The quantity $\mathcal{J}^T \mathcal{G}$ is the main building block of consensus optimization Mescheder et al. (2017), whereas Letcher et al. (2019) argues that using the antisymmetric part only $\mathcal{A}^T\mathcal{G}$ enables convergence to stable fixed points (Symplectic Gradient Adjustment).

This framework gives us an empirical way to quantify the nature the interactions between LP and LT agents, that we introduce in definition 3.9. The weights ω^A, ω^S are computed empirically during training, and tell us to which extent the interactions between two players are potential, or (weak) Hamiltonian.

Definition 3.9. *Let \mathcal{P} be a subset of players in $[1, n]$ associated to the strategy vector θ , and denote $\tilde{\mathcal{J}}$ the restriction of the game Jacobian \mathcal{J} to \mathcal{P} . Let $\tilde{\mathcal{J}} := \tilde{\mathcal{D}} + \tilde{\mathcal{S}} + \tilde{\mathcal{A}}$ be the (unique) decomposition of $\tilde{\mathcal{J}}$ into diagonal, symmetric (with zero diagonal) and antisymmetric matrices. We define the Hamiltonian and potential weights of the game as:*

$$\omega^A(\theta) := \frac{\|\tilde{\mathcal{A}}^T \mathcal{G}\|}{\|\tilde{\mathcal{A}}^T \mathcal{G}\| + \|\tilde{\mathcal{S}}\mathcal{G}\|}, \quad \omega^S(\theta) := 1 - \omega^A(\theta) \quad (15)$$

Note that by Ramponi and Restelli (2021); Shen et al. (2019), the game Jacobian \mathcal{J} is computed, in the case of RL, for $i \neq j$:

$$[\mathcal{J}(\theta)]_{ij} = \frac{1}{B} \sum_{b=1}^B \sum_{t=0}^T \mathcal{R}_{t,b}^i \sum_{t'=0}^t \nabla_{\theta_i} \ln \pi_{\theta_i} \left(a_{t',b}^{(i)} | s_{t',b}^{(i)} \right) \nabla_{\theta_j} \ln \pi_{\theta_j} \left(a_{t',b}^{(j)} | s_{t',b}^{(j)} \right)^T$$

where B is the number of episodes sampled and:

$$[\mathcal{J}(\theta)]_{ii} = \frac{1}{B} \sum_{b=1}^B \nabla_{\theta_i} g_b^i \nabla_{\theta_i} \ln \pi_{\theta_i} \left(a_{t',b}^{(i)} | s_{t',b}^{(i)} \right) + \nabla_{\theta_i}^2 g_b^i$$

$$g_b^i := \frac{1}{B} \sum_{b=1}^B \sum_{t=0}^T \mathcal{R}_{t,b}^i \sum_{t'=0}^t \nabla_{\theta_i} \ln \pi_{\theta_i} \left(a_{t',b}^{(i)} | s_{t',b}^{(i)} \right)$$

In figure 6 we illustrate the Hamiltonian weight of definition 3.9 during training, in two situations.

In the first case (left), we consider a game between a PnL-driven LP ($\omega = 1$) and a PnL-driven LT ($\omega = 1$), and no ECN. We see that the game is quite balanced with $\omega^A \approx 0.6$. Remember that in a potential game, there exists a quantity (the potential) that both players are trying to maximize, and in particular, by the example we discussed earlier, a game can be both zero-sum and potential. In this case, the potential component $\omega^S \approx 0.4$ comes from the fact that there is a common skill that both the LP and LT are trying to learn, namely how to earn PnL. The Hamiltonian component comes from the fact that learning this skill does not happen independently from the other player, i.e. there is competition, or coupling, between both players, where the PnL is a function of both players' strategies. We then introduce a second LP, identical to the first. We see the interesting observation that the Hamiltonian weight between the LP and the LT decreases to 0.2, while that between the two

LPs reaches 0.6. The interpretation is that the competition that was initially occurring between the LP and the LT in the 1v1 case, switches to taking place between the two LPs in the second phase, thus benefiting the LT. In this case, the link between the two LPs becomes slightly more adversarial, which makes the link between the LP and the LT almost cooperative. In simple terms, competition between service providers benefits the customer.

In the second situation (right), we compare the 1v1 game between a PnL-driven LP and a PnL-driven LT discussed above with a 1v1 game between a PnL-driven LP and a flow-driven LT ($\omega = 0$), with even quantity targets $q^a = q^b = 0.5$. We see that for the latter case, there is almost no potential component, $\omega^A \approx 1$. This is expected since the objective of the flow LT is completely unrelated to that of the LP, which is PnL. Hence, it is expected that there is no common quantity, or skill, that both players are trying to learn.

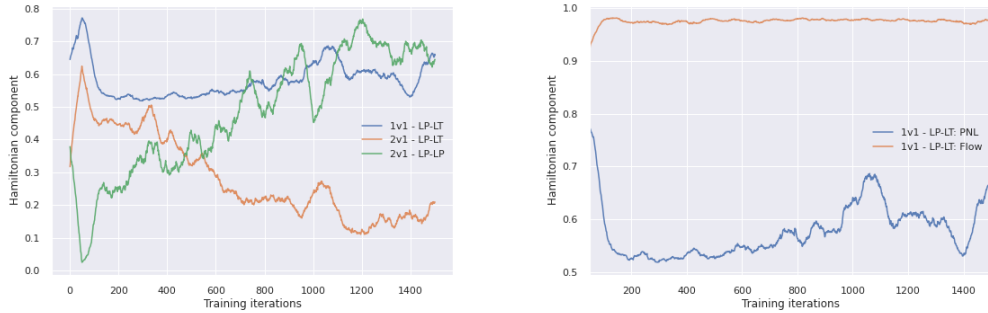


Figure 6: (Left) Hamiltonian component ω^A for a game between 1 LP and 1 LT (1v1), and between 2 LPs and 1 LT (2v1). The link LP-LT is fairly balanced in the 1v1 case. $\omega^S \approx 0.4$ since there is a skill that both players are trying to learn (earning PnL), $\omega^A \approx 0.6$ comes from the competition between players. This link vanishes in the 2v1 case where the competition occurs between the two LPs instead. In other words, competition between service providers benefits the customer. (Right) Hamiltonian component ω^A for a game between 1 LP and 1 PnL LT ($\omega = 1$), and between 1 LP and 1 Flow LT ($\omega = 0$). In the latter case, $\omega^S \approx 0$ since the objective of the LT is entirely unrelated to that of the LP.

4 Calibration of agent supertypes to equilibrium targets

In this section, we present a novel RL-based equilibrium calibration algorithm which we found performed well both on toy data and our internal market data. Due to the confidentiality of the latter, we use HSBC EURUSD data taken from Barzykin et al. (2021b) in section 5.2, however the results that we display match the accuracy we observed using our internal data.

Calibration refers to acting on the supertype profile $\Lambda := (\Lambda^{LP}, \Lambda^{LT})$ so as to match externally specified targets on the shared equilibrium. In a game that satisfies the conditions of theorem 3.6, agents will reach a shared equilibrium associated to Λ . For the simulation to accurately model specific real world observations, we would like the emergent behavior of agents in that equilibrium to satisfy certain constraints. For example, these constraints can be on LPs' market share, individual trade distribution (section 5.1), or flow response curve (section 5.2). As mentioned in the recent work Avegliano and Sichman (2019), there is currently no consensus on how to calibrate parameters of agent-based models. Most methods studied so far build a surrogate of the simulator Avegliano and Sichman (2019); Lamperti et al. (2018). The difficulty is that for every choice of Λ , one should in principle train agents until equilibrium is reached and record the associated calibration loss, and repeat this process until the loss is small enough, which is prohibitively expensive. The baseline we consider in our experiments follows this philosophy by periodically trying new Λ obtained via Bayesian optimization (BO). One issue is that BO can potentially perform large moves in the supertype space, hence changing Λ too often could prevent the shared policy to correctly learn an equilibrium since it would not be given sufficient time to adapt.

Our solution is therefore to smoothly vary Λ during training: we introduce a RL calibrator agent with a stochastic policy, whose goal is to optimally pick Λ and who learns jointly with RL agents learning a shared equilibrium, but under a slower timescale. The two-timescale stochastic approximation

framework is widely used in RL Dalal et al. (2018); Konda and Tsitsiklis (2004) and is well-suited to our problem as it allows the RL calibrator's policy to be updated more slowly than the agents' shared policy, yet simultaneously, thus giving enough time to agents to approximately reach an equilibrium. This RL-based formulation allows us to further exploit smoothness properties of specific RL algorithms such as PPO Schulman et al. (2017), where a KL penalty controls the policy update. Since the calibrator's policy is stochastic, this is a distributional approach (in that at every training iteration, you have a distribution of supertype profiles rather than a fixed one) which will contribute to further smooth the objective function in (17), cf. Salimans et al. (2017). Note that our formulation of section 2.1 is general enough to accommodate the case where Λ is a distribution $f(\Lambda)$ over supertype profiles: indeed, define new supertypes $\widetilde{\Lambda}_i := f_i$, where f_1 is the marginal distribution of Λ_1 , and for $i \geq 2$, f_i is the distribution of Λ_i conditional on $(\Lambda_k)_{k \leq i-1}$ (induced by f). This means that instead of a fixed Λ , one can choose a distribution $f(\Lambda)$ by simply defining supertypes appropriately, and in that case it is important to see that the shared policy at equilibrium will depend on the distribution f rather than on a fixed supertype profile.

The RL calibrator's *state* is the current supertype Λ , and its *action* is a vector of increments $\delta\Lambda$ to apply to the supertypes, resulting in new supertypes $\Lambda + \delta\Lambda$, where we assume that Λ_i takes value in some subset of \mathbb{R}^d . This approach is in line with the literature on "learning to learn" Andrychowicz et al. (2016); Li and Malik (2017), since the goal of the RL calibrator is to learn optimal directions to take in the supertype space, given a current location. The RL calibrator has full knowledge of the information across agents $\mathbf{z}_t := (\mathbf{z}_t^{LP}, \mathbf{z}_t^{LT})$ and is given K externally specified targets $f_*^{(k)} \in \mathbb{R}$ for functions of the form $f_{cal}^{(k)}((\mathbf{z}_t)_{t \geq 0})$. Its *reward* r^{cal} will then be a weighted sum of the reciprocal of losses ℓ_k ¹³:

$$r^{cal} = \sum_{k=1}^K w_k \ell_k^{-1} (f_*^{(k)} - f_{cal}^{(k)}((\mathbf{z}_t)_{t \geq 0})) \quad (16)$$

The result is algorithm 1, where at stage $m = 1$, the supertype profile Λ_1 is sampled across episodes b as $\Lambda_1^b \sim \Lambda_0 + \delta\Lambda^b$, with $\delta\Lambda^b \sim \pi_1^\Lambda(\cdot | \Lambda_0)$ and where we denote $\widetilde{\pi}_1^\Lambda := \Lambda_0 + \pi_1^\Lambda(\cdot | \Lambda_0)$ the resulting distribution of Λ_1 . Then, we run multi-agent episodes b according to (9), each one of them with its supertype profile Λ_1^b , and record the reward r_b^{cal} , thus corresponding to the calibrator state Λ_0 , and action $\delta\Lambda^b$. The process is repeated, yielding for each episode b at stage $m \geq 2$, $\Lambda_m^b \sim \Lambda_{m-1}^b + \pi_m^\Lambda(\cdot | \Lambda_{m-1}^b)$, resulting in a distribution $\widetilde{\pi}_m^\Lambda$ for Λ_m , empirically observed through the sampled $\{\Lambda_m^b\}_{b=1..B}$. As a result, the calibrator's policy π^Λ optimizes the following objective at stage m :

$$V_{\pi_m}^{calib}(\pi_m^\Lambda) := \mathbb{E}_{\Lambda \sim \widetilde{\pi}_{m-1}^\Lambda, \Lambda' \sim \pi_m^\Lambda(\cdot | \Lambda) + \Lambda, \lambda_i \sim p_{\Lambda'_i}, a_t^{(i)} \sim \pi_m(\cdot | \cdot, \lambda_i)} [r^{cal}] \quad (17)$$

Algorithm 1 (CALSHEQ) Calibration of Shared Equilibria

Input: learning rates $(\beta_m^{cal}), (\beta_m^{shared})$ satisfying assumption 4.1, initial calibrator and shared policies π_0^Λ, π_0 , initial supertype profile $\Lambda_0^b = \Lambda_0$ across episodes $b \in [1, B]$.

- 1: **while** π_m^Λ, π_m not converged **do**
- 2: **for** each episode $b \in [1, B]$ **do**
- 3: Sample supertype increment $\delta\Lambda^b \sim \pi_m^\Lambda(\cdot | \Lambda_{m-1}^b)$ and set $\Lambda_m^b := \Lambda_{m-1}^b + \delta\Lambda^b$
- 4: Sample multi-agent episode with supertype profile Λ_m^b and shared policy π_m , with $\lambda_i \sim p_{\Lambda_m^b}, a_t^{(i)} \sim \pi_m(\cdot | \cdot, \lambda_i), i \in [1, n]$ cf. (9)
- 5: update π_m with learning rate β_m^{shared} based on gradient (19) and episodes $b \in [1, B]$
- 6: update π_m^Λ with learning rate β_m^{cal} based on gradient (20) associated to (17) with episodes $b \in [1, B]$

Let θ_m and θ_m^Λ be the (neural net) parameters of the shared policy and calibrator policy at stage m , so that π_m and π_m^Λ are shorthand for, respectively, π_{θ_m} and $\pi_{\theta_m^\Lambda}^\Lambda$. Let β_m^{shared} and β_m^{cal} be the learning rates at stage m , according to which θ_m and θ_m^Λ will be updated.

¹³ ℓ_k^{-1} denotes the reciprocal of ℓ_k .

The idea of two-timescale stochastic approximation in our case is that from the point of view of the shared policy, the distribution of supertypes being chosen by the calibrator should be seen as "quasi-static", i.e. frozen, which, informally, will give enough time to the shared policy to approximately reach an equilibrium. This is reflected in assumption 4.1, standard under the two-timescale framework Tamar et al. (2012); Borkar (1997), and ensures that π_m in (17) is updated faster compared to π_m^Λ and thus can be considered as having converged to an equilibrium depending on π_m^Λ . π^Λ is then updated based on (17) using a classical single-agent RL gradient update. This process ensures that π^Λ is updated smoothly during training and learns optimal directions to take in the supertype space, benefiting from the multiple locations Λ_m^b experienced across episodes and over training iterations. Our framework shares some similarities with the work on learning to optimize in swarms of particles Cao et al. (2019), since at each stage m , we have a distribution of supertype profiles empirically observed through the B episodes, where each Λ_m^b can be seen as a particle.

Assumption 4.1. *The learning rates (β_m^{cal}) , (β_m^{shared}) satisfy $\frac{\beta_m^{cal}}{\beta_m^{shared}} \xrightarrow{m \rightarrow +\infty} 0$, as well as the Robbins-Monro conditions, that is their respective sum is infinite, and the sum of their squares is finite.*

Assumption 4.2. *Let Λ_0 and θ_0^Λ be fixed, and the sequence $(\theta_m^\Lambda)_{m>0}$ generated as in (20). There exists a family of distributions $\bar{\pi}_\theta^\Lambda$ parametrized by θ , such that for any $m \geq 0$, $\tilde{\pi}_m^\Lambda = \bar{\pi}_{\theta_m^\Lambda}^\Lambda$, where we recall that $\tilde{\pi}_m^\Lambda$ is the distribution of Λ_m generated through the recursion $\Lambda_k \sim \Lambda_{k-1} + \pi_{\theta_k^\Lambda}^\Lambda(\cdot | \Lambda_{k-1})$.*

The idea behind assumption 4.2 is to have the distribution of Λ_m only depend on the past through θ_m^Λ . We need it to express our parameter updates in the standard two-timescale framework (19)-(20). It can always be achieved by taking π_θ^Λ of the form $\pi_\theta^\Lambda(\cdot | \Lambda) := \bar{\pi}_\theta^\Lambda(\cdot) - \Lambda$ for some $\bar{\pi}_\theta^\Lambda$. More generally, the recursion $\Lambda_k \sim \Lambda_{k-1} + \pi_{\theta_k^\Lambda}^\Lambda(\cdot | \Lambda_{k-1})$ generates a Markov chain on \mathbb{R}^d , and the assumption is that $\tilde{\pi}_{m-1}^\Lambda$ is a stationary distribution of the transition kernel $P_m(x, A) := x + \pi_{\theta_m^\Lambda}^\Lambda(A - x | x)$, where A is a Borel subset of \mathbb{R}^d . In practice, it means that $\tilde{\pi}_m^\Lambda$ is mostly driven by π_m^Λ as learning progresses. By assumption 4.2, we can use the following notation for the gradient $\nabla_{\theta, B}^{shared}$ in (10):

$$\begin{aligned} x_m &:= \nabla_{\theta_m, B}^{shared}, & \hat{x}(\theta_m, \theta_m^\Lambda) &:= \mathbb{E}_{\pi_{\theta_m}, \tilde{\pi}_{\theta_m}^\Lambda} [x_m] \\ X_{m+1} &:= \beta_m^{shared}(x_m - \hat{x}(\theta_m, \theta_m^\Lambda)) \end{aligned} \tag{18}$$

The update of θ_m reads:

$$\theta_{m+1} = \theta_m + \beta_m^{shared} \hat{x}(\theta_m, \theta_m^\Lambda) + X_{m+1} \tag{19}$$

X is a martingale difference sequence, namely $\mathbb{E}[X_{m+1} | \mathcal{F}_m] = 0$, where \mathcal{F}_m is the sigma-algebra generated by the discrete-time processes θ and θ^Λ up to time m . Similarly, the update of θ_m^Λ reads:

$$\theta_{m+1}^\Lambda = \theta_m^\Lambda + \beta_m^{cal} \hat{y}(\theta_m, \theta_m^\Lambda) + Y_{m+1} \tag{20}$$

where y_m is associated to the gradient of V^{calib} with respect to the calibrator policy parameter θ^Λ in (17):

$$\begin{aligned} y_m &:= \frac{1}{B} \sum_{b=1}^B \nabla_{\theta^\Lambda} \ln \pi_m^\Lambda(\delta \Lambda^b | \Lambda_m^b) r_b^{cal} \\ \hat{y}(\theta_m, \theta_m^\Lambda) &:= \mathbb{E}_{\pi_{\theta_m}, \tilde{\pi}_{\theta_m}^\Lambda} [y_m], & Y_{m+1} &:= \beta_m^{cal}(y_m - \hat{y}(\theta_m, \theta_m^\Lambda)) \end{aligned} \tag{21}$$

The updates of θ and θ^Λ are now expressed in the standard two-timescale setting as described in Borkar (1997); Leslie and Collins (2002), which yields theorem 4.4.

Assumption 4.3. *i) The policy networks π_θ and π_θ^Λ are Lipschitz with respect to θ ; ii) $\sup_m \|\theta_m^\Lambda\| + \|\theta_m\| < \infty$; iii) for each fixed θ^Λ , the ordinary differential equation $\dot{\theta} = \hat{x}(\theta, \theta^\Lambda)$ has a unique globally asymptotically stable equilibrium point $\xi(\theta^\Lambda)$ such that it is Lipschitz in θ^Λ ; iv) the ordinary differential equation $\dot{\theta} = \hat{y}(\xi(\theta), \theta)$ has a global asymptotically stable attractor J ¹⁴.*

¹⁴A nonempty, compact, invariant set J is an attractor if it has a neighborhood N such that $\lim_{t \rightarrow \infty} d(\theta_t^\Lambda(z), J) = 0$ for $z \in N$, where $\theta_t^\Lambda(z)$ denotes the solution of the o.d.e. started at z Leslie and Collins (2002).

Theorem 4.4. Assume that assumptions 4.1, 4.2, 4.3 hold true and let J and ξ as in assumption 4.3. Then, the iterates $(\theta_m, \theta_m^\Lambda)$ generated by algorithm 1 converge almost surely to a point $(\xi(\theta_*^\Lambda), \theta_*^\Lambda)$, where $\theta_*^\Lambda \in J$.

Proof. The proof follows from Borkar (1997) (see also Leslie and Collins (2002), theorem 5, Tamar et al. (2012) theorem 4.3). \square

5 Experiments

Both shared LP, shared LT and calibrator policies were trained jointly using Proximal Policy Optimization Schulman et al. (2017), an extension of TRPO Schulman et al. (2015), with a KL penalty to control the smoothness of policy updates Schulman et al. (2017). We used configuration parameters in line with Schulman et al. (2017), that is a clip parameter of 0.3, an adaptive KL penalty with a KL target of 0.01 (so as to smoothly vary the supertype profile) and a learning rate of 10^{-4} . We found that entropy regularization was not specifically helpful in our case. Episodes were taken of length 100 time steps, using $B = 60$ parallel runs in between policy updates. As a result, each policy update was performed with a batch size of $n \cdot 100 \cdot B$ timesteps for the shared policy (where n is the number of agents per policy), and B timesteps for the calibrator's policy, together with 30 iterations of stochastic gradient descent. We used for each policy a fully connected neural net with 2 hidden layers, 256 nodes per layer, and tanh activation. Since our action space is continuous, the outputs of the neural net are the mean and stDev of a standard normal distribution, which is then used to sample actions probabilistically (the covariance matrix across actions is chosen to be diagonal).

For all experiments, we check empirically that we reach convergence for π^{LT} and π^{LP} . We investigate calibration of such empirical equilibria, as well as emergent behavior learnt by our agents. All our LT and LP agents are RL-based, and hence they learn all aspects of the game purely from its rules, precisely LT trading, and LP hedging, pricing. Experiments were conducted in the RLLib multi-agent framework Liang et al. (2018), ran on AWS using a EC2 C5 24xlarge instance with 96 CPUs, resulting in a training time of approximately half a day per experiment.

5.1 Calibration: the case of stationary LTs on toy data

Experimental setup. First, we consider calibration in the case of stationary LTs on toy data: they are assumed at every point in time t to either want to buy or sell with equal probability a fixed quantity q_{LT} . This corresponds to the case $\omega = 0$, $q^a = q^b = 0.5$ in section 2.2.2, but here we do not train π^{LT} to achieve such objective. We split 500 LTs into 10 supertypes, supertype $i \in [1, 10]$ being associated to $q_{LT} = i$.

LPs are assumed to have PnL weight $\omega = 1$. We consider 2 distinct supertypes for 5 to 10 LPs (depending on the experiment), where LP1 is assigned supertype 1 and the $n - 1$ others are assigned supertype 2. These are respectively vectors of size 12 and 11, resulting in 23 parameters to calibrate in total. For each supertype we have i) 10 probabilities to be connected to LT supertypes, ii) the LP risk aversion, which is 1 parameter for supertype 1, and the mean/variance of a (clipped) normal random variable for supertype 2. The corresponding ranges for the the calibrator's state Λ and action $\delta\Lambda$ are reported in table 3. In contrast, experimental results in Lamperti et al. (2018) only calibrate 8 or 12 parameters, although not in a RL context. Remember that in a given episode, a LP may be connected differently to LTs in a given supertype, however it has the same probability to be connected to each one of them, the episode connectivities being sampled randomly at the beginning of it as Bernoulli random variables.

The calibration targets we consider are related to i) LP market share, ii) the distribution of per-timestep individual trade quantities that a given LP receives. The constraint is on 9 percentiles of the distribution, for each supertype.

Table 3: RL calibrator state and action spaces.

Supertype parameter flavor j	state $\Lambda_i(j)$ range	action $\delta\Lambda_i(j)$ range
LT supertype connectivity probability	$[0, 1]$	$[-1, 1]$
LP risk aversion Gaussian mean	$[0, 5]$	$[-5, 5]$
LP risk aversion Gaussian stDev	$[0, 2]$	$[-2, 2]$

We give in table 5 a breakdown of the calibrator reward subobjectives corresponding to equation (16). For each experiment, all sub-objectives are required to be achieved simultaneously. Precisely, the reward formulation associated to table 5 are given below, where we denote $m_{super_1} = m_{super_1}((z_t)_{t \geq 0})$ the market share of supertype 1 observed throughout an episode, m_{total} the sum of all LPs market share, $\hat{v}_{super_j}(p)$ the observed $(10p)^{th}$ percentile of supertype j 's per timestep individual trade quantity distribution.

In experiment 1, $r = (1 + r^{(1)} + 0.2r^{(2)})^{-1}$, with $v_{super_1} = [8, 8, 8, 9, 9, 9, 10, 10, 10]$, $r^{(1)} = \frac{1}{2}(\max(0.15 - m_{super_1}, 0) + \max(0.8 - m_{total}, 0))$, $r^{(2)} = \frac{1}{9} \sum_{p=1}^9 |v_{super_1}(p) - \hat{v}_{super_1}(p)|$. In experiment 2/3, $r = (1 + r^{(1)} + 0.2r^{(2)} + 0.2r^{(3)})^{-1}$, with $v_{super_1} = [8, 8, 8, 9, 9, 9, 10, 10, 10]$, $v_{super_2} = [2, 3, 3, 4, 5, 5, 6, 6, 7]$, $r^{(1)} = \frac{1}{2}(\max(0.15 - m_{super_1}, 0) + \max(0.8 - m_{total}, 0))$, $r^{(j+1)} = \frac{1}{9} \sum_{p=1}^9 |v_{super_j}(p) - \hat{v}_{super_j}(p)|$, $j \in \{1, 2\}$. In experiment 4, $r = (1 + r^{(1)} + r^{(2)})^{-1}$, with $r^{(1)} = |0.25 - m_{super_1}|$, $r^{(2)} = \max(0.8 - m_{total}, 0)$.

Table 4: Summary of experiment configuration.

Experiment #	# LP Agents	Budget # Training Steps (10^6)	# distinct LP Supertypes	# LP Supertype parameters to be calibrated	Total # Calibration Targets
1	5	40	2	20	11
2	5	40	2	20	20
3	10	20	2	20	20
4	10	20	2	23	2

Table 5: Calibration target breakdown

Experiment #	# Calibration Targets	Calibration Target Type
1	9	trade quantity distribution supertype 1
		percentiles 10% – 90% target 8, 8, 9, 9, 9, 10, 10, 10
2	18	market share supertype 1 $\geq 15\%$ + total $\geq 80\%$
		trade quantity distribution Supertypes 1+2
3	18	supertype 1 - percentiles 10% – 90% target 8, 8, 9, 9, 9, 10, 10, 10
		supertype 2 - percentiles 10% – 90% target 2, 3, 3, 4, 5, 5, 6, 6, 7
4	1	market share supertype 1 $\geq 15\%$ + total $\geq 80\%$
		trade quantity distribution Supertypes 1+2
3	18	supertype 1 - percentiles 10% – 90% target 8, 8, 9, 9, 9, 10, 10, 10
		supertype 2 - percentiles 10% – 90% target 2, 3, 3, 4, 5, 5, 6, 6, 7
4	1	market share supertype 1 $\geq 15\%$ + total $\geq 80\%$
		market share supertype 1 = 25%
	1	total market share $\geq 80\%$

Baseline. There is currently no consensus on how to calibrate parameters of agent-based models Avegliano and Sichman (2019), but existing literature suggests using surrogate-based methods Lamperti et al. (2018). The baseline we consider here is Bayesian optimization (BO), a method that has been used for hyperparameter optimization. The latter can be considered as similar to this calibration task, and BO will allow us to periodically record the calibration loss related to a certain choice of supertype Λ , and suggest an optimal point to try next, via building a Gaussian Process-based surrogate of the simulator.

Every M training iterations, we record the calibrator's reward, and use Bayesian optimization to suggest the next best Λ to try. We empirically noticed that if M was taken too low ($M \sim 10$), the shared policy couldn't adapt as the supertype profile changes were too frequent (and potentially too drastic), thus leading to degenerate behaviors (e.g. LPs not trading at all). We tested values of $M = 10$, $M = 50$, $M = 100$, $M = 200$, and opted for $M = 100$ as we found it was a good trade-off between doing sufficiently frequent supertype profile updates and at the same time giving enough time to the shared policy to adapt. We chose an acquisition function of upper confidence bound (UCB) type Srinivas et al. (2016). Given the nature of our problem where agents on the shared policy need to be given sufficient time to adapt to a new supertype profile choice Λ , we opted for a relatively low UCB exploration parameter of $\kappa = 0.5$, which we empirically found yielded a good trade-off between exploration and exploitation (taking high exploration coefficient can yield drastic changes in the supertype profile space, which can prevent agents to learn correctly an equilibrium). In figure 21 we perform an ablation study focused on experiment 1: we look at the impact of the

choice of M in the EI (expected improvement) and UCB (exploration parameter of $\kappa = 1.5$) cases and find that different choices of M and of the acquisition function yield similar performance. We also look at the case "CALSHEQ_no_state" where the calibrator policy directly samples supertype values (rather than increments) without any state information (i.e. the calibrator policy's action is conditioned on a constant), and find that it translates into a significant decrease in performance. We further note that decreasing M has a cost, especially when Λ is high dimensional, since the BO step will become more and more expensive with increasing observation history length. For example, in the case of experiment 1, we observed with $M = 1$ that the training hadn't reached the 20M timestep budget after 2 days (for a calibrator reward in line with other values of M). The covariance function of the Gaussian process was set to a Matern kernel with $\nu = 2.5$.

Performance metrics. We evaluate our findings according to the following three criteria 1) calibrator reward in (17), quantifying the accuracy of the equilibrium fit to the target(s), where one equals perfect fit, 2) convergence of LP agents' rewards to an equilibrium and 3) smoothness of the supertype profile Λ as a function of training iterations, ensuring that equilibria is given sufficient time to be reached, cf. discussion in section 4.

Results. In figure 7 we display calibrator and agents' reward evolution during training. It is seen that *CALSHEQ* outperforms BO in that i) the RL calibrator's rewards converge more smoothly and achieve on average better results in less time, ii) in experiment 4, supertype 1's reward in the BO case converges to a negative value, which should not happen as LPs always have the possibility to earn zero income by making their prices not competitive. The reason for it is that as mentioned in section 4, BO can potentially perform large moves in the supertype space when searching for a solution, and consequently agents may not be given sufficient time to adapt to new supertype profiles Λ . This fact is further seen in figures 30-33 where we show a sample of supertype parameters during training. It is seen that *CALSHEQ* smoothly varies these parameters, giving enough time to agents on the shared policy to adapt, and preventing rewards to diverge as previously discussed.

The RL calibrator's total reward in (17) is computed as weighted sum of various sub-objectives. In figures 26-29, we zoom on the individual components that constitute the overall reward, together with the associated externally specified target values. It is seen that *CALSHEQ* converges more smoothly and more accurately than BO to the target values.

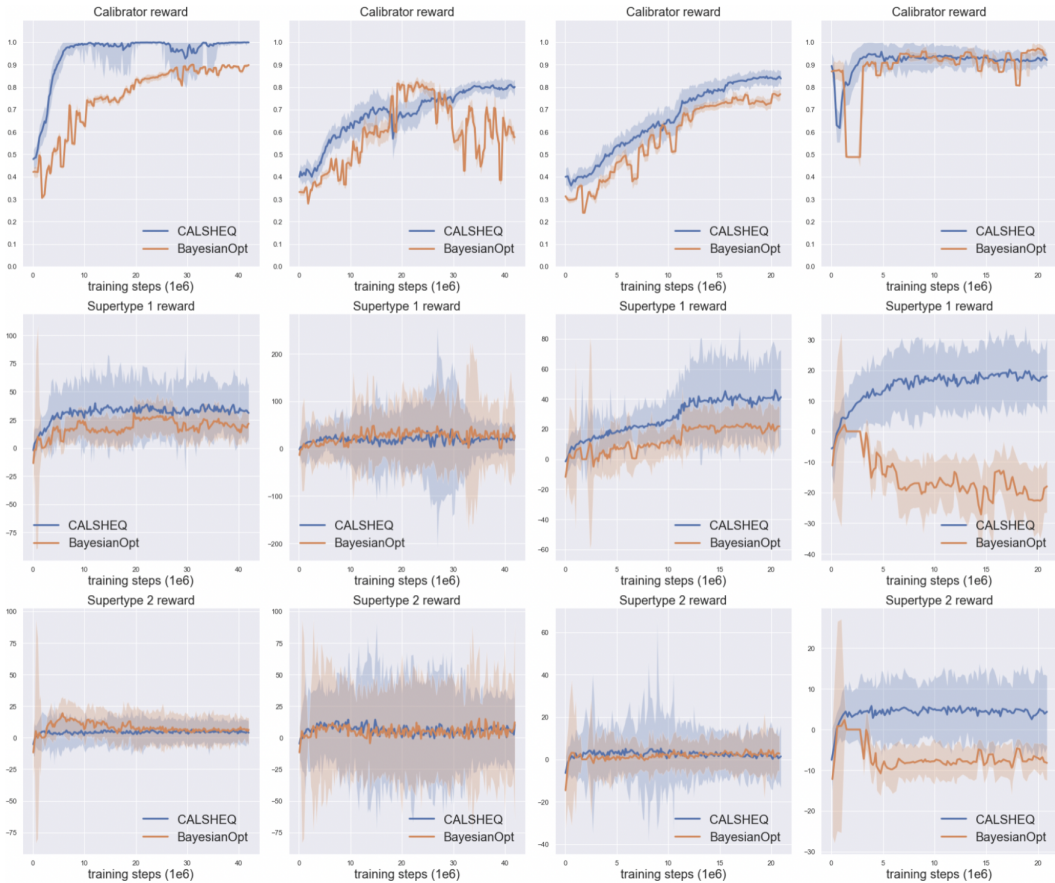


Figure 7: Rewards during training, averaged over episodes B - Calibrator (**Top**), LP Supertypes 1/2 (**Mid/Bottom**) - experiments 1-2-3-4. *CALSHEQ* (ours) and baseline (Bayesian optimization). Shaded area represents ± 1 stDev.

5.2 Calibration: the general case on real data

In this section, similar to section 5.1, we consider calibration targets for a given LP, on its own supertype, but this time i) we consider HSBC EURUSD data taken from Barzykin et al. (2021b), and ii) we calibrate and train the LT agent population as well. Precisely, we take from the latter work the flow response curve $\epsilon \rightarrow \mathcal{F}(\epsilon)$ displayed in figure 8 and table 6, namely the trade quantity it gets as a function of its pricing (cf. definition in section 5.3). When the price is competitive, the LP gets more flow than when it is not, so it is clear that this curve is non-increasing. Our target will be on the shape of that curve, namely on the three coefficients of the 2nd order polynomial fit to this curve. In order to make the calibration problem more challenging and show the flexibility of our approach, we require in addition the LP’s marketshare to be 40 %.

We consider a total of 5 LPs and 30 LTs split into 3 LP supertypes and 5 LT supertypes, where the LP to be calibrated has its own supertype. This corresponds to a total of 36 parameters to be calibrated corresponding to connectivities and reward function parameters, cf. section 2.2.2 and tables 7-9.

We see in figure 8 and table 6 that our RL-based calibration outperforms significantly Bayesian optimization, consistent with section 5.1. We consider various configurations for the Bayesian optimization acquisition function, upper confidence bound (UCB) with exploration parameter ranging from 0.5 to 2.5, and expected improvement (EI).

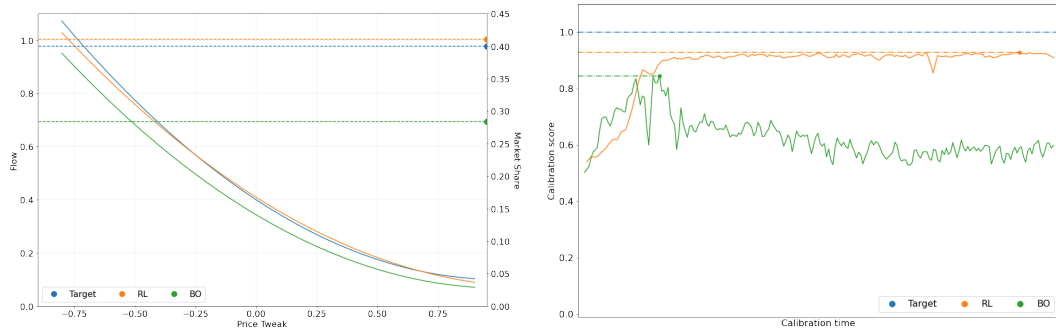


Figure 8: HSBC EURUSD data, taken from Barzykin et al. (2021b) (January to April 2021) (**left**) calibration fit for both market share and the flow response curve $\epsilon \rightarrow \mathcal{F}(\epsilon)$ (**right**) calibration score as a function of training iterations. RL-based calibration outperforms significantly Bayesian optimization on the dual marketshare + flow response curve objective. Target (blue), RL (orange), BO (green).

Table 6: Summary of calibration scores for HSBC EURUSD data, taken from Barzykin et al. (2021b) (January to April 2021). BO UCB is presented for exploration parameter ranging from 0.5 to 2.5. Flow_k represents the *k*th coefficient of the 2nd order polynomial fit to the target in figure 8.

Algorithm	Score (%)	Flow ₀	Flow ₁	Flow ₂	MarketShare
Target	100	0.4	-0.6	0.3	0.4
RL	97	0.41	-0.58	0.25	0.41
BO-UCB-2.0	85	0.34	-0.55	0.27	0.28
BO-UCB-2.5	85	0.44	-0.71	0.16	0.28
BO-UCB-1.5	84	0.32	-0.62	0.27	0.46
BO-UCB-1.0	77	0.36	-0.41	0.14	0.20
BO-UCB-0.5	74	0.25	-0.47	0.21	0.37
BO-EI	68	0.22	-0.36	0.21	0.30

5.3 Emergent agent behavior

In this section, we train shared policies π^{LT} and π^{LP} , and investigate several emergent behaviors learnt by our agents.

We consider a base agent configuration for which we vary the attributes of the first LP and study its learnt behavior as a function of that variation. We consider 2 LP supertypes with risk aversion $\gamma = 0.5$, and respectively 1 and 2 agents; 2 LT supertypes consisting of respectively 12 flow LTs ($\omega = 0$) and 2 PnL LTs ($\omega = 1$) all connected to the ECN. The network of agents and ECN is set to be fully connected.

We train both shared policies π^{LT} and π^{LP} by randomizing the following attributes of the first LP: connectivity to flow and PnL LTs, PnL weight, risk aversion, and proceed to analyzing its learnt emergent behaviors as a function of these attributes. Precisely, we define the supertype of the first LP to sample uniformly the latter quantities over $[0, 1]$ for connectivities and PnL weight, and $[0, 2]$ for risk aversion. We display in figures 19-20 the rewards during training. Once the two policies have been trained, we compute metrics of interest from the point of view of the first LP by running a fixed number of episodes (100) per chosen set of agent types and aggregating the corresponding data. For example, if we look at the LP's inventory as a function of its risk aversion, we run 100 episodes per chosen value of risk aversion, and compute the average inventory over those episodes.

At a given time t , let $\mathcal{O}_t^{ask}, \mathcal{O}_t^{bid}$ be the sets of trades performed by a given LP with the various LTs on both sides. For a given side $\alpha \in \{\text{bid, ask}\}$, we define $\mathcal{F}_t(\alpha)$ the *flow* of a LP as the sum of absolute trade quantities, and $\epsilon_{t,\alpha}$ its related price:

$$\mathcal{F}_t(\alpha) := \sum_{q:q \in \mathcal{O}_t^\alpha} |q|, \quad \epsilon_{t,\alpha} := \begin{cases} \frac{1}{2}\epsilon_{t,\text{spread}} + \epsilon_{t,\text{skew}} & \text{if } \alpha = \text{ask} \\ \frac{1}{2}\epsilon_{t,\text{spread}} - \epsilon_{t,\text{skew}} & \text{if } \alpha = \text{bid} \end{cases} \quad (22)$$

Note that with this convention, the lower $\epsilon_{t,\alpha}$, the more attractive the price from a LT standpoint. We further define the *flow response curve* $\epsilon \rightarrow \mathcal{F}(\epsilon)$ the average flow obtained for a given price level ϵ :

$$\mathcal{F}(\epsilon) := \frac{\sum_{\alpha \in \{\text{bid, ask}\}} \sum_{t=1}^T \mathcal{F}_t(\alpha) \mathbf{1}_{\{\epsilon_{t,\alpha} = \epsilon\}}}{\sum_{\alpha \in \{\text{bid, ask}\}} \sum_{t=1}^T \mathbf{1}_{\{\epsilon_{t,\alpha} = \epsilon\}}} \quad (23)$$

Skewing intensity. Recall that $2\epsilon_{t,\text{skew}} = \epsilon_{t,\text{ask}} - \epsilon_{t,\text{bid}}$ exactly captures the LP pricing asymmetry between bid and ask sides, and that *skewing* refers to setting prices asymmetrically on both sides so as to reduce, or internalize, one's inventory. The more positive the inventory, the more we expect the LP to want to sell, i.e. the more negative $\epsilon_{t,\text{skew}}$. We define the *skewing intensity* as the slope of the linear regression to the cloud of points $\epsilon_{t,\text{skew}} = f(q_t)$, where q_t is the LP's net inventory at time t . In figure 9 we look at this regression line for various connectivities to flow LTs. We see that the more connected, the more the LP learns to skew, materialized by the slope getting more negative, cf. figure 11. This is because flow LTs trade independently of PnL, hence provide to the LP a stream of liquidity available at all times: the LP learns that the more connected to these LTs, the more it can reduce its inventory by setting its prices asymmetrically via $\epsilon_{t,\text{skew}}$. Similarly, we see on figure 11 that the more risk averse, the more intense the skewing. This is because the more risk averse, the more eager to reduce its inventory. We display in figure 10 the absolute inventory as a function of risk aversion, and indeed observe the decreasing pattern. The more the PnL weight, the less intense the skewing: this is because skewing intensely costs PnL. The more connected to PnL LTs, the more intense the skewing: this is because PnL LTs play a role similar to risk aversion, since from the point of view of the LP, both penalize mid-price variations via inventory PnL in section 2.2.2. The corresponding plots of $\epsilon_{t,\text{skew}}$ vs. inventory are presented in figures 22, 23, 24, and the skew intensity distribution in figure 25.

Hedge fraction. We plot the LP hedge fraction ϵ_{hedge} in figure 12. The more risk averse, the more eager the LP is to liquidate its inventory, hence the more hedging. Similarly, hedging is an increasing function of connectivity to PnL LTs, since we discussed that they play a similar role as risk aversion. The more the PnL weight, the less the hedging: this is because hedging costs PnL. Finally, the more connected to flow LTs, the less the hedging, since the easier it is to reduce one's inventory, as discussed when analyzing skewing intensity.

Pricing. We plot in figure 15 the average price $\epsilon_{t,\alpha}$ in (22). Remember that the lower the latter, the more competitive the pricing. As expected the higher the PnL weight, the higher the impact of the

pricing on the LP, hence the less competitive the pricing. The more the connectivity to PnL LTs, the more the LP's PnL suffers, hence the less competitive the pricing so as to compensate the related loss. The more connected to flow LTs, the more competitive the pricing: this is because the LP gets more revenue, so can afford to be more competitive on its prices.

Inventory holding time. We define the *inventory holding time* τ of a given inventory q_t the first time where $q_{t+\tau}$ has opposite sign than q_t , i.e. the first time where the inventory goes back to zero. We plot in figure 13 the average inventory holding time, and in figure 14 a more granular view of the holding time as a function of inventory. The higher the PnL weight, the higher the holding time, since reducing one's inventory is done via skewing or hedging, which both cost PnL. The more risk averse, the more the hedging and skewing, hence the lower the holding time. The more connected to flow LTs, the lower the holding time since the more intense the skewing. The more connected to PnL LTs, the less competitive the pricing, hence the higher the holding time.

Flow. We plot in figure 16 the flow $\mathcal{F}(\epsilon)$ received by the LP from each LT agent class, where we normalize each curve by the number of agents of that class connected to the LP. This way, such curves represent the typical flow shape received by the LP from a representative flow or PnL LT. As the PnL weight increases, it is interesting to see that the flow from PnL LTs decreases more abruptly than that from flow LTs: this is because the price $\epsilon_{t,\alpha}$ gets significantly less competitive, to which the PnL LTs respond more intensely as their objective is PnL related. As flow LT connectivity increases, we saw in figure 9 that the LP tailors its pricing to this class of LT as they are lucrative from a PnL point of view and help reduce inventory, hence it becomes gradually less focused on PnL LTs, and consequently gets less related flow.

Market share and PnL. We present market share and PnL in figures 17, 18. As PnL weight increases, the LP's objective becomes more weighted towards market share and hence market share decreases and PnL increases. Connectivity to PnL LTs penalizes PnL as expected, and interestingly it also penalizes market share since we saw that the price $\epsilon_{t,\alpha}$ gets less competitive on average. PnL is also a decreasing function of risk aversion.

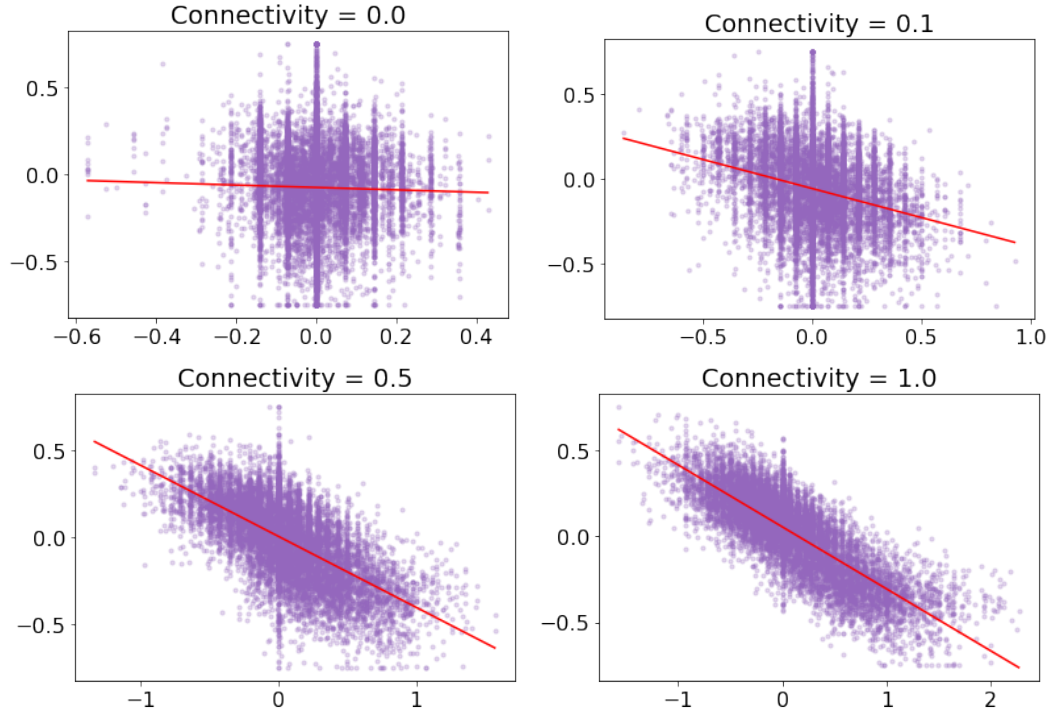


Figure 9: Skew $\epsilon_{t,\text{skew}}$ vs. inventory as a function of flow LT connectivity. The more connected to flow LTs, the more intensely the LP skews, i.e. price asymmetrically as a function of its inventory. This is quantified by the slope of the regression line getting more negative (skewing intensity), cf. also figure 11.

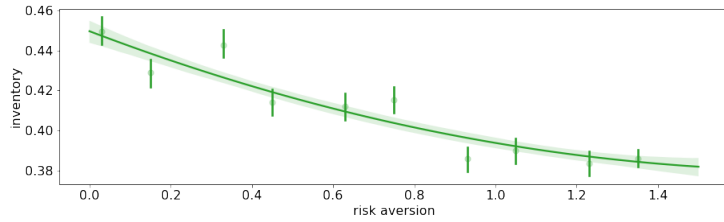


Figure 10: Average absolute LP inventory $|q_t|$ as a function of risk aversion.

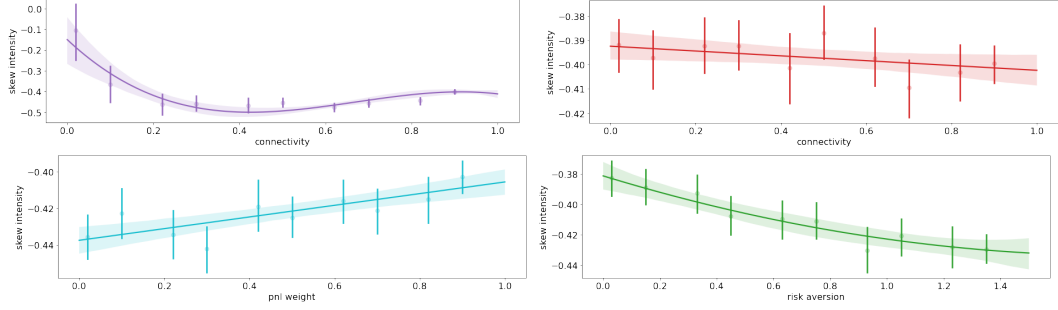


Figure 11: Skew intensity as a function of flow LT connectivity (top left), PnL LT connectivity (top right), PnL weight (bottom left), risk aversion (bottom right). The more intense the skewing, the more negative the skewing intensity (the lower).

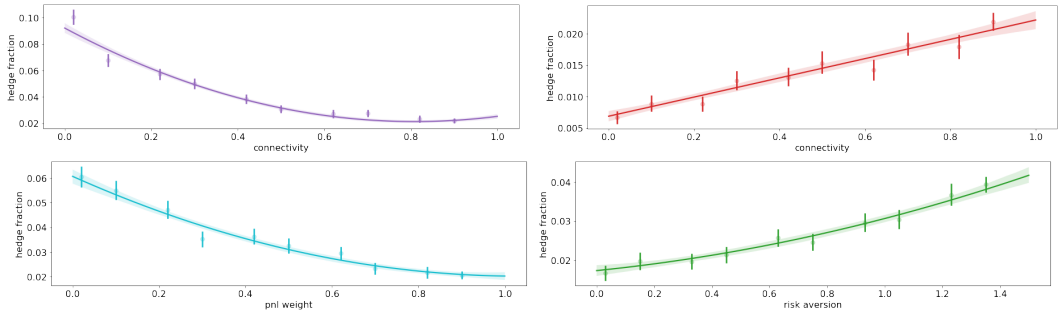


Figure 12: Hedge fraction as a function of flow LT connectivity (top left), PnL LT connectivity (top right), PnL weight (bottom left), risk aversion (bottom right).

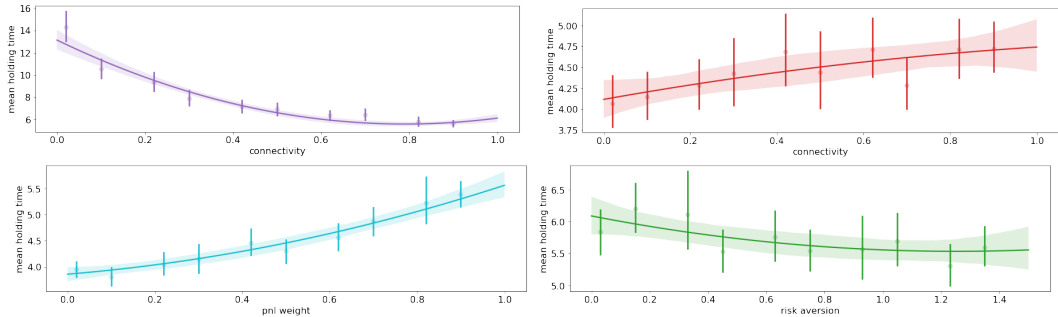


Figure 13: Mean inventory holding time as a function of flow LT connectivity (top left), PnL LT connectivity (top right), PnL weight (bottom left), risk aversion (bottom right).

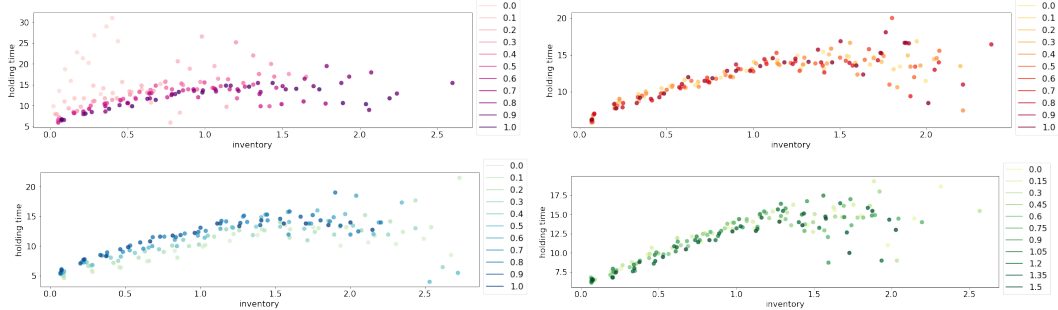


Figure 14: Inventory holding time as a function of inventory, for various values of flow LT connectivity (top left), PnL LT connectivity (top right), PnL weight (bottom left), risk aversion (bottom right).

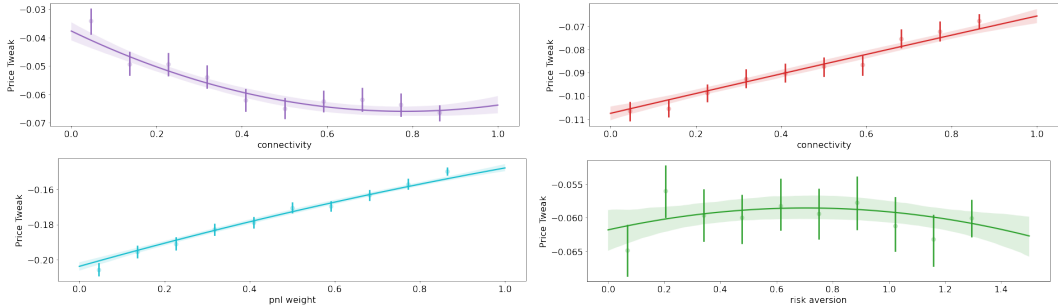


Figure 15: Average price $\epsilon_{t,\alpha}$ in (22) as a function of flow LT connectivity (top left), PnL LT connectivity (top right), PnL weight (bottom left), risk aversion (bottom right).

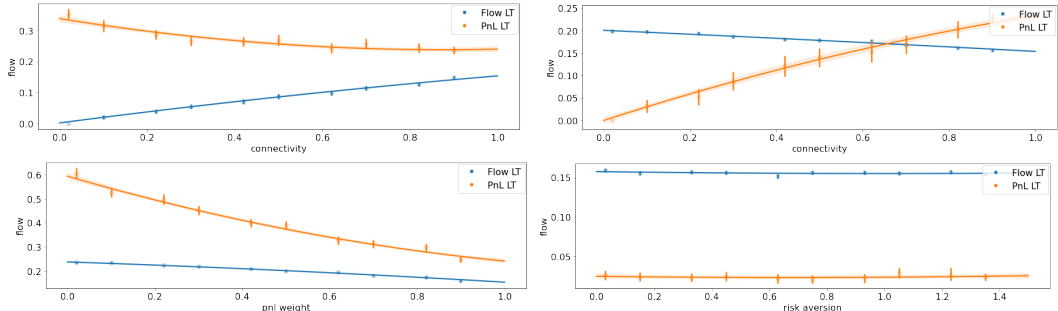


Figure 16: Flow as a function of flow LT connectivity (top left), PnL LT connectivity (top right), PnL weight (bottom left), risk aversion (bottom right). Flow curves are normalized by the number of LT agents in each agent class that the LP is connected to.

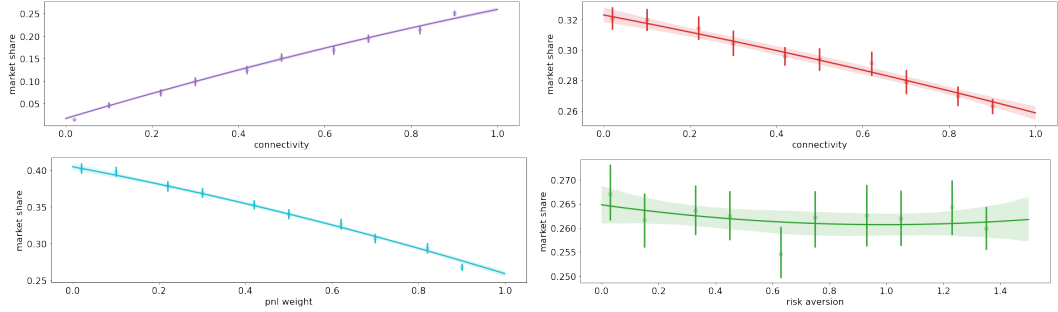


Figure 17: Market Share as a function of flow LT connectivity (top left), PnL LT connectivity (top right), PnL weight (bottom left), risk aversion (bottom right).

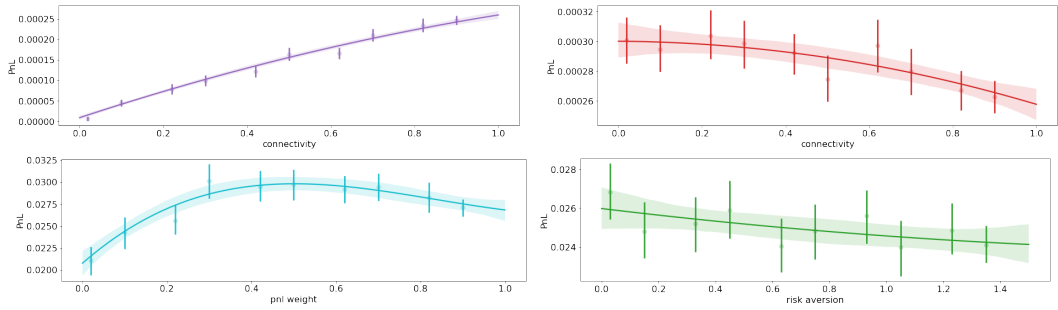


Figure 18: PnL as a function of flow LT connectivity (top left), PnL LT connectivity (top right), PnL weight (bottom left), risk aversion (bottom right).

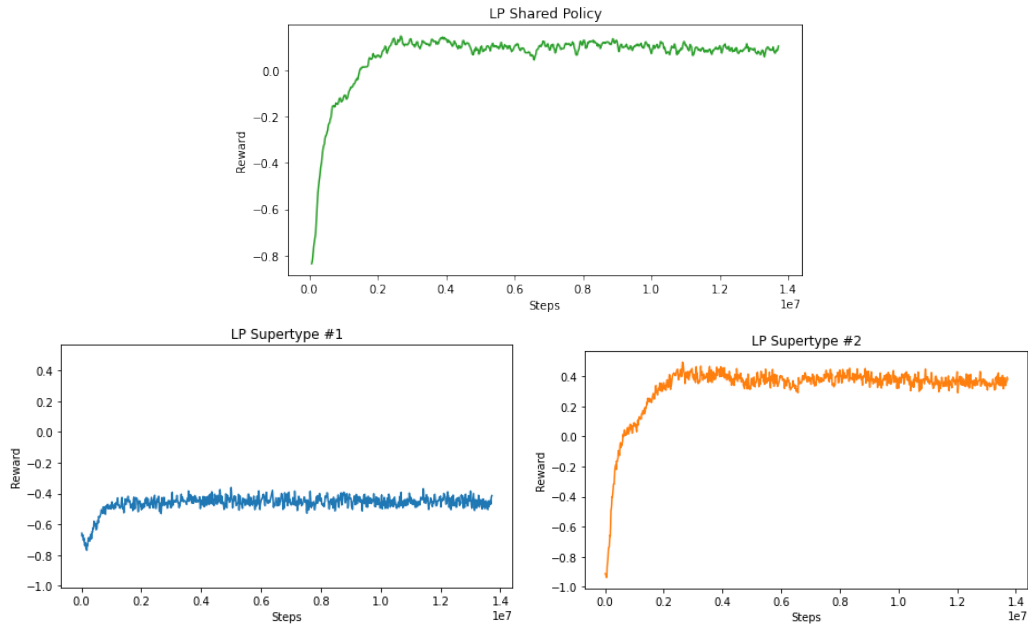


Figure 19: LP reward during training: shared policy, and supertypes 1 and 2.

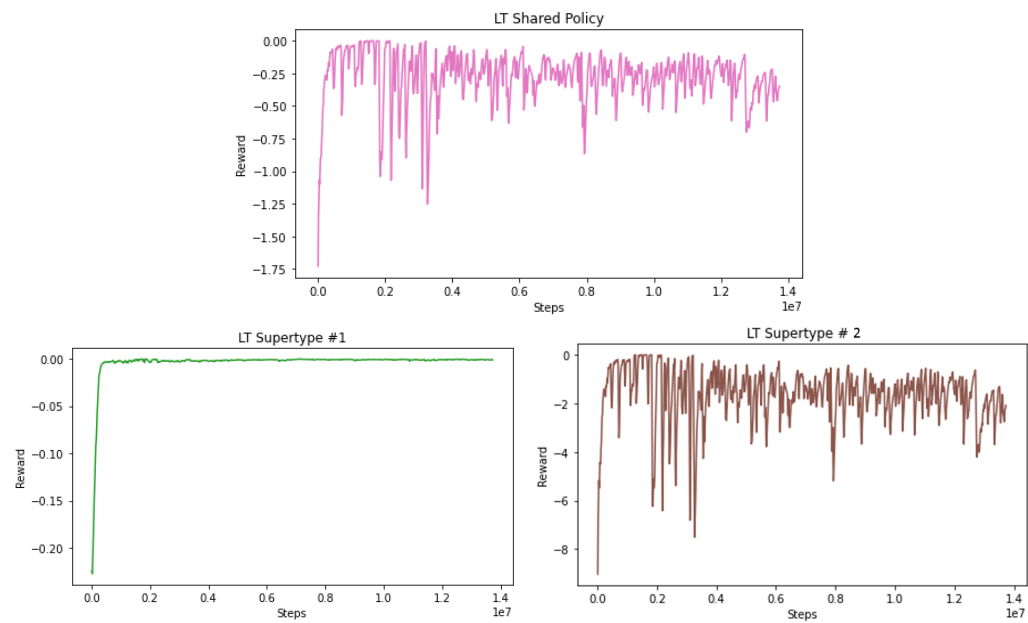


Figure 20: LT reward during training: shared policy, and supertypes 1 and 2.

6 Conclusion

In this work, we formalized the interactions between liquidity providers and liquidity takers in a dealer market as a multi-stage, multi-type stochastic game. We showed how a suitable design of parametrized families of reward functions coupled with shared policy learning makes our reinforcement-learning-driven agents learn emergent behaviors relative to a wide spectrum of incentives encompassing profit-and-loss, optimal execution and market share, by playing against each other. In particular, we find that liquidity providers naturally learn to balance hedging and skewing as a function of their incentives, where the latter refers to setting their pricing asymmetrically on the bid and ask sides as a function of their inventory. We introduced a novel RL-based equilibrium calibration algorithm which we found performed well at imposing constraints on the game equilibrium, both on toy and real market data. In particular, we find interesting that we are able to find a specific agent population - fully RL-driven - that explains the HSBC EURUSD flow response curve of a specific LP in Barzykin et al. (2021b).

Disclaimer

This paper was prepared for information purposes by the Artificial Intelligence Research group of JPMorgan Chase & Co and its affiliates (“JP Morgan”), and is not a product of the Research Department of JP Morgan. JP Morgan makes no representation and warranty whatsoever and disclaims all liability, for the completeness, accuracy or reliability of the information contained herein. This document is not intended as investment research or investment advice, or a recommendation, offer or solicitation for the purchase or sale of any security, financial instrument, financial product or service, or to be used in any way for evaluating the merits of participating in any transaction, and shall not constitute a solicitation under any jurisdiction or to any person, if such solicitation under such jurisdiction or to such person would be unlawful. © 2022 JPMorgan Chase & Co. All rights reserved.

References

Amihud, Y. and Mendelson, H. (1980). Dealership market: Market-making with inventory. *Journal of financial economics*, 8(1):31–53.

Andrychowicz, M., Denil, M., Gomez, S., Hoffman, M. W., Pfau, D., TomSchaul, Shillingford, B., and Freitas, N. D. (2016). Learning to learn by gradient descent by gradient descent. In *Advances in Neural Information Processing Systems*.

Ardon, L., Vadori, N., Spooner, T., Xu, M., Vann, J., and Ganesh, S. (2021). Towards a fully RL-based market simulator. *Proceedings of the 2nd International Conference on AI in Finance*.

Avegliano, P. and Sichman, J. S. (2019). Using surrogate models to calibrate agent-based model parameters under data scarcity. In *AAMAS*.

Avellaneda, M. and Stoikov, S. (2008). High-frequency trading in a limit order book. *Quantitative Finance*, 8(3):217–224.

Baldazzi, D., Garnelo, M., Bachrach, Y., Czarnecki, W., Perolat, J., Jaderberg, M., and Graepel, T. (2019). Open-ended learning in symmetric zero-sum games. In Chaudhuri, K. and Salakhutdinov, R., editors, *Proceedings of the 36th International Conference on Machine Learning*, volume 97 of *Proceedings of Machine Learning Research*, pages 434–443, Long Beach, California, USA. PMLR.

Bank, P., Ekren, I., and Muhle-Karbe, J. (2021). Liquidity in competitive dealer markets. *Mathematical Finance*.

Barzykin, A., Bergault, P., and Guéant, O. (2021a). Algorithmic market making in foreign exchange cash markets with hedging and market impact. <http://arxiv.org/abs/2106.06974>.

Barzykin, A., Bergault, P., and Guéant, O. (2021b). Market making by an fx dealer: tiers, pricing ladders and hedging rates for optimal risk control. <http://arxiv.org/abs/2112.02269>.

Borkar, V. S. (1997). Stochastic approximation with two time scales. *Systems & Control Letters*.

Brown, G. W. (1951). Iterative solution of games by fictitious play. *Activity Analysis of Production and Allocation*.

Candogan, O., Menache, I., Ozdaglar, A., and Parrilo, P. A. (2011). Flows and Decompositions of Games: Harmonic and Potential Games. *Mathematics of Operations Research*, 36(3):474–503.

Cao, Y., Chen, T., Wang, Z., and Shen, Y. (2019). Learning to optimize in swarms. In *Advances in Neural Information Processing Systems*.

Chan, N. T. and Shelton, C. (2001). An electronic Market-Maker. *Technical Report, MIT AI Lab*.

Cont, R. and Müller, M. S. (2021). A stochastic partial differential equation model for limit order book dynamics. *SIAM Journal on Financial Mathematics*, 12(2):744–787.

Cont, R. and Xiong, W. (2022). Dynamics of market making algorithms in dealer markets: Learning and tacit collusion.

Czarnecki, W. M., Gidel, G., Tracey, B., Tuyls, K., Omidshafiei, S., Balduzzi, D., and Jaderberg, M. (2020). Real world games look like spinning tops. In Larochelle, H., Ranzato, M., Hadsell, R., Balcan, M., and Lin, H., editors, *Advances in Neural Information Processing Systems*, volume 33, pages 17443–17454. Curran Associates, Inc.

Dalal, G., Szörényi, B., Thoppe, G., and Mannor, S. (2018). Finite sample analysis of two-timescale stochastic approximation with applications to reinforcement learning. In *Proc. Conference on Learning Theory (COLT)*.

Darley, V., Outkin, A., Plate, T., and Gao, F. (2000). Sixteenths or pennies? observations from a simulation of the nasdaq stock market. In *Proceedings of the IEEE/IAFE/INFORMS 2000 Conference on Computational Intelligence for Financial Engineering (CIFEr) (Cat. No.00TH8520)*, pages 151–154.

Das, S. (2005). A learning market-maker in the Glosten-Milgrom model. In *Quantitative Finance*.

Das, S. (2008). The effects of market-making on price dynamics. In *Proceedings of the 7th international joint conference on Autonomous agents and multiagent systems - Volume 2*, pages 887–894. International Foundation for Autonomous Agents and Multiagent Systems.

Duersch, P., Oechssler, J., and Schipper, B. (2012). Pure strategy equilibria in symmetric two-player zero-sum games. In *Int J Game Theory*, volume 41, pages 553–564.

Eiben, A., Horvath, M., Kowalczyk, W., and Schut, M. (2007). Reinforcement learning for online control of evolutionary algorithms. *Engineering Self-Organising Systems*, pages 151–160.

Ethier, S. and Kurtz, T. (1986). *Markov Processes: Characterization and Convergence*. Wiley.

Finn, C., Levine, S., and Abbeel, P. (2016). Guided cost learning: Deep inverse optimal control via policy optimization. In *Proceedings of the 33rd International Conference on International Conference on Machine Learning - Volume 48*, ICML’16, page 49–58. JMLR.org.

Foerster, J. N., Assael, Y. M., de Freitas, N., and Whiteson, S. (2016). Learning to communicate with deep multi-agent reinforcement learning. *Proceedings of the 30th International Conference on Neural Information Processing Systems*, pages 2145–2153.

Ganesh, S., Vadori, N., Xu, M., Zheng, H., Reddy, P., and Veloso, M. (2019). Reinforcement learning for market making in a multi-agent dealer market. *NeurIPS 2019 Workshop on Robust AI in Financial Services*.

Garman, M. B. (1976). Market microstructure. *Journal of financial economics*, 3(3):257–275.

Ghoshal, S. and Roberts, S. (2016). Optimal FX market making under inventory risk and adverse selection constraints. Technical report, Working paper.

Glosten, L. R. and Milgrom, P. R. (1985). Bid, ask and transaction prices in a specialist market with heterogeneously informed traders. *Journal of financial economics*, 14(1):71–100.

Guéant, O. (2017). Optimal market making. *Applied Mathematical Finance*.

Guéant, O., Lehalle, C.-A., and Fernandez-Tapia, J. (2013). Dealing with the inventory risk: a solution to the market making problem. *Mathematics and Financial Economics*, 7(4):477–507.

Gupta, J. K., Egorov, M., and Kochenderfer, M. (2017). Cooperative multi-agent control using deep reinforcement learning. In *Autonomous Agents and Multiagent Systems*, pages 66–83. Springer International Publishing.

Ha, D. and Schmidhuber, J. (2018). Recurrent world models facilitate policy evolution. *Advances in Neural Information Processing Systems (NeurIPS)*.

Hambly, B. M., Xu, R., and Yang, H. (2021). Policy gradient methods find the nash equilibrium in n -player general-sum linear-quadratic games. <https://dx.doi.org/10.2139/ssrn.3894471>.

Hansen, E. A., Bernstein, D. S., and Zilberstein, S. (2004). Dynamic programming for partially observable stochastic games. *AAAI*.

Hefti, A. (2017). Equilibria in symmetric games: theory and applications. *Theoretical Economics*, 12:979–1002.

Ho, T. and Stoll, H. R. (1981). Optimal dealer pricing under transactions and return uncertainty. *Journal of financial economics*, 9(1):47–73.

Jumadinova, J. and Dasgupta, P. (2010). A comparison of different automated market-maker strategies. In *12th Workshop on Agent-Mediated Electronic Commerce*, pages 141–154.

Konda, V. R. and Tsitsiklis, J. (2004). Convergence rate of linear two-timescale stochastic approximation. *The Annals of Applied Probability*, 14(2):796–819.

Lamperti, F., Roventini, A., and Sani, A. (2018). Agent-based model calibration using machine learning surrogates. *Journal of Economic Dynamics and Control*, 90:366–389.

Lanctot, M., Zambaldi, V., Gruslys, A., Lazaridou, A., Tuyls, K., Perolat, J., Silver, D., and Graepel, T. (2017). A unified game-theoretic approach to multiagent reinforcement learning. In Guyon, I., Luxburg, U. V., Bengio, S., Wallach, H., Fergus, R., Vishwanathan, S., and Garnett, R., editors, *Advances in Neural Information Processing Systems*, volume 30.

Leonardos, S., Overman, W., Panageas, I., and Piliouras, G. (2021). Global convergence of multiagent policy gradient in markov potential games. *Advances in Neural Information Processing Systems (NeurIPS)*.

Leslie, D. S. and Collins, E. (2002). Convergent multiple-timescales reinforcement learning algorithms in normal form games. *Annals of App. Prob.*

Letcher, A., Balduzzi, D., Racaniere, S., Martens, J., Foerster, J., Tuyls, K., and Graepel, T. (2019). Differentiable Game Mechanics. *Journal of Machine Learning Research*.

Li, K. and Malik, J. (2017). Learning to Optimize. *ICLR*.

Li, Z. and Wellman, M. P. (2020). Structure learning for approximate solution of Many-Player games. In *AAAI*, pages 2119–2127.

Li, Z. and Wellman, M. P. (2021). Evolution Strategies for Approximate Solution of Bayesian Games. *Proceedings of the AAAI Conference on Artificial Intelligence*.

Liang, E., Liaw, R., Nishihara, R., Moritz, P., Fox, R., Goldberg, K., Gonzalez, J., Jordan, M., and Stoica, I. (2018). RLLib: Abstractions for distributed reinforcement learning. In *Proceedings of the 35th International Conference on Machine Learning*, volume 80 of *Proceedings of Machine Learning Research*, pages 3053–3062.

Lim, Y.-S. and Gorse, D. (2018). Reinforcement learning for High-Frequency market making. In *ESANN*.

Lockhart, E., Lanctot, M., Pérolat, J., Lespiau, J.-B., Morrill, D., Timbers, F., and Tuyls, K. (2019). Computing approximate equilibria in sequential adversarial games by exploitability descent. In *Proceedings of the 28th International Joint Conference on Artificial Intelligence (IJCAI)*.

Lowe, R., Wu, Y., Tamar, A., Harb, J., Abbeel, P., and Mordatch, I. (2017). Multi-agent actor-critic for mixed cooperative-competitive environments. *Neural Information Processing Systems (NIPS)*.

Mahajan, A., Rashid, T., Samvelyan, M., and Whiteson, S. (2019). Maven: Multi-agent variational exploration. In Wallach, H., Larochelle, H., Beygelzimer, A., d'Alché-Buc, F., Fox, E., and Garnett, R., editors, *Advances in Neural Information Processing Systems*, volume 32. Curran Associates, Inc.

McMahan, H. B., Gordon, G. J., and Blum, A. (2003). Planning in the presence of cost functions controlled by an adversary. In *Proceedings of the Twentieth International Conference on International Conference on Machine Learning*, ICML'03, page 536–543. AAAI Press.

Mescheder, L., Nowozin, S., and Geiger, A. (2017). The Numerics of GANs. *NeurIPS*.

Mnih, V., Badia, A. P., Mirza, M., Graves, A., Harley, T., Lillicrap, T. P., Silver, D., and Kavukcuoglu, K. (2016). Asynchronous methods for deep reinforcement learning. In *Proceedings of the 33rd International Conference on International Conference on Machine Learning - Volume 48*, ICML'16, page 1928–1937. JMLR.org.

Monderer, D. and Shapley, L. S. (1996). Potential Games. *Games and Economic Behavior*, 14:124–143.

Perrin, S., Lauriere, M., Perolat, J., Elie, R., Geist, M., and Pietquin, O. (2022). Generalization in mean field games by learning master policies. *AAAI*.

Ramponi, G. and Restelli, M. (2021). Newton optimization on helmholtz decomposition for continuous games. *AAAI*.

Rashid, T., Samvelyan, M., de Witt, C. S., Farquhar, G., Foerster, J. N., and Whiteson, S. (2018). Qmix - monotonic value function factorisation for deep multi-agent reinforcement learning. In *International Conference on Machine Learning*.

Salimans, T., Ho, J., Chen, X., and Sutskever, I. (2017). Evolution Strategies as a Scalable Alternative to Reinforcement Learning. <https://arxiv.org/abs/1703.03864>.

Schulman, J., Levine, S., Abbeel, P., Jordan, M., and Moritz, P. (2015). Trust region policy optimization. In Bach, F. and Blei, D., editors, *Proceedings of the 32nd International Conference on Machine Learning*, volume 37 of *Proceedings of Machine Learning Research*, pages 1889–1897.

Schulman, J., Wolski, F., Dhariwal, P., Radford, A., and Klimov, O. (2017). Proximal Policy Optimization Algorithms. <https://arxiv.org/abs/1707.06347>.

Shen, Z., Ribeiro, A., Hassani, H., Qian, H., and Mi, C. (2019). Hessian aided policy gradient. *Proceedings of the 36th International Conference on Machine Learning*, volume 97 of *Proceedings of Machine Learning Research*.

Spooner, T., Fearnley, J., Savani, R., and Koukorinis, A. (2018). Market making via reinforcement learning. In *Proceedings of the 17th International Conference on Autonomous Agents and MultiAgent Systems*, AAMAS '18, page 434–442, Richland, SC. International Foundation for Autonomous Agents and Multiagent Systems.

Spooner, T. and Savani, R. (2020). Robust market making via adversarial reinforcement learning. In Bessiere, C., editor, *Proceedings of the Twenty-Ninth International Joint Conference on Artificial Intelligence, IJCAI-20*, pages 4590–4596. International Joint Conferences on Artificial Intelligence Organization. Special Track on AI in FinTech.

Srinivas, N., Krause, A., Kakade, S., and Seeger, M. (2016). Gaussian process optimization in the bandit setting: No regret and experimental design. *ICML*.

Srinivasan, S., Lanctot, M., Zambaldi, V., Pérolat, J., Tuyls, K., Munos, R., and Bowling, M. (2018). Actor-critic policy optimization in partially observable multiagent environments. In *Advances in Neural Information Processing Systems (NeurIPS)*.

Sunehag, P., Lever, G., Gruslys, A., Czarnecki, W. M., Zambaldi, V. F., Jaderberg, M., Lanctot, M., Sonnerat, N., Leibo, J. Z., Tuyls, K., and Graepel, T. (2018). Value-decomposition networks for cooperative multi-agent learning based on team reward. In *International Conference on Autonomous Agents and Multiagent Systems*.

Tamar, A., Di Castro, D., and Mannor, S. (2012). Policy gradients with variance related risk criteria. In *ICML*.

Vadori, N., Ganesh, S., Reddy, P., and Veloso, M. (2020). Calibration of Shared Equilibria in General Sum Partially Observable Markov Games. *Advances in Neural Information Processing Systems (NeurIPS)*.

Wah, E., Wright, M., and Wellman, M. P. (2017). Welfare effects of market making in continuous double auctions. *Journal of Artificial Intelligence Research*, 59:613–650.

Yu, C., Velu, A., Vinitsky, E., Wang, Y., Bayen, A., and Wu, Y. (2021). The surprising effectiveness of ppo in cooperative, multi-agent games. <https://arxiv.org/abs/2103.01955>.

Zheng, S., Trott, A., Srinivasa, S., Naik, N., Gruesbeck, M., Parkes, D. C., and Socher, R. (2020). The AI Economist: Improving equality and productivity with AI-driven tax policies. <https://arxiv.org/abs/2004.13332>.

A Appendix

Proof of theorem 2.2. The strategy consists in applying convergence results in Ethier and Kurtz (1986) (theorem 4.2, ch. 7). We need to show that for every $r > 0$, $x > 0$:

$$\lim_{\epsilon \rightarrow 0} \sup_{\|V\| \leq r} \epsilon^{-1} \mathbb{P}[\|V_{n+1}^\epsilon - V_n^\epsilon\| \geq x | V_n^\epsilon = V] = 0 \quad (24)$$

$$\lim_{\epsilon \rightarrow 0} \sup_{\|V\| \leq r} \|\epsilon^{-1} \mathbb{E}[V_{n+1}^\epsilon - V_n^\epsilon | V_n^\epsilon = V] - b(V)\| = 0 \quad (25)$$

$$\lim_{\epsilon \rightarrow 0} \sup_{\|V\| \leq r} \|\epsilon^{-1} \mathbb{E}[(V_{n+1}^\epsilon - V_n^\epsilon)(V_{n+1}^\epsilon - V_n^\epsilon)^T | V_n^\epsilon = V] - Q(V)\| = 0 \quad (26)$$

where $V_n^\epsilon := (V_{i,n}^\epsilon)_{i \in [1,2m]}$, \odot is the elementwise product, and $b(V) := -\mu^- \odot V + \mu^+$. (25), (26) both follow by direct computation. Indeed, we have $V_{n+1}^\epsilon - V_n^\epsilon = -\delta_{n,\epsilon}^- \odot V_n^\epsilon + \delta_{n,\epsilon}^+$, and therefore $\epsilon^{-1} \mathbb{E}[V_{n+1}^\epsilon - V_n^\epsilon | V_n^\epsilon = V] = b(V)$. This proves (25). For (26), we proceed again by direct computation, denoting $\tilde{\delta}_{i,n}^\pm := \delta_{i,n}^\pm - \mu_i^\pm$:

$$\begin{aligned} \epsilon^{-1} \mathbb{E}[(V_{i,n+1}^\epsilon - V_{i,n}^\epsilon)(V_{j,n+1}^\epsilon - V_{j,n}^\epsilon) | V_n^\epsilon = V] &= \\ &\mathbb{E}[\tilde{\delta}_{i,n}^+ \tilde{\delta}_{j,n}^+] - V_i \mathbb{E}[\tilde{\delta}_{i,n}^- \tilde{\delta}_{j,n}^+] - V_j \mathbb{E}[\tilde{\delta}_{j,n}^- \tilde{\delta}_{i,n}^+] + V_i V_j \mathbb{E}[\tilde{\delta}_{i,n}^- \tilde{\delta}_{j,n}^-] \end{aligned}$$

Expanding the latter yields $\epsilon^{-1} \mathbb{E}[(V_{i,n+1}^\epsilon - V_{i,n}^\epsilon)(V_{j,n+1}^\epsilon - V_{j,n}^\epsilon) | V_n^\epsilon = V] = [Q(V)]_{ij}$, and hence (26). We complete the proof by showing (24). Conditionally on $V_n^\epsilon = V$, we have:

$$\begin{aligned} \|V_{n+1}^\epsilon - V_n^\epsilon\| &= \|\epsilon(\mu^+ - \mu^- \odot V) + \sqrt{\epsilon}(\tilde{\delta}_n^+ - \tilde{\delta}_n^- \odot V)\| \\ &\leq \epsilon c_V + \sqrt{\epsilon}(\|\tilde{\delta}_n^+\| + 2\|V\|) \end{aligned}$$

where $c_V := \|\mu^+\| + \|\mu^-\| \|V\|$ is a constant only dependent on V , and remembering that δ^- takes value in $[0, 1]$ almost surely. We now apply Chebyshev's inequality, since by assumption $\delta_{i,n}^+$ are bounded in $L^{2+\eta}$:

$$\begin{aligned} &\mathbb{P}[\|V_{n+1}^\epsilon - V_n^\epsilon\| \geq x | V_n^\epsilon = V] \\ &\leq \mathbb{P}[\epsilon c_V + \sqrt{\epsilon}(\|\tilde{\delta}_n^+\| + 2\|V\|) \geq x] \\ &\leq \frac{\epsilon^{1+\frac{\eta}{2}}}{(x - \epsilon c_V)^{2+\eta}} \mathbb{E}[(\|\tilde{\delta}_n^+\| + 2\|V\|)^{2+\eta}] \\ &\leq \frac{\epsilon^{1+\frac{\eta}{2}}}{(x - \epsilon c_V)^{2+\eta}} (m_\eta + 2^{1+\eta}(2\|V\|)^{2+\eta}) \end{aligned}$$

where the last inequality comes from Holder's inequality and $m_\eta := \mathbb{E}[\|\tilde{\delta}_n^+\|^{2+\eta}]$. We thus have for $\|V\| \leq r$, $c_r := \|\mu^+\| + \|\mu^-\| r$ and $\epsilon \in (0, \frac{x}{2c_r})$:

$$\epsilon^{-1} \mathbb{P}[\|V_{n+1}^\epsilon - V_n^\epsilon\| \geq x | V_n^\epsilon = V] \leq \epsilon^{\frac{\eta}{2}} \left(\frac{2}{x}\right)^{2+\eta} (m_\eta + 8^{2\eta} r^{2+\eta})$$

which shows (24). \square

Proof of proposition 2.3. Denoting $u_n := \mathbb{E}[V_{i,n}]$, we have from the recursion equation $u_{n+1} = (1 - \mu_i^-)u_n + \mu_i^+$, from which $u_n = \mu_i^\infty + (V_{i,0} - \mu_i^\infty)(1 - \mu_i^-)^n$. The limit of u_n follows. Denoting $u_t := \mathbb{E}[V_{i,t}^*]$, taking expectations we have the ODE $u'_t = \mu_i^- (\mu_i^\infty - u_t)$, from which the limit of u_t follows, similar to the Ornstein-Uhlenbeck case. The covariance follows the same way. Indeed, let $z_n := \mathbb{E}[V_{i,n} V_{j,n}] - \mu_i^\infty \mu_j^\infty$, then we have, assuming without loss of generality that $V_{i,0} = \mu_i^\infty$:

$$z_{n+1} = z_n (1 - \mu_i^- - \mu_j^- + \mu_i^- \mu_j^- + \rho_{ij}^- \sigma_i^- \sigma_j^-) + \sigma_{ij}^\infty$$

which is of the form $z_{n+1} = (1 - a)z_n + b$. The limit of z_n follows directly as $\frac{b}{a}$. For the continuous-time limit $z_t := \mathbb{E}[V_{i,t}^* V_{j,t}^*] - \mu_i^\infty \mu_j^\infty$, simply observe that the rescaling by ϵ replaces n by $\lfloor \epsilon^{-1} t \rfloor$,

μ_i^\pm by $\epsilon\mu_i^\pm$ and σ_i^\pm by $\sqrt{\epsilon}\sigma_i^\pm$. Hence the discounting term $(1 - \mu_i^- - \mu_j^- + \mu_i^- \mu_j^- + \rho_{ij}^- \sigma_i^- \sigma_j^-)^n$ becomes $(1 - \epsilon\gamma + o(\epsilon))^{\lfloor \epsilon^{-1}t \rfloor}$, with $\gamma := \mu_i^- + \mu_j^- - \rho_{ij}^- \sigma_i^- \sigma_j^-$. The Riemann sum $\sum_{k=0}^{\lfloor \epsilon^{-1}t \rfloor} (1 - \gamma\epsilon + o(\epsilon))^k$ then converges to $\int_0^t e^{-\gamma x} dx$, which goes to γ^{-1} as $t \rightarrow \infty$ and yields the desired result.

Proof of proposition 2.6. We have:

$$\mathcal{V}(x) := Q(x) - Q(0) = \sigma^{-2}x^2 + 2\sigma^- (\mu^\infty \sigma^- - \rho \sigma^+) x$$

It is clear that if $\sigma^- = 0$, $\mathcal{V}(x) = 0 \forall x$. The roots of \mathcal{V} are 0 and $2 \left(\rho \frac{\sigma^+}{\sigma^-} - \mu^\infty \right)$. Since $x = V^* - \mu^\infty$, the roots are $V^* = \mu^\infty$ and $V^* = 2\rho \frac{\sigma^+}{\sigma^-} - \mu^\infty$. We denote $\gamma_* \leq \gamma^*$ these 2 roots. The leading order coefficient of \mathcal{V} is positive, therefore \mathcal{V} is negative in the region $V^* \in (\gamma_*, \gamma^*)$, and nonnegative otherwise.

V^* is never self-inhibiting if and only if $\gamma_* = \gamma^*$, i.e. $\mu^\infty = 2\rho \frac{\sigma^+}{\sigma^-} - \mu^\infty$, i.e. $\sigma^+ \mu^- \rho = \sigma^- \mu^+$.

We note that γ_* and γ^* depend on the model parameters only through the ratios $\frac{\sigma^+}{\sigma^-} \rho$ and $\frac{\mu^+}{\mu^-}$. Finally, we have $\partial_\rho \mathcal{V}(x) = -2\sigma^- \sigma^+ x$, which is positive if and only if x is negative.

Lemma A.1. *Every extended transitive game with payoff f has at least one (f, ϵ) -self-play sequence for every $\epsilon > 0$, and every such sequence is finite.*

Proof. First note that such a game has at least one (f, ϵ) -self-play sequence for every $\epsilon > 0$ since every (x, x) is a (f, ϵ) -self-play sequence of size 0 (cf. definition 2). Then, let (x_n, y_n) be a (f, ϵ) -self-play sequence. By definition of the self-play sequence we have $f(x_{2n+1}, x_{2n}) > f(x_{2n}, x_{2n}) + \epsilon$. By extended transitivity (cf. assumption 1) this implies $T(x_{2n+1}) > T(x_{2n}) + \delta_\epsilon$. But $x_{2n+1} = x_{2n+2}$ by definition of the self-play sequence, hence $T(x_{2n+2}) > T(x_{2n}) + \delta_\epsilon$. By induction $T(x_{2n}) > T(x_0) + n\delta_\epsilon$ for $n \geq 1$. If the sequence is not finite and since $\delta_\epsilon > 0$, one can take the limit as $n \rightarrow \infty$ and get a contradiction, since T is bounded by extended transitivity assumption. \square

Theorem A.2. *An extended transitive game with payoff f has a symmetric pure strategy ϵ -Nash equilibrium for every $\epsilon > 0$, which further can be reached within a finite number of steps following a (f, ϵ) -self-play sequence.*

Proof. Let $\epsilon > 0$. Take a (f, ϵ) -self-play sequence. By lemma A.1, such a sequence exists and is finite, hence one may take a (f, ϵ) -self-play sequence of maximal size, say $2N_\epsilon$. Assume that its end point (x, x) is not an ϵ -Nash equilibrium. Then $\exists y: f(y, x) > f(x, x) + \epsilon$, which means that one can extend the (f, ϵ) -self-play sequence to size $2N_\epsilon + 2$ with entries (y, x) and (y, y) , which violates the fact that such a sequence was taken of maximal size. \square

Theorem A.3. *An extended transitive game with continuous payoff f and compact strategy set has a symmetric pure strategy Nash equilibrium.*

Proof. By theorem A.2, take a sequence of ϵ_n -Nash equilibria with $\epsilon_n \rightarrow 0$ and corresponding (f, ϵ_n) -self-play sequence endpoints (x_n, x_n) . By compactness assumption, this sequence has a converging subsequence (x_{m_n}, x_{m_n}) , whose limit point (x_*, x_*) belongs to the strategy set. We have by definition of ϵ_{m_n} -Nash equilibrium that $f(x_{m_n}, x_{m_n}) \geq \sup_y f(y, x_{m_n}) - \epsilon_{m_n}$. Taking the limit as $n \rightarrow \infty$ and using continuity of f , we get $f(x_*, x_*) \geq \sup_y f(y, x_*)$, which shows that (x_*, x_*) is a symmetric pure strategy Nash equilibrium. \square

Proof of theorem 3.6. The first part of the theorem follows from theorem A.2. Then, we have by assumption that $\mathcal{S}, \mathcal{A}, \mathcal{S}^\lambda$ are finite. Denote $m := |\mathcal{S}| \cdot |\mathcal{A}| \cdot |\mathcal{S}^\lambda|$. In that case \mathcal{X} is given by:

$$\mathcal{X} = \{(x_a^{s, \lambda}) \in [0, 1]^m : \forall s \in [1, |\mathcal{S}|], \lambda \in [1, |\mathcal{S}^\lambda|], \sum_{a=1}^{|\mathcal{A}|} x_a^{s, \lambda} = 1\}$$

\mathcal{X} is a closed and bounded subset of $[0, 1]^m$, hence by Heine–Borel theorem it is compact. Note that closedness comes from the fact that summation to 1 is preserved by passing to the limit. By

assumption, the rewards are bounded, so by lemma 1, V_{Λ_i} is continuous for all i , which yields continuity of \widehat{V} , hence we can apply theorem A.3 to conclude.

Finally, if $(\pi_{\theta_n})_{n \geq 0}$ is a sequence of policies obtained following the gradient update (4) with $\widehat{V}(\pi_{\theta_{n+1}}, \pi_{\theta_n}) > \widehat{V}(\pi_{\theta_n}, \pi_{\theta_n}) + \epsilon$, then the self-play sequence generated by $(\pi_{\theta_n})_{n \geq 0}$ is finite by lemma A.1, and its endpoint is necessarily a symmetric pure strategy ϵ -Nash equilibrium according to the proof of theorem A.2, hence an ϵ -shared equilibrium. \square

Proof of lemma 3.5. Since by assumption \mathcal{S}^{LP} , \mathcal{A}^{LP} and $\mathcal{S}^{\lambda^{LP}}$ are finite, we will use interchangeably sum and integral over these spaces. Let us denote the total variation metric for probability measures π_1, π_2 on \mathcal{X}^{LP} :

$$\rho_{TV}(\pi_1, \pi_2) := \frac{1}{2} \max_{s, \lambda} \sum_{a \in \mathcal{A}} |\pi_1(a|s, \lambda) - \pi_2(a|s, \lambda)|$$

and let us equip the product space $\mathcal{X}^{LP} \times \mathcal{X}^{LP}$ with the metric:

$$\rho_{TV}((\pi_1, \pi_2), (\pi_3, \pi_4)) := \rho_{TV}(\pi_1, \pi_3) + \rho_{TV}(\pi_2, \pi_4).$$

We work for simplicity with the discounted infinite horizon case with discount factor $\gamma > 0$, but the finite horizon-case is dealt with the same way. In the calculations below, we omit the policy π^{LT} of the LT agents since it is fixed and hence can be subsumed in the transition dynamics \mathcal{T} , similarly we omit the LP superscript, since it is clear we are dealing with agents of such class and there is no ambiguity. Remember that $z_t^{(i)} := (s_t^{(i)}, a_t^{(i)}, \lambda_i)$. Let:

$$V_{\Lambda_i}(\pi_1, \pi_2, \mathbf{s}, \boldsymbol{\lambda}) := \mathbb{E}_{a_t^{(i)} \sim \pi_1(\cdot|s_i, \lambda_i), a_t^{(j)} \sim \pi_2(\cdot|s_j, \lambda_j)} \left[\sum_{t=0}^{\infty} \gamma^t \mathcal{R}(z_t^{(i)}, \mathbf{z}_t^{(-i)}) | \mathbf{s}_0 = \mathbf{s} \right], \quad j \neq i$$

so that:

$$V_{\Lambda_i}(\pi_1, \pi_2) = \int_{\mathbf{s}} \int_{\boldsymbol{\lambda}} V_{\Lambda_i}(\pi_1, \pi_2, \mathbf{s}, \boldsymbol{\lambda}) \cdot \Pi_{j=1}^n [\mu_{\lambda_j}^0(ds_j) p_{\Lambda_j}(d\lambda_j)]$$

Then we have:

$$\begin{aligned} V_{\Lambda_i}(\pi_1, \pi_2, \mathbf{s}, \boldsymbol{\lambda}) &= \int_{\mathbf{a}} \mathcal{R}(z^{(i)}, \mathbf{z}^{(-i)}) \pi_1(da_i|s_i, \lambda_i) \Pi_{j \neq i} \pi_2(da_j|s_j, \lambda_j) \\ &+ \gamma \int_{\mathbf{a}} \int_{\mathbf{s}'} \mathcal{T}(\mathbf{z}, d\mathbf{s}') V_{\Lambda_i}(\pi_1, \pi_2)(\mathbf{s}', \boldsymbol{\lambda}) \pi_1(da_i|s_i, \lambda_i) \Pi_{j \neq i} \pi_2(da_j|s_j, \lambda_j) \end{aligned}$$

The goal is to compute $|V_{\Lambda_i}(\pi_1, \pi_2, \mathbf{s}, \boldsymbol{\lambda}) - V_{\Lambda_i}(\pi_3, \pi_4, \mathbf{s}, \boldsymbol{\lambda})|$ and show that the latter is small provided that $\rho_{TV}((\pi_1, \pi_2), (\pi_3, \pi_4))$ is small. Let us use the notation:

$$c_1(\pi_1, \pi_2) := \int_{\mathbf{a}} \mathcal{R}(z^{(i)}, \mathbf{z}^{(-i)}) \pi_1(da_i|s_i, \lambda_i) \Pi_{j \neq i} \pi_2(da_j|s_j, \lambda_j)$$

Since by assumption $|\mathcal{R}|$ is bounded, say by \mathcal{R}_{max} we have:

$$\begin{aligned} &|c_1(\pi_1, \pi_2) - c_1(\pi_3, \pi_4)| \\ &\leq \mathcal{R}_{max} \int_{\mathbf{a}} |\pi_1(da_i|s_i, \lambda_i) \Pi_{j \neq i} \pi_2(da_j|s_j, \lambda_j) - \pi_3(da_i|s_i, \lambda_i) \Pi_{j \neq i} \pi_4(da_j|s_j, \lambda_j)| \\ &\leq \mathcal{R}_{max} \int_{a_i} |\pi_1(da_i|s_i, \lambda_i) - \pi_3(da_i|s_i, \lambda_i)| \\ &\quad + \mathcal{R}_{max} \int_{\mathbf{a}_{-i}} |\Pi_{j \neq i} \pi_2(da_j|s_j, \lambda_j) - \Pi_{j \neq i} \pi_4(da_j|s_j, \lambda_j)| \\ &\leq 2\mathcal{R}_{max} \rho_{TV}(\pi_1, \pi_3) + 2\mathcal{R}_{max} (n-1) \rho_{TV}(\pi_2, \pi_4) \leq 2n\mathcal{R}_{max} \rho_{TV}((\pi_1, \pi_2), (\pi_3, \pi_4)) \end{aligned}$$

Now, let us use the notation:

$$c_2(\pi_1, \pi_2) := \int_{\mathbf{a}} \int_{\mathbf{s}'} \mathcal{T}(\mathbf{z}, d\mathbf{s}') V_{\Lambda_i}(\pi_1, \pi_2)(\mathbf{s}', \boldsymbol{\lambda}) \pi_1(da_i|s_i, \lambda_i) \Pi_{j \neq i} \pi_2(da_j|s_j, \lambda_j)$$

For the term $|c_2(\pi_1, \pi_2) - c_2(\pi_3, \pi_4)|$, we can split:

$$\begin{aligned}
& V_{\Lambda_i}(\pi_1, \pi_2)(\mathbf{s}', \boldsymbol{\lambda}) \pi_1(da_i|s_i, \lambda_i) \Pi_{j \neq i} \pi_2(da_j|s_j, \lambda_j) \\
& \quad - V_{\Lambda_i}(\pi_3, \pi_4)(\mathbf{s}', \boldsymbol{\lambda}) \pi_3(da_i|s_i, \lambda_i) \Pi_{j \neq i} \pi_4(da_j|s_j, \lambda_j) \\
& = V_{\Lambda_i}(\pi_1, \pi_2)(\mathbf{s}', \boldsymbol{\lambda}) [\pi_1(da_i|s_i, \lambda_i) \Pi_{j \neq i} \pi_2(da_j|s_j, \lambda_j) - \pi_3(da_i|s_i, \lambda_i) \Pi_{j \neq i} \pi_4(da_j|s_j, \lambda_j)] \\
& \quad + \pi_3(da_i|s_i, \lambda_i) \Pi_{j \neq i} \pi_4(da_j|s_j, \lambda_j) [V_{\Lambda_i}(\pi_1, \pi_2)(\mathbf{s}', \boldsymbol{\lambda}) - V_{\Lambda_i}(\pi_3, \pi_4)(\mathbf{s}', \boldsymbol{\lambda})]
\end{aligned}$$

Since V_{Λ_i} is bounded by $\mathcal{R}_{max}(1 - \gamma)^{-1}$, and noting that we have, as for c_1 , that:

$$\begin{aligned}
& \int_a |\pi_1(da_i|s_i, \lambda_i) \Pi_{j \neq i} \pi_2(da_j|s_j, \lambda_j) - \pi_3(da_i|s_i, \lambda_i) \Pi_{j \neq i} \pi_4(da_j|s_j, \lambda_j)| \\
& \leq 2n \rho_{TV}((\pi_1, \pi_2), (\pi_3, \pi_4))
\end{aligned}$$

we then have:

$$\begin{aligned}
|c_2(\pi_1, \pi_2) - c_2(\pi_3, \pi_4)| & \leq 2n \mathcal{R}_{max}(1 - \gamma)^{-1} \rho_{TV}((\pi_1, \pi_2), (\pi_3, \pi_4)) \\
& \quad + \max_{\mathbf{s}, \boldsymbol{\lambda}} |V_{\Lambda_i}(\pi_1, \pi_2, \mathbf{s}, \boldsymbol{\lambda}) - V_{\Lambda_i}(\pi_3, \pi_4, \mathbf{s}, \boldsymbol{\lambda})|
\end{aligned}$$

We then have, collecting all terms together:

$$\begin{aligned}
|V_{\Lambda_i}(\pi_1, \pi_2, \mathbf{s}, \boldsymbol{\lambda}) - V_{\Lambda_i}(\pi_3, \pi_4, \mathbf{s}, \boldsymbol{\lambda})| & \leq 2n \mathcal{R}_{max}(1 + \gamma(1 - \gamma)^{-1}) \rho_{TV}((\pi_1, \pi_2), (\pi_3, \pi_4)) \\
& \quad + \gamma \max_{\mathbf{s}, \boldsymbol{\lambda}} |V_{\Lambda_i}(\pi_1, \pi_2, \mathbf{s}, \boldsymbol{\lambda}) - V_{\Lambda_i}(\pi_3, \pi_4, \mathbf{s}, \boldsymbol{\lambda})|
\end{aligned}$$

Taking the maximum over $\mathbf{s}, \boldsymbol{\lambda}$ on the left hand-side and rearranging terms finally yields:

$$\begin{aligned}
|V_{\Lambda_i}(\pi_1, \pi_2) - V_{\Lambda_i}(\pi_3, \pi_4)| & \leq \max_{\mathbf{s}, \boldsymbol{\lambda}} |V_{\Lambda_i}(\pi_1, \pi_2, \mathbf{s}, \boldsymbol{\lambda}) - V_{\Lambda_i}(\pi_3, \pi_4, \mathbf{s}, \boldsymbol{\lambda})| \\
& \leq 2n(1 - \gamma)^{-1} \mathcal{R}_{max}(1 + \gamma(1 - \gamma)^{-1}) \rho_{TV}((\pi_1, \pi_2), (\pi_3, \pi_4)) \\
& = 2n(1 - \gamma)^{-2} \mathcal{R}_{max} \rho_{TV}((\pi_1, \pi_2), (\pi_3, \pi_4))
\end{aligned}$$

which yields the desired continuity result. \square

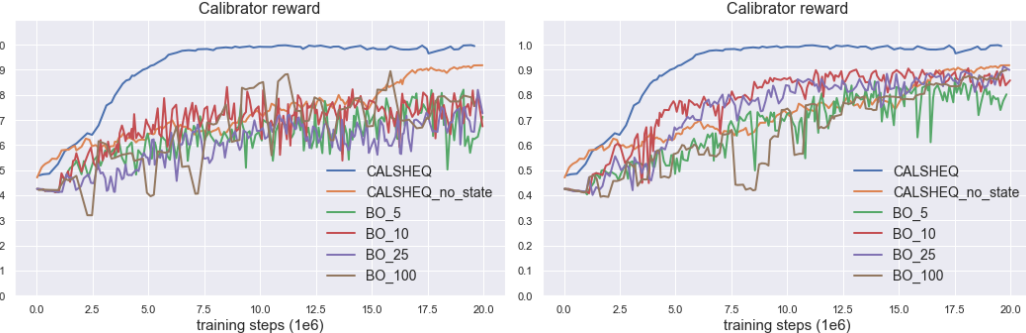


Figure 21: Calibrator Reward during training for various number of BO frequencies M - Experiment 1 - **(Left)** BO Expected Improvement (EI) - **(Right)** BO UCB with exploration parameter $\kappa = 1.5$.

Table 7: Calibrated connectivity matrix for the HSBC EURUSD data taken from Barzykin et al. (2021b)

		ECN	LP	
		0	0	1
		1	0%	100%
LT	2	100%	0%	4% 96%
	3	0%	100%	0% 0%
	4	0%	0%	100% 0%

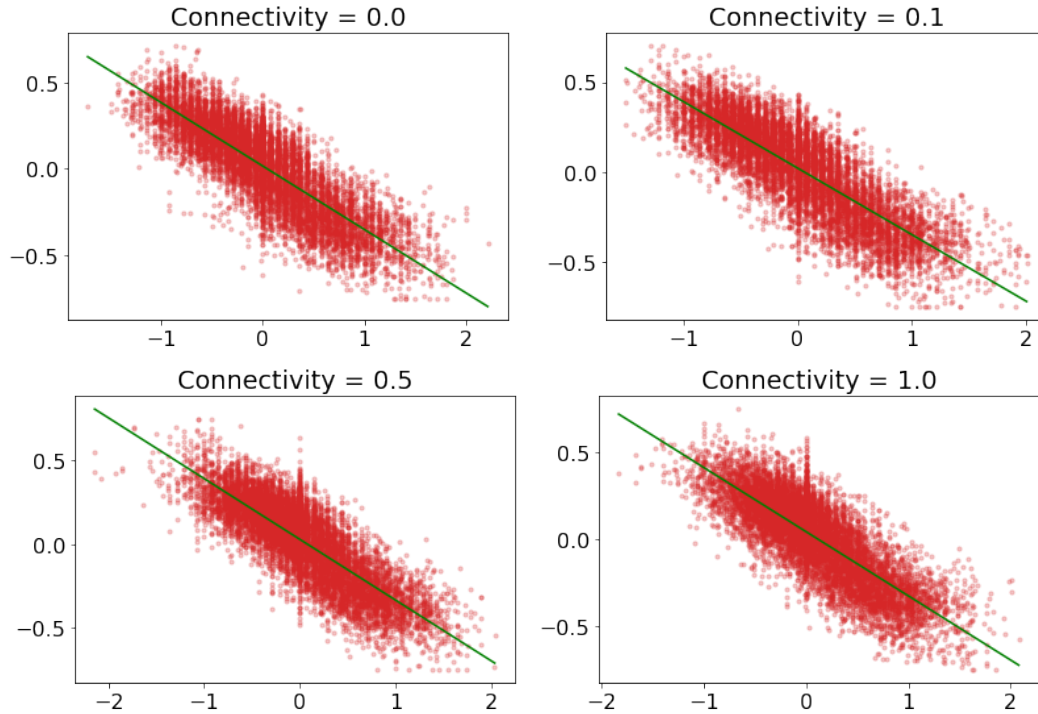


Figure 22: Skew $\epsilon_{t,\text{skew}}$ vs. inventory as a function of PnL LT connectivity.

Table 8: LP calibrated parameters for the HSBC EURUSD data taken from Barzykin et al. (2021b)

LP	PnL Weight ω	Risk Aversion γ
0	0%	0
1	100%	0.08
2	0%	1.13

Table 9: LT calibrated parameters for the HSBC EURUSD data taken from Barzykin et al. (2021b)

LT	PnL Weight ω	Risk Aversion γ
0	0%	1.5
1	0%	0.
2	0%	1.5
3	0%	1.5
4	0%	0.34

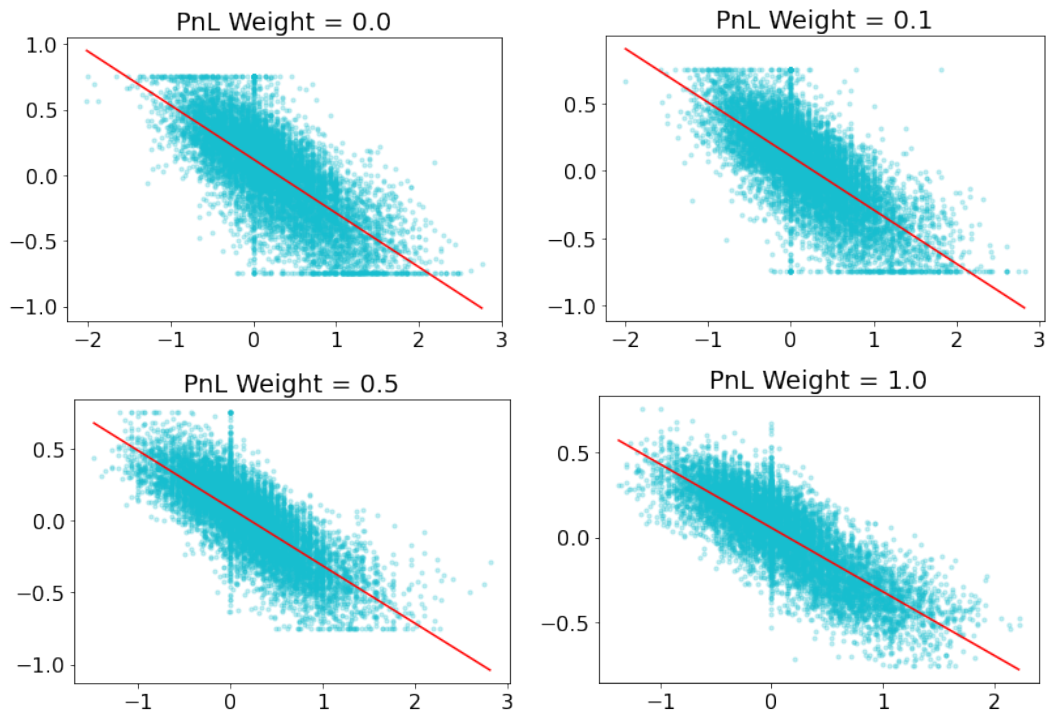


Figure 23: Skew $\epsilon_{t,skew}$ vs. inventory as a function of PnL weight.

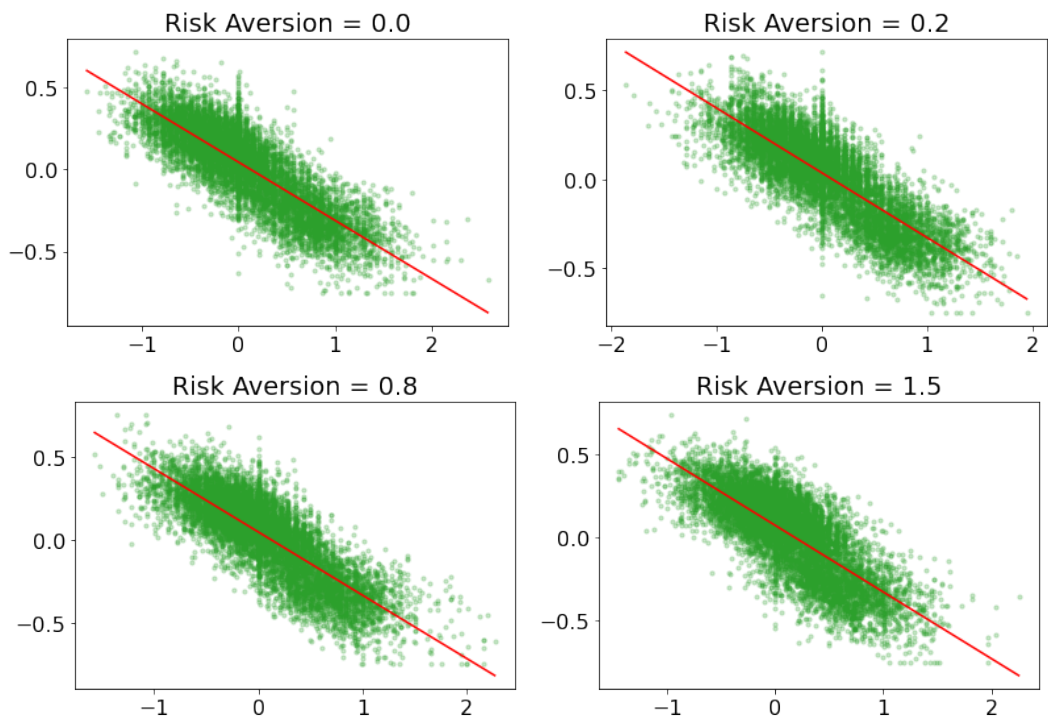


Figure 24: Skew $\epsilon_{t,skew}$ vs. inventory as a function of risk aversion.

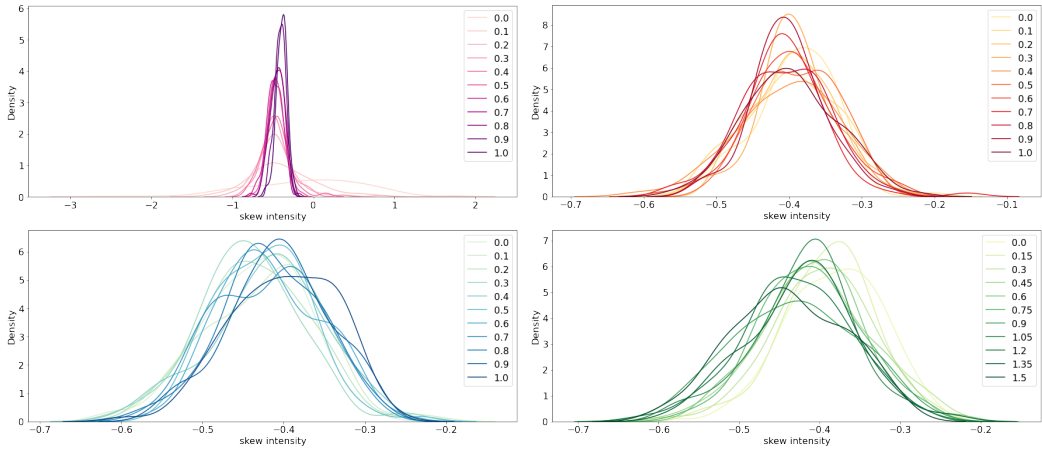


Figure 25: Skew intensity distribution as a function of flow LT connectivity (top left), PnL LT connectivity (top right), PnL weight (bottom left), risk aversion (bottom right).

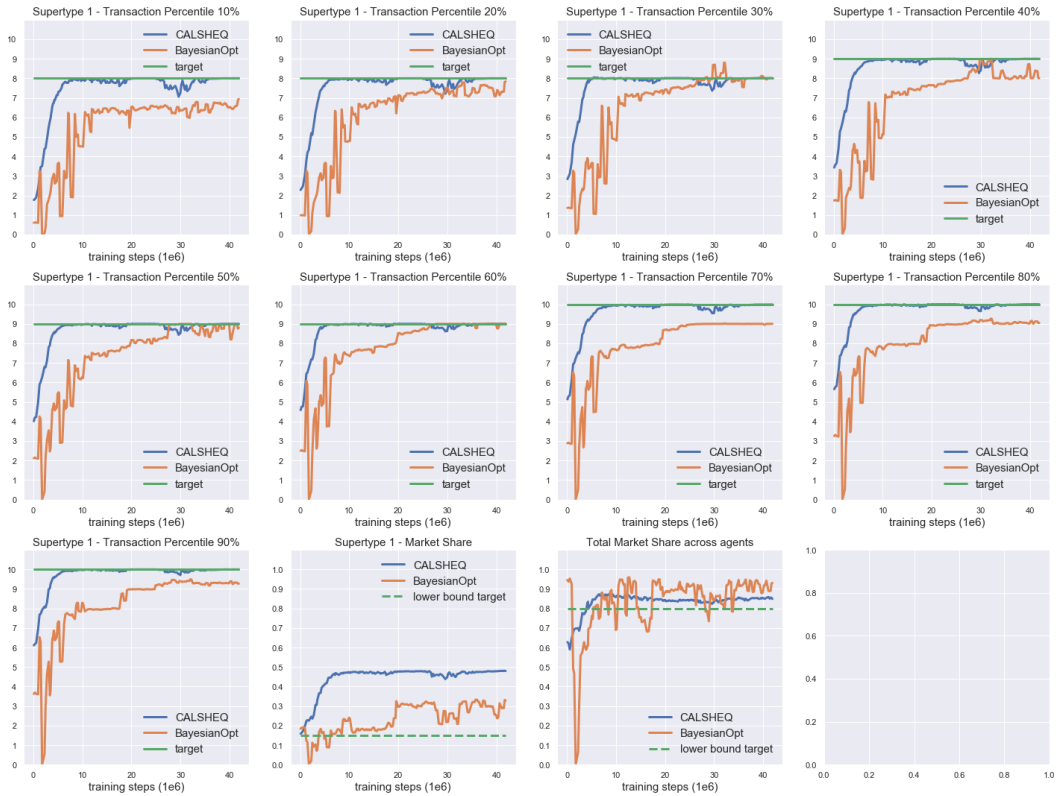


Figure 26: Experiment 1 - Calibration target fit for trade quantity distribution percentile and Market Share during training, averaged over episodes B . Dashed line target indicates that the constraint was set to be greater than target (not equal to it). *CALSHEQ* (ours) and baseline (Bayesian optimization).

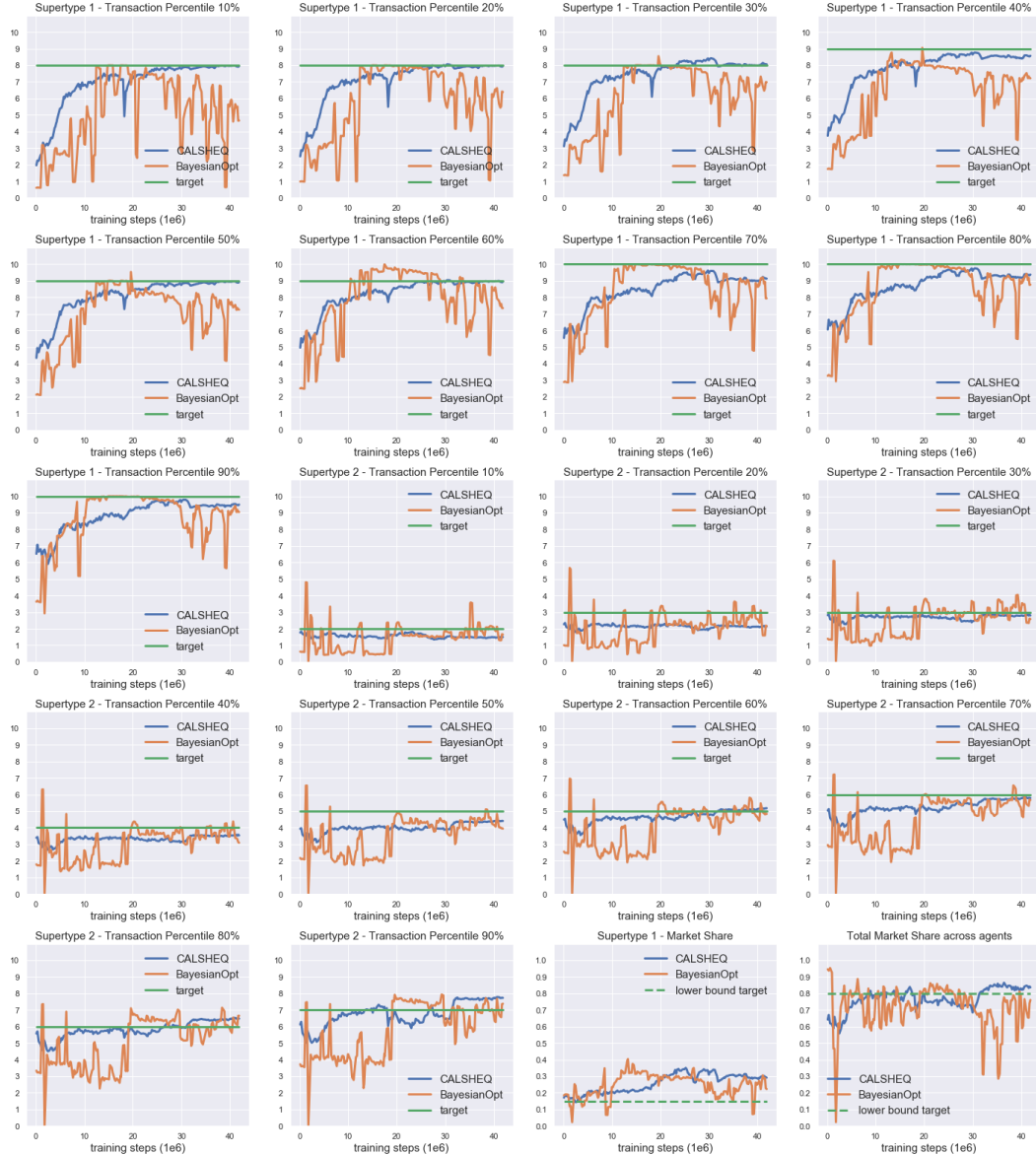


Figure 27: Experiment 2 - Calibration target fit for trade quantity distribution percentile and Market Share during training, averaged over episodes B . Dashed line target indicates that the constraint was set to be greater than target (not equal to it). *CALSHEQ* (ours) and baseline (Bayesian optimization).



Figure 28: Experiment 3 - Calibration target fit for trade quantity distribution percentile and Market Share during training, averaged over episodes B . Dashed line target indicates that the constraint was set to be greater than target (not equal to it). *CALSHEQ* (ours) and baseline (Bayesian optimization).

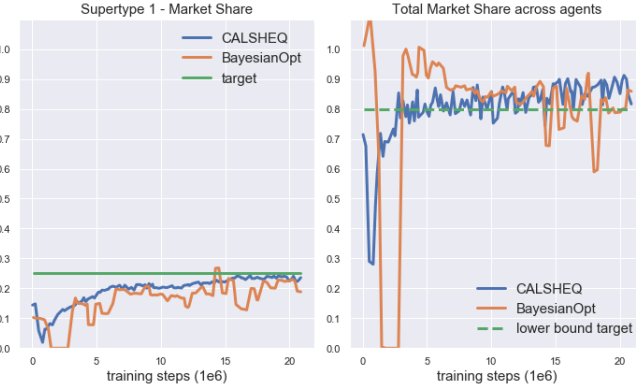


Figure 29: Experiment 4 - Calibration target fit for Market Share during training, averaged over episodes B . Dashed line target indicates that the constraint was set to be greater than target (not equal to it). *CALSHEQ* (ours) and baseline (Bayesian optimization).

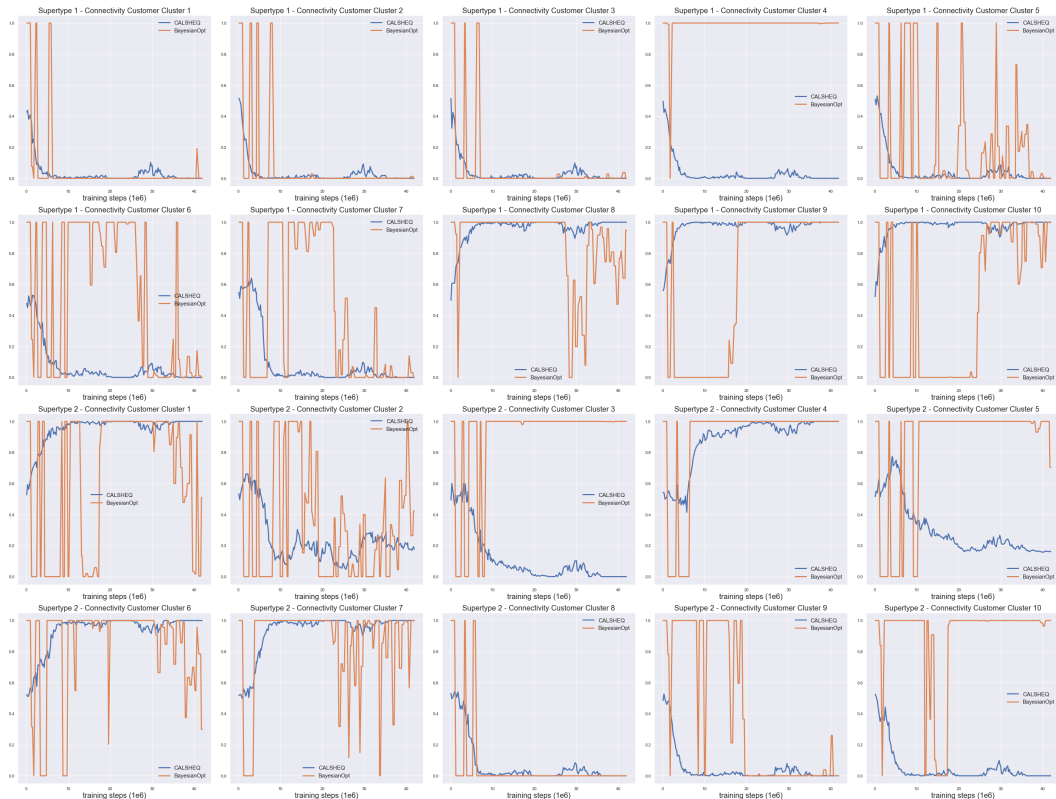


Figure 30: Experiment 1 - Calibrated parameters, averaged over episodes B . *CALSHEQ* (ours) and baseline (Bayesian optimization).

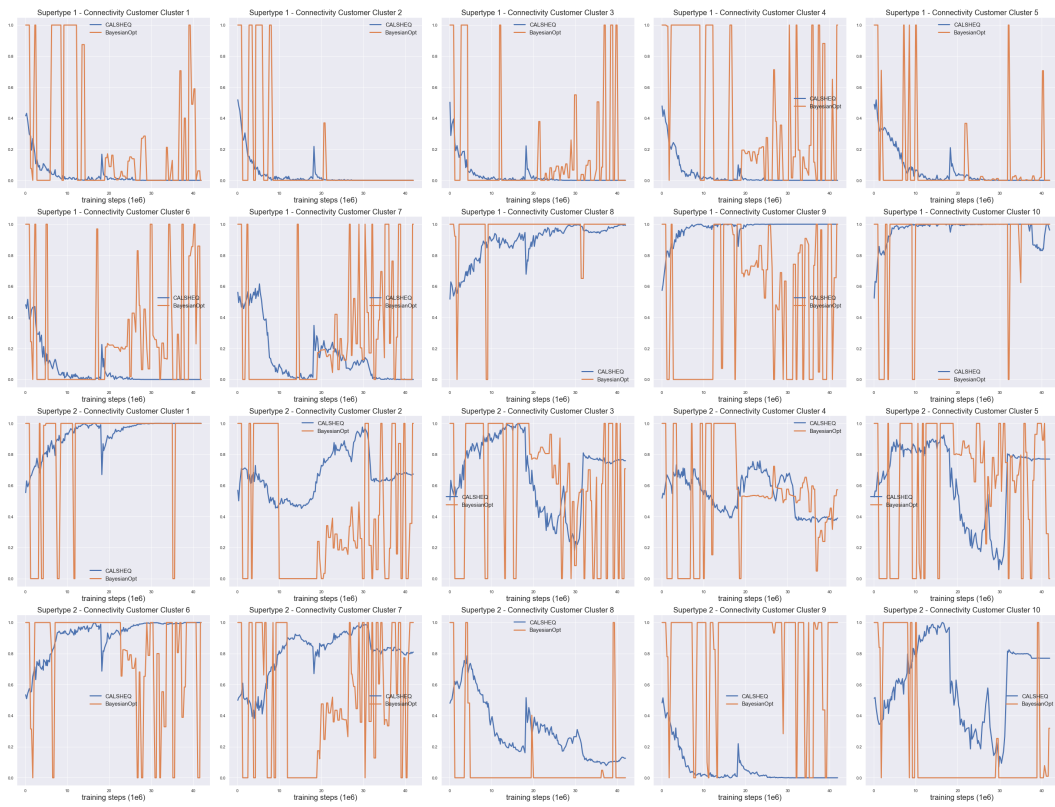


Figure 31: Experiment 2 - Calibrated parameters, averaged over episodes B . *CALSHEQ* (ours) and baseline (Bayesian optimization).

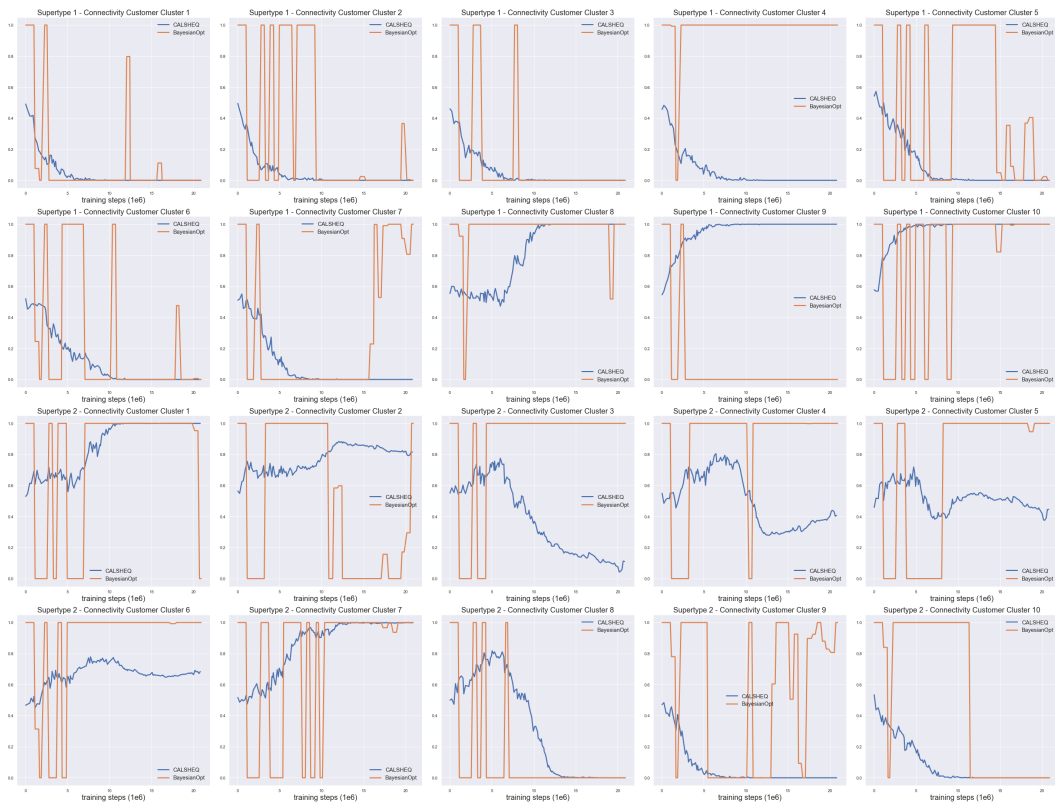


Figure 32: Experiment 3 - Calibrated parameters, averaged over episodes B . *CALSHEQ* (ours) and baseline (Bayesian optimization).

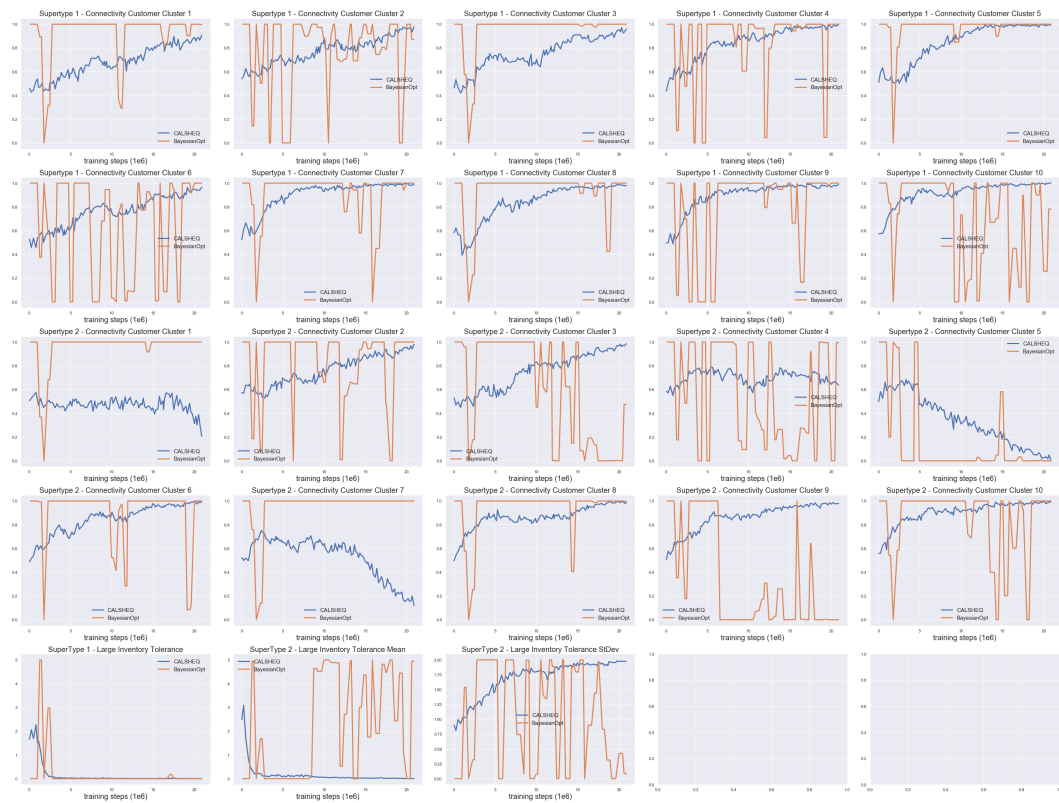


Figure 33: Experiment 4 - Calibrated parameters, averaged over episodes *B*. *CALSHEQ* (ours) and baseline (Bayesian optimization).